DNA ELECTROPHORESIS IN PHOTOPOLYMERIZED POLYACRYLAMIDE GELS ON A MICROFLUIDIC DEVICE

A Dissertation

by

CHIH-CHENG LO

Submitted to the Office of Graduate Studies of
Texas A&M University
in partial fulfillment of the requirements for the degree of

DOCTOR OF PHILOSOPHY

May 2008

Major Subject: Chemical Engineering

DNA ELECTROPHORESIS IN PHOTOPOLYMERIZED POLYACRYLAMIDE GELS ON A MICROFLUIDIC DEVICE

A Dissertation

by

CHIH-CHENG LO

Submitted to the Office of Graduate Studies of
Texas A&M University
in partial fulfillment of the requirements for the degree of

DOCTOR OF PHILOSOPHY

Approved by:

Chair of Committee,	Victor M. Ugaz
Committee Members,	Yue Kuo
	Michael A. Bevan
	Gyula Vigh
Head of Department,	Michael V. Pishko

May 2008

Major Subject: Chemical Engineering

ABSTRACT

DNA Electrophoresis in Photopolymerized Polyacrylamide Gels

on a Microfluidic Device. (May 2008)

Chih-Cheng Lo, B.S., National Chung Hsing University;

M.E., Texas A&M University

Chair of Advisory Committee: Dr. Victor M. Ugaz

DNA gel electrophoresis is a critical analytical step in a wide spectrum of genomic analysis assays. Great efforts have been directed to the development of miniaturized microfluidic systems ("lab-on-a-chip" systems) to perform low-cost, high-throughput DNA gel electrophoresis. However, further progress toward dramatic improvements of separation performance over ultra-short distances requires a much more detailed understanding of the physics of DNA migration in the sieving gel matrix than is currently available in literature. The ultimate goal would be the ability to quantitatively determine the achievable level of separation performance by direct measurements of fundamental parameters (mobility, diffusion, and dispersion coefficients) associated with the gel matrix instead of the traditional trial-and-error process.

We successfully established this predicting capability by measuring these fundamental parameters on a conventional slab gel DNA sequencer. However, it is dif-

ficult to carry out fast and extensive measurements of these parameters on a conventional gel electrophoresis system using single-point detection (2,000 hours on the slab gel DNA sequencer we used).

To address this issue, we designed and built a new automated whole-gel scanning detection system for a systematic investigation of these governing parameters on a microfluidic gel electrophoresis device with integrated on-chip electrodes, heaters, and temperature sensors. With this system, we can observe the progress of DNA separation along the whole microchannel with high temporal and spatial accuracy in nearly real time. This is in contrast to both conventional slab gel imaging where the entire gel can be monitored, but only at one time frame after completion of the separation, and capillary electrophoresis systems that allows detection as a function of time, but only at a single detection location.

With this system, a complete set of mobility, diffusion, and dispersion data can be collected within one hour instead of days or even months of work on a conventional sequencer under the same experimental conditions. The ability to acquire both spatial and temporal data simultaneously provides a more detailed picture of the separation process that can potentially be used to refine theoretical models and improve separation performance over ultra-short distances for the next-generation of electrophoresis technology.

DEDICATION

To

my parents, Mr. Sung-Ken Lo and Ms. Mei-Ying Huang,

my wife, Mei-Cheng, and daughter, Sophia, and all my friends

Thank you all for your love, support, and encouragement.

ACKNOWLEDGEMENTS

I would like to express my sincerest and heartfelt gratitude to my research advisor, Dr. Victor M. Ugaz, for his patience and guidance in my course of this study. All I have learned from him is indispensable and will benefit me in the long run.

I also thank my committee members, Dr. Kuo, Dr. Bevan, and Dr. Vigh, for their guidance and support throughout the course of this research.

Thanks also go to my friends and colleagues, Arjun, Nitin, Faisal, Jen-Huang, Serdar, and Yu-Wen for their participation in my student life at Texas A&M University. I also want to extend my gratitude to the faculty and staff of the Artie McFerrin Department of Chemical Engineering for making my time at Texas A&M University a great experience.

Last but not least, I want to thank my parents for their support and encouragement, and my wife and daughter for their patience and love.

NOMENCLATURE

%T	Monomer concentration
%C	Crosslinker concentration
bp	base pairs
BRM	Biased reptation model
BRF	Biased reptation with fluctuations
DNA	Deoxyribonucleic acid
dsDNA	Double-stranded DNA
ssDNA	Single-stranded DNA
WCID	Whole-column image detection

TABLE OF CONTENTS

CHAPTER Page

Page

LIST OF FIGURES

FIGURE Page

FIGURE Page

FIGURE Page

FIGURE Page

FIGURE Page

LIST OF TABLES

CHAPTER I

INTRODUCTION*

Recent advances in genomic analysis assays provide capabilities to directly access whole-genome information of many organisms. This benefits research in many applications, ranging from agriculture and farming to diagnosis of pathogens and treatments of human genetic diseases. In most of these assays, gel electrophoresis plays an important role due to its ability to perform size-selective fractionation of DNA fragments in sizes ranging from a few bases to several kilobases. Each assay has its specific requirement on separation resolutions, depending on the number and length of the DNA fragments to be separated (Table I-1) [1]. For example, DNA sequencing has the highest requirements on separation resolution due to its need to accurately distinguish single-base differences between single-stranded DNA (ssDNA) fragments. Such requirements are now routinely satisfied by capillary electrophoresis (CE) technology in separations of DNA fragments up to 1000 bases in length. However, sequencing whole genome of organisms still remains a prohibitively expensive endeavor, e.g. $100,000 USD for a mammalian-sized genome [2], and it takes months or years to finish.

This dissertation follows the style of *Electrophoresis*.

* Part of the data reported in this chapter is reprinted with permission from: Microfabricated electrophoresis systems for DNA sequencing and genotyping applications: current technology and future directions by Ugaz, V. M., Elms, R. D., Lo, R.C., Shaikh, F. A., and Burns, M. A., *Phil. Trans. R. Soc. Lond. A* (2004) **362**, 1105-1129.

Table I-1. Summary and associated separation resolution requirements of some typical genomic analysis assays making use of gel electrophoresis.

Assay	Description	Fragment Size Range (bases)	Resolution
False Positive PCR	Diagnostic to verify PCR amplification of correct DNA targets to avoid false positive identifications.	50 – 5,000	10 base
Gene Expression	"Northern blot" analysis consisting of size fractionation by gel electrophoresis followed by immobilization on a membrane.	200 – 20,000	10 base
Gene Expression	Reverse transcription PCR (RT-PCR) in which an RNA sample is converted to DNA (reverse transcription), which is subsequently amplified using PCR.	200 – 5,000	10 base
Restriction Digestion	Assays involving cleavage of a specific DNA sequence by a restriction enzyme, followed by size fractionation using gel electrophoresis.	$100 – 10^6$	10 base
Nucleic Acid-Protein Interactions	Examination of specific interactions between proteins and nucleic acids by monitoring the migration of DNA-protein hybrids relative to that of the DNA alone.	100 – 5,000	10 base
Human Identification Genotyping	PCR amplification of a modest number of identity loci (7 to 20), each of which is known to have a large number of alleles in the human population (4 to 20).	100 – 1,000	2 – 4 base
Single Nucleotide Polymorphism (SNP) Assays	Primer extension or "mini sequencing" methods employ PCR amplification followed by primer extension in the presence of specific dideoxynucleotide/ deoxynucleotide mixtures.	20 – 40	2 – 8 base
DNA Sequencing	Size-selective fractionation of DNA fragments generated by Sanger dideoxy sequencing reactions.	50 – 1,000	1 base

In addition, current gel electrophoresis technology still requires laboratory infrastructure and trained personnel to operate, and the gel electrophoresis device is still too big to be portable. These issues limits applications of DNA assays in remote locations, such as doctor's clinics and battlefields, to diagnose diseases or to detect pathogens in biological weapons. As a result, there is a compelling need to develop a new generation of fast and high-performance DNA gel electrophoresis technology.

1.1 Theory of DNA migration in a gel matrix

1.1.1 Mobility

Gel electrophoresis techniques rely on inducing a size-dependent difference in the migration velocity of negatively charged DNA molecules in the presence of an applied electric field. In practice, mobility ($\mu = v/E$, where v is the migration velocity, and E the applied electric field) is used instead of migration velocity to characterize DNA migration behavior. For example, in free solution, the mobility of short dsDNA fragments first increases with increasing size, then levels off, and eventually becomes size-independent after a threshold size of ~ 170 bp [3]. The detailed mechanism of this change in mobility size dependence is still not fully understood, but it is speculated to result from the transition form a rod-like to a coil-like conformation, because the persistent length for dsDNA is ~ 150 bp [4]. Longer DNA (> 170 bp) adopts a 'free draining coil' configuration in which all segments along the contour length of the molecule are uniformly exposed to the surrounding aqueous buffer environment [5]. Consequently, DNA fragments in free solution migrate at a uniform speed (expressed by the free solution mobility μ_0) that is

independent of their size. This can be explained by considering the forces acting on the fragments.

Electrostatic:

$$F_e = qE \tag{I-1}$$

where F_e is the electrostatic driving force, q the effective charge, and E the applied electric field.

Hydrodynamic drag:

$$F_d = fv \tag{I-2}$$

where F_d is the frictional drag force, f the friction coefficient, and v the migration velocity.

Force balance:

$$F_e = F_d$$

$$qE = fv$$

$$v = (q/f)E = \mu E \tag{I-3}$$

The force balance shows that differences in migration velocity can arise through size dependence of either the effective charge or friction. A closer look at these two factors reveals that the effective charge, q, scales as the number of segments (bases), N, ($q \sim N$) because of constant charge per unit mass of DNA molecules (-0.05e per base for ssDNA; -0.1e per base pair for dsDNA [6]) , and the drag, f, also has the same scaling relationship ($f \sim N$) due to equal contribution from each segment in the free draining coil. This results in a uniform migration velocity for DNA fragments of different sizes in free solution electrophoresis. As a result, a length dependence must be introduced through some

other means in order to achieve efficient separation. The most commonly used approach to introducing this size dependence is to induce electrophoretic migration to occur through a gel matrix so that interactions with the porous network will alter the mobility of the migrating DNA fragments. Specifically, smaller fragments experience less resistance as they travel through the gel matrix, and therefore are eluted more quickly than larger fragments. The gel matrix used in DNA electrophoresis has numerous nanopores extending in all directions throughout the whole structure. When a negatively charged DNA molecule migrates through the gel under the influence of an external electric field, the details of its motion depend on the size of the polymer coil relative to the pore size of the gel.

1.1.1.1 Ogston sieving

When the DNA fragment is smaller than the gel pore size ($R_g < a$, where R_g is the radius of gyration of a DNA fragment's equilibrium coil configuration and a is the mean gel pore size), the fragments retain equilibrium random coil configuration during migration between pores (Figure I-1a). Ogston first analyzed this migration scheme as a spherical particle moving through a random network of infinitely long, rigid cylinders [7]. Rodbard *et al.* further extended this model for the mobility scaling of DNA fragments migrating in gel matrix of a given concentration [8].

$$\log(\mu) = \log(\mu_0) - K_r C \tag{I-4a}$$

$$K_r = c_1 (R_g + r)^2 \tag{I-4b}$$

where μ is the DNA mobility in the sieving gel, μ_0 the DNA mobility in free solution, K_r the retardation coefficient, C the gel concentration, and c_1 the constant for a given electrophoresis system. The radius of gyration for a DNA molecule can be computed with the Kratky-Porod equation [9].

$$R_g^2 = \frac{pL_c}{3}[1 - 3(\frac{p}{L_c}) + 6(\frac{p}{L_c})^2 - 6(\frac{p}{L_c})^3(1 - e^{-\frac{L_c}{p}})] \qquad \text{(I-5)}$$

where L_c is the contour length of the DNA molecule, and p is the persistence length (L_c = 0.43 (nm/base) X DNA molecular size (M), and p = 3 nm for ssDNA [10-12]). From eqs. (I-4) and (I-5), we can find that log(μ) scales linearly with the DNA molecular size (M). In this regime, the gel matrix serves as a molecular sieve.

1.1.1.2 Entropic trapping

The DNA fragment selectively "jumps" between larger pores in the gel matrix when its size is comparable to that of the mean gel pore size ($R_g \approx a$; Figure I-1b). The scaling of mobility was reported as follows [13].

$$\mu \propto \frac{1}{\mathrm{M}^{1+\gamma}};\ \gamma > 0 \qquad \text{(I-6)}$$

In this regime, the DNA fragment has to migrate through narrow pores that connect to larger ones in the gel matrix to reach its maximum conformational entropy.

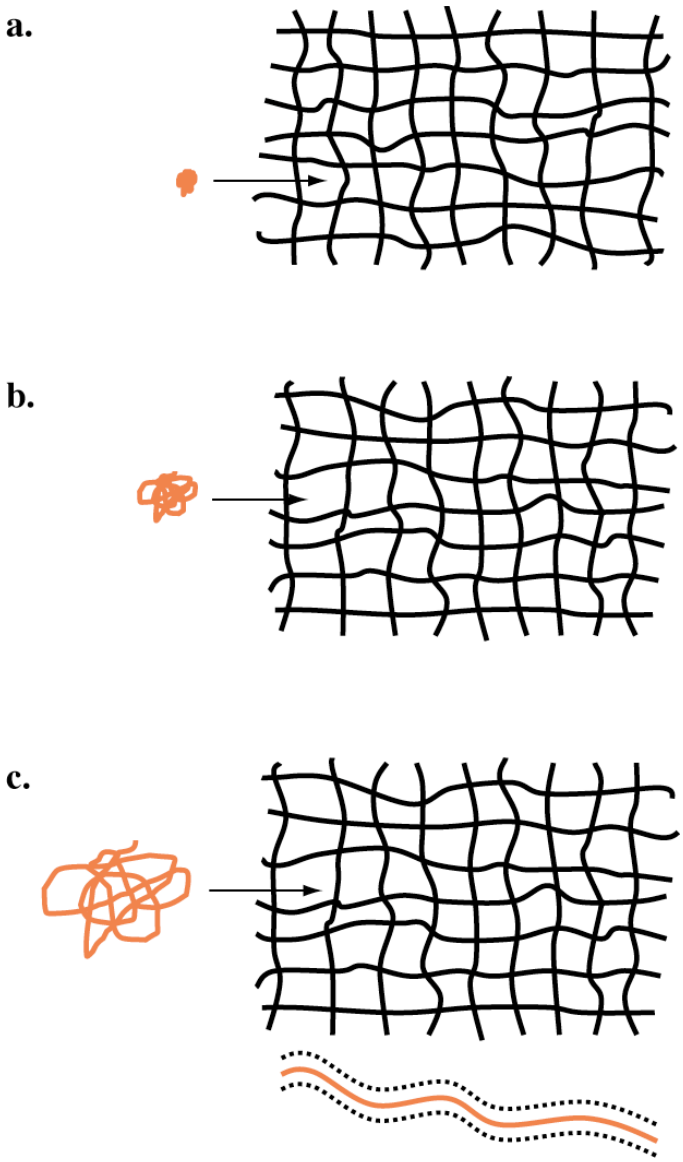

Figure I-1 Schemes of DNA migrating in the sieving gel. (a) In the Ogston sieving regime, the gel pore size is larger than the DNA fragment, and therefore it can easily be sieved through the gel matrix. (b) In the entropic trapping regime, the gel pore size is approximately that of the DNA fragment, and the DNA fragment "hops" through the gel matrix by some larger pores. (c) In the biased reptation regime, the gel pore size is smaller than the DNA fragment, and the DNA fragment travels head first through the gel matrix in an imaginary tube.

1.1.1.3 Biased reptation

Under conditions where the equilibrium coil size of the migrating DNA fragments is larger than the mean gel pore size ($R_g > a$; Figure I-1c), the migration of DNA fragments can be described in terms of a reptation mechanism in which the leading end of the molecule threads its way through the gel matrix by an imaginary tube under the influence of an external electric field [14-16]. The *biased reptation model* (BRM) [17-20] predicts that the mobility of a large DNA fragment scales inversely with its size.

$$\mu = \mu_0(\frac{1}{3N} + \frac{\varepsilon^2}{9}) \qquad \text{(I-7a)}$$

$$\varepsilon = \frac{Eqa}{kT} \qquad \text{(I-7b)}$$

where N (often referred to as the number of "blobs") is the ratio of the total fragment length (M) to the fragment length whose equilibrium coil size is equal to the mean pore diameter (M_a), and ε is the reduced electric field. Here E is the electric field, q the effective charge per blob, a the mean gel pore size, k the Boltzmann constant, and T the Kelvin temperature. This model correctly predicts the inverse scaling between mobility and DNA fragment size that was experimentally observed. When N is small, the size-dependent term dominates and accounts for the scaling of $\mu \sim N^{-1}$. For large N, the second term dominates and predicts that the mobility of long DNA molecules becomes dependent on the electric field instead of size. This qualitatively captures the scaling relationship between the experimentally observed mobility and DNA fragment size. However, the BRM model does not quantitatively predict a correct scaling relationship for

long fragments migrating under low field strengths. It predicts $\mu \sim \varepsilon^2$ instead of $\mu \sim \varepsilon^1$ observed experimentally [21].

The *biased reptation with fluctuations* (BRF) model [19, 20, 22-24] takes into account the effect of an external electric field on tube length fluctuations, which affect the orientation of the reptating DNA molecule. The scaling of mobility is as follows.

$$\mu = \mu_0(\frac{1}{3N} + f(\varepsilon)) \tag{I-8a}$$

$$\varepsilon = \frac{\eta a^2 \mu_0 E}{kT} \tag{I-8b}$$

where the term *f(ε)* takes into account electrohydrodynamic forces on the blob, and η is the solvent viscosity. Predictions of the BRF model are quantitatively in good agreement with the scaling relationship between experimentally measured mobility and DNA fragment size [21, 25-27].

1.1.2 Diffusion

The theory of DNA electrophoresis has been studied by many researches, but only a few have investigated the band broadening caused by thermal motion of the DNA molecules [28]. In dilute polymer solutions, the Zimm model can be applied to describe hydrodynamics of isolated polymer chains. The diffusion coefficient of the polymer chain is given as follows [29].

$$D \sim \frac{kT}{\eta R_g}$$

$$R_g \sim N^{\nu}$$

$$D \sim N^{-\nu} \qquad \text{(I-9)}$$

For random walk polymer chains, the exponent ν is 0.5 [30]. In the Ogston sieving regime, the diffusion coefficient of the DNA fragment scales in the same way as predicted by the Zimm model [31]. In the reptation regime, the diffusion coefficient scales as [15, 16]:

$$D \sim N^{-3+2\nu} \qquad \text{(I-10)}$$

This predicts that the diffusion coefficient scales as $D \sim N^{-2}$.

1.1.3 Dispersion

Although the thermal motion of DNA molecules is attributed to band broadening in gel electrophoresis, this cannot account for the overall band-broadening process [28, 32-34]. In addition to the thermal motion of DNA molecules, the presence of an electric field also contributes to the band broadening process. To distinguish from the effect of thermal motion, this effect is termed as *dispersion coefficient* (D^E). The Stokes-Einstein equation was initially used to determine the dispersion coefficient [28, 33].

$$D^E = D(\frac{\mu^E}{\mu^0}) \qquad \text{(I-11)}$$

where μ^E is the mobility with the presence of an electric field, and μ^E is the zero-field mobility. The scaling of dispersion coefficient is predicted to be $D \sim N^{-2}$ for small DNA fragments and $D \sim N^{-1}$ for large ones [28]. However, it was pointed out that the Stokes-

Einstein equation could only be applied to very small DNA molecules at nearly zero electric field [28, 31, 35]. This contradicts the actual DNA gel electrophoresis process.

The BRF model takes into account the effect of the presence of an electric field on the orientation of DNA molecules and the electrohydrodynamic forces on each blob of the chain. It predicts three scaling relationships for dispersion coefficients [36]:

$$\text{Regime 1:} \quad D^E \sim N^{-2}\,\varepsilon^{0},\ N < \varepsilon^{-2/3} \tag{I-12a}$$

$$\text{Regime 2:} \quad D^E \sim N^{-0.5}\,\varepsilon^{1},\ \varepsilon^{-1} > N > \varepsilon^{-2/3} \tag{I-12b}$$

$$\text{Regime 3:} \quad D^E \sim N^{0}\,\varepsilon^{1.5},\ N > \varepsilon^{-1} \tag{I-12c}$$

It is important to note that the modeling of dispersion coefficients in BRF only considers the effects of the orientation DNA molecules. However, there are other factors that contribute to the band broadening process, such as temperature gradients and inhomogeneities in buffer conductivity.

1.2 Separation resolution of DNA gel electrophoresis

A typical electrophoresis experiment involves injecting a small volume of fluorescently labeled DNA into the gel matrix and recording migration of the separated fragments as they travel past a fixed downstream detection point. The sensitivity of the experiment is determined by the ability to distinguish adjacent peaks as they migrate through the detection window. Neighboring fragments are most easily resolved when the difference in their respective mobilities is as large as possible. However, the separated zones also experience diffusion as they travel through the gel resulting in a broadening of the ob-

served peaks that makes closely spaced bands more difficult to resolve. During electrophoresis, this band broadening process occurs at a faster rate than can be accounted for by molecular diffusion alone (here, the term *dispersion* is used to distinguish between electrophoretic band broadening and thermally-driven molecular diffusion in the absence of an electric field).

Following the analytical framework developed in chromatography theory, the ability to distinguish neighboring peaks can be quantified in terms of a parameter called the *separation resolution, R*, defined as the ratio of the distance between peaks ($t_2 - t_1$) to the sum of their half-widths at the base (Figure I-2) [37]. If the peaks are assumed to follow a Gaussian profile, the half width at the base of each peak can be taken as twice its standard deviation σ, in which case resolution can be defined as follows.

$$R = \frac{t_2 - t_1}{2(\sigma_1 + \sigma_2)} \tag{I-13}$$

Using this definition of base half width, a value of R = 1.5 corresponds to two completely separated peaks, while values less than 1.5 indicate some degree of overlap. By convention, a value of $R \geq 0.5$ is often taken as a criterion to indicate that two neighboring peaks are clearly distinguishable [37]. However, for DNA sequencing applications, base-calling algorithms are able to make use of information from four individual lanes so that sequence data can be correctly inferred even at considerably lower values of R.

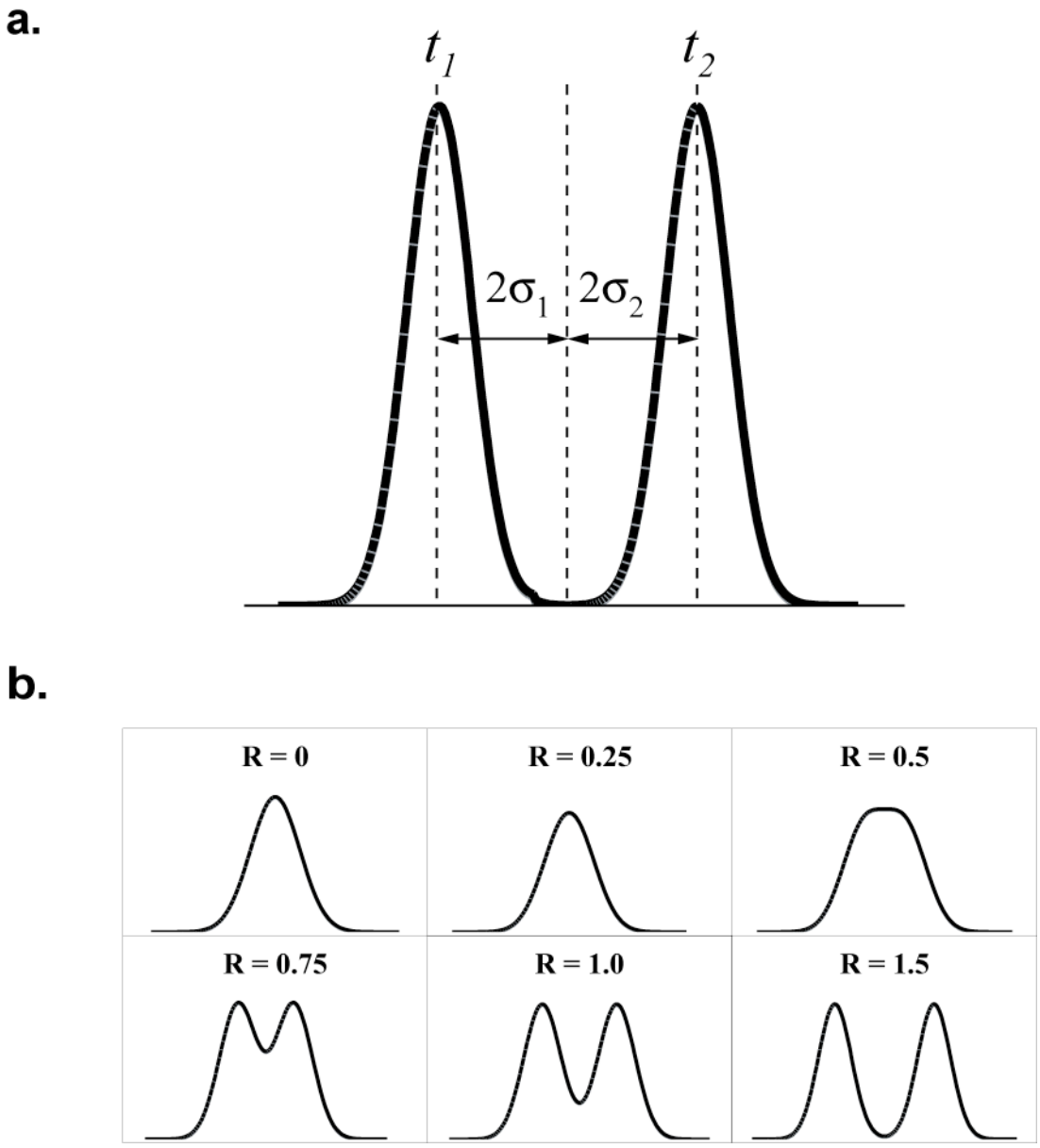

Figure I-2. Separation resolution. (a) Illustration of parameters involved in determining separation resolution I from a time series of intensity measurements in terms of peak spacings and widths. (b) Examples of representative peak spacings associated with different *R* values. Neighboring peaks become increasingly distinguishable with increasing *R* values.

By expressing the quantities in equation (I-13) in terms of mobility and dispersion coefficients, it is possible to obtain an equivalent expression for separation resolution in terms of parameters associated with the physical processes involved in DNA migration through the gel [33, 38].

$$R = \frac{1}{4}\left(\frac{\Delta\mu}{\mu}\right)\frac{L}{\sqrt{2D^{E}(L/\mu E)}} \qquad \text{(I-14)}$$

Here, the term $\Delta\mu/\mu$ is referred to as the *selectivity* (a parameter characterizing relative mobilities between neighboring fragments of different length), μ is the average mobility of the neighboring fragments, and L is the effective separation length (the distance between injection and detection points). D^{E} is the longitudinal dispersion coefficient of the DNA fragments in the gel, where the superscript E indicates the electric field dependence of this parameter. Consequently, models developed to characterize the physics of gel electrophoresis (e.g. biased reptation) can be used to estimate values of the mobility and dispersion coefficients so that separation resolution can, in principle, be directly predicted using equation (I-14).

In practice, however, separation performance is sensitive to a number of factors including chemical composition and pore size distribution of the gel matrix, ionic composition of the running buffer (including denaturant additives, if present), electric field strength, and operating temperature. In addition, experiments to measure diffusion and dispersion can be very tedious and time consuming to perform, especially when electric field dependence is to be investigated.

Consequently, very few comprehensive studies have been undertaken to measure these parameters, and the limited data that are available have been acquired over a relatively narrow window of operating conditions that are generally not consistent among different research groups. These inconsistencies have made it difficult, if not impossible, to reliably estimate separation performance using equation (I-14) with the existing body of physical data alone.

This lack of data has also hindered progress toward developing improved models of DNA migration during gel electrophoresis because the process of assessing their ability to capture experimentally observed behavior is often not straightforward. As an example, consider the variability that exists in measured values of the free solution mobility [13, 27, 38-42] and dispersion coefficients [27, 38, 43, 44] of ssDNA (Tables I-2 and I-3). These discrepancies arise in large part from the variability in experimental conditions employed, where a variety of different instruments, gel compositions, and experimental conditions (temperature, electric field, buffer composition) have been used. These inconsistencies make the process of comparing data obtained by different research groups, establishing trends, and evaluating scaling relationships obtained from theoretical models an extremely challenging undertaking.

Table I-2. Summary of measured free solution mobilities of ssDNA

Reference	Sieving Matrix	Instrument	Temp. (°C)	Electric Field (V/cm)	DNA Sample	Buffer	Free Solution Mobility (cm^2/Vs)	Calculation Method for Free Solution Mobility	Experiment Preconditions
Brahmasandra, Burke *et al.* [38]	Cross-linked polyacrylamide [a]	Slab gel sequencer	55	20	ssDNA (50-500 bases	1.5X TBE/ 7M urea	$2.85x10^{-4}$	Extrapolation to 0%T gel concentration	Gel prerun for 5 hours
Rousseau, Drouin *et al.* [13]	Cross-linked polyacrylamide [b]	Slab gel sequencer	40	18.3	ssDNA (50-500 bases)	0.5x TBE/ 8.0 M urea	$2.9x10^{-4}$ $3.76x10^{-4}$ [f]	Extrapolation to 0%Tgel concentration	Gel prerun at 40°C for 8.4 hours
Rousseau, Drouin *et al.* [42]	Cross-linked polyacrylamide [c]	Slab gel sequencer	55	9.58	ssDNA (17-6557 bases)	0.5x TBE/ 8.0 M urea	$3.8x10^{-4}$	Extrapolation to 0%Tgel concentration	Gel degassed and then prerun at 55°C before use
Pluen, Tinland *et al.* [27]	Cross-linked polyacrylamide [d]	Slab gel sequencer	21	5	ssDNA (410-5386 bases)	0.01 M TBE/ 8.0 M urea	$1.7x10^{-4}$ $3.30x10^{-4}$ [f]	Direct measurement in free solution	None
Heller [40]	Linear pDMA[e]	CE sequencer	25/50	210	ssDNA (50-500 bases)	0.5x TBE/ 4 M urea	$3.58x10^{-4}$ [g] $4.64x10^{-4}$ [h] $4.60x10^{-4}$ [i] $5.0x10^{-4}$ [f]	Both direct experiment in free solution and extrapolation to 0%T gel concentration	Gel degassed and then incubated at 25°C overnight before use
Nkodo, Garnier *et al.* [45]	Free solution	CE sequencer	30	35-250	ssDNA (50-250 bases)	1x TAPS/ pH 8.5	$1.83x10^{-4}$ $2.9x10^{-4}$ [f]	Slope of the fit line for migration velocity vs. field strength	None
Fabrizio, Nadim *et al.* [39]	Free solution	Microfluidic chip	22	588	ssDNA (9-21 bases)	10x TBE/ pH 8.3	$1.04x10^{-4}$ $1.97x10^{-4}$ [f]	Direct measurement in free solution	None

a) Chemically polymerized, 6-12 %T and 5 %C
b) Chemically polymerized, 3.25-12 %T and 5 %C
c) Chemically polymerized, 2.25-4.5 %T and 5 %C
d) Chemically polymerized, 4-8 %T and 3 %C
e) Chemically polymerized, 1-10%
f) Corrected to 55°C by scaling with ratio of viscosity of water at the two temperatures ($\mu_2 = \mu_1(\eta_1/\eta_2)$) [46]
g) ssDNA at 25°C free solution
h) ssDNA at 50°C free solution
i) Extrapolation to 0%T gel concentration for 75 bases at 50°C

Table I-3. Summary of measured dispersion coefficients of ssDNA

Reference	Sieving Matrix	Instrument	Temp. (°C)	Electric Field (V/cm)	DNA Sample	Buffer	Measured Dispersion Coefficient (cm^2/s)	Experiment Preconditions
Brahmasandr, Burke *et al* [38]	Cross-linked polyacrylamide[a]	Slab gel sequencer	55	20-60	ssDNA (50-500 bases)	1.5X TBE/ 7M urea	$1.74x10^{-8}$~$1.03x10^{-7}$ [e] $7.6x10^{-9}$~$2.8x10^{-8}$ [f] $2.28x10^{-9}$~$1.19x10^{-8}$ [g]	Gel prerun for 5 hours
Ugaz, Burke *et al.* [44]	Cross-linked polyacrylamide[b]	Microfluidic chip	50	20	ssDNA (50-500 bases)	2.0X TBE	$2.5x10^{-7}$~$4x10^{-8}$ [h]	None
Pluen, Tinland *et al.* [27]	Cross-linked polyacrylamide[c]	Slab gel sequencer	21	5-100	ssDNA (410-5386 bases)	0.01 M TBE/ 8.0 M urea	$3.1x10^{-8}$~$5.5x10^{-7}$ [i]	None
Schmalzing, Adourian *et al.* *[43]*	Linear polyacrylamide[d]	Microfluidic chip	45	200	ssDNA (40-520 bases)	1X TBE/ 3.5 M urea/ 30% (v/v) formamide/ pH 8.3	$2.43x10^{-7}$~$4.3x10^{-8}$ [j]	Pre-electrophoresis for 10 min. at 200 V/cm and 45 °C

a) Chemically polymerized, 6-12 %T and 5 %C
b) ReproGel High Resolution, UV-polymerized, 8 %T
c) Chemically polymerized, 4-8 %T and 3 %C
d) Chemically polymerized, 2-6%
e) 400 bases at 6 %T
f) 400 bases at 9 %T
g) 400 bases at 12 %T
h) 50-500 bases at 8 %T
i) 410 bases at 4 %T
j) 40-520 bases at 4 %T

Although there is currently a lack of systematic experimental data for mobility, diffusion, and dispersion under a consistent range of operating conditions, these data are essential in order to establish the validity of current and future theoretical models for the physics of gel electrophoresis. In addition, the need for improved characterization of sieving gels is becoming increasingly critical as the development of advanced genomic analysis technology continues to place greater demands on separation performance.

1.3 Current technology

1.3.1 Slab gel electrophoresis

Slab gel electrophoresis has been routinely employed in many DNA analysis assays that require size-based separation of DNA mixtures, such as DNA sequencing, detection of restriction fragment length polymorphisms (RFLP), and Southern blotting. Crosslinked polyacrylamide and agarose gels are generally used as the sieving matrices in these systems [47]. A slab gel is cast by loading liquid gel solutions into a vertical (or horizontal) mold, and a comb is inserted to produce sample wells with its teeth (Figure I-3). The whole set is immersed in a buffer solution after polymerization of the gel and removal of the comb. To run slab gel electrophoresis, a fluorescently labeled DNA sample is loaded into sample wells and is driven through the sieving matrix by an external electric field. The fluorescence signal of labeled DNA fragments is recorded and then analyzed on a computer.

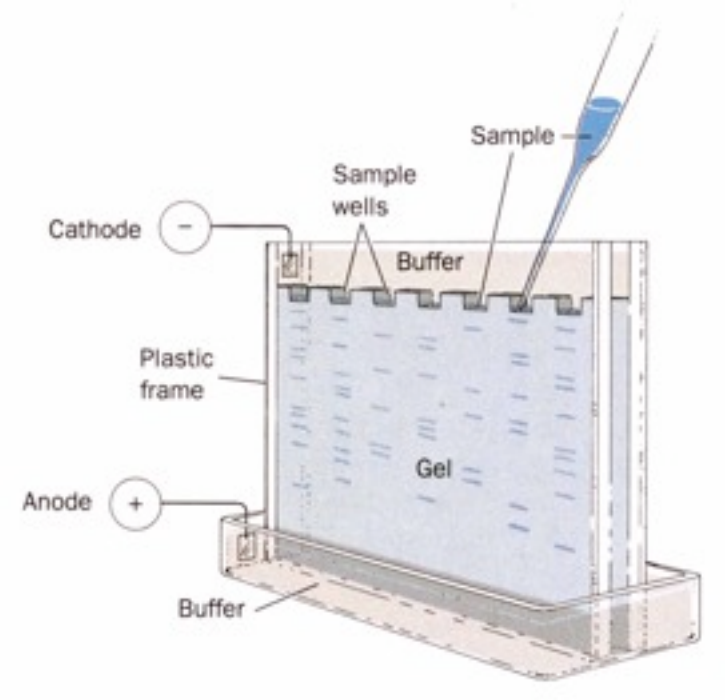

Figure I-3. A schematic presentation of slab gel electrophoresis. The DNA mixture is manually loaded into the sample wells and is then driven through the gel from the cathode to the anode by an external electric field. Picture adapted from http://www.science.fau.edu/chemistry/Mari/.

Slab gel electrophoresis has several advantages. Firstly, it provides high-resolving power for separation of DNA fragments. Crosslinked polyacrylamide provides very high resolving power, because the pore size can be easily adjusted by control on monomer/crosslinker concentrations, and it is UV transparent, which is very important for DNA detection. Secondly, the separated DNA samples can be used for further study. Specific DNA bands could be cut out from the gel and purified for further manipulation. Thirdly, a large amount of DNA sample can be process in one run. A slab gel has many sample wells (e.g., 40 lanes for the ALFExpress II DNA analysis system), and many

samples can run in parallel, allowing side-by-side comparisons of electrophoresis results. However, the major disadvantage of this technology is the need to cast a new gel for each new experiment. This takes a lot of time and makes it very difficult to automate. In addition, trained personnel are needed to prepare slab gels and to operate separation runs due to the toxicity of acrylamide monomers and impurities in agarose gels. Joule heating due to electric current moving through the gel also posts a significant limitation on the performance of slab gel electrophoresis because of the problem of thermal convection in the gel.

1.3.2 Capillary electrophoresis

Capillary gel electrophoresis (Figure I-4) was invented in the 1970s and advanced in the 80s and 90s [48-52]. It served as the workhorse of the Human Genome Project in the quest to decode the whole human genome. Linear polyacrylamide is usually employed as the sieving matrix in capillary electrophoresis [47]. In general, a commercially available fused silica/quartz capillary has a 50-100 μm inner diameter and a wall thickness of about 150 μm. A thin layer (10 μm) of polyimide is coated on the exterior of the capillary to make it flexible and easy to handle. To perform a separation run, the gel liquid solutions are loaded into the capillary that is then connected to buffer reservoirs, and a fluorescently labeled DNA sample is loaded into the capillary by either electrokinetic or hydrodynamic injection. An external electric field is applied to drive DNA samples through the sieving gel. The signal of fluorescently labeled DNA fragments is recorded and later analyzed on a computer.

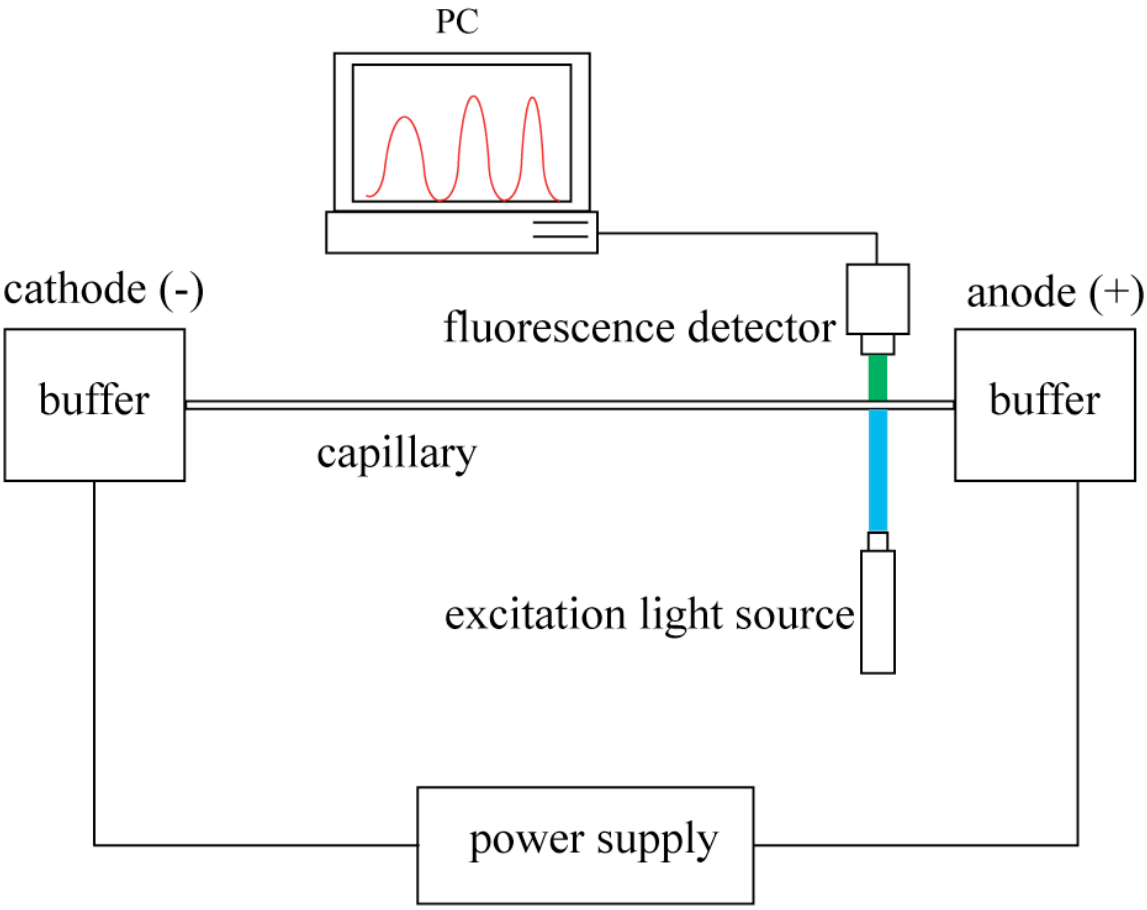

Figure I-4. A schematic presentation of capillary gel electrophoresis. The DNA sample is driven through the capillary from cathode to anode. The fluorescently labeled DNA fragments are excited by a laser beam at the detector, and the signal is collected to a personal computer for further analysis.

Capillary gel electrophoresis has several advantages. Firstly, a high throughput DNA gel electrophoresis can be achieved. Joule heat during gel electrophoresis can be efficiently dissipated by the high ratio of the surface area to volume in a capillary. A high electric field can be used to perform the separation in a much shorter run time (generally in about 20 minutes compared to 2-20 hours required by slab gel electrophoresis) [47].

Secondly, complete automation of the capillary gel electrophoresis instrument can be accomplished when reloadable sieving matrices are used. The DNA sample can be automatically introduced into the capillary by hydrodynamic or electrokinetic injection, and the replacement of the used sieving matrix can also be automated when the separation run is completed. Thirdly, the small volume of a capillary results in reduced consumption of samples and reagents. This makes capillary gel electrophoresis very suitable for analytical purposes, because the required sample volume is much smaller (nL) than that of slab gel electrophoresis (μL). However, a fully automated capillary gel electrophoresis instrument is very expensive, e.g., $325,000 USD for a MegaBACE 4000 system, and it is too large to be portable.

1.3.3 Microchip electrophoresis

Although current technology of capillary gel electrophoresis can provide fully automated, high-throughput DNA analysis, great effort has been directed to developing *microfabricated gel electrophoresis devices*, which are cheap, portable, high-throughput, and ready to be integrated with other analytical components to make completely self-contained DNA-analysis devices (Figure I-5). Such microfabricated gel electrophoresis devices require high resolving power in very short separation distances and have a size small enough to permit large-scale production using current photolithographic fabrication technology employed in microelectronics industry. Such size reduction of microfabricated electrophoresis devices can be accomplished by using high performance sieving matrices in shorter separation distances or by developing new designs to allow longer

separation channels on a microfabricated gel electrophoresis device. Different polymers, such as agarose, pluronic gels, linear polyacrylamide, and crosslinked polyacrylamide, have been tested on microfabricated electrophoresis devices as sieving matrices [44]. Among these polymers, UV-polymerized crosslinked polyacrylamide proves to be very promising, because it has high resolving power in a short separation distance, requires significantly less polymerization time, and gives precise control on the location and shape of the gel interface in the separation channel (Figure 1 in [53]).

To perform a separation run, DNA samples are electrokinetically injected into the separation channel by applying a voltage between the reservoirs on the shorter injection channels intersecting the separation channel. After injection, the voltage is switched, so that the electric field is applied between the buffer reservoirs across the separation channel.

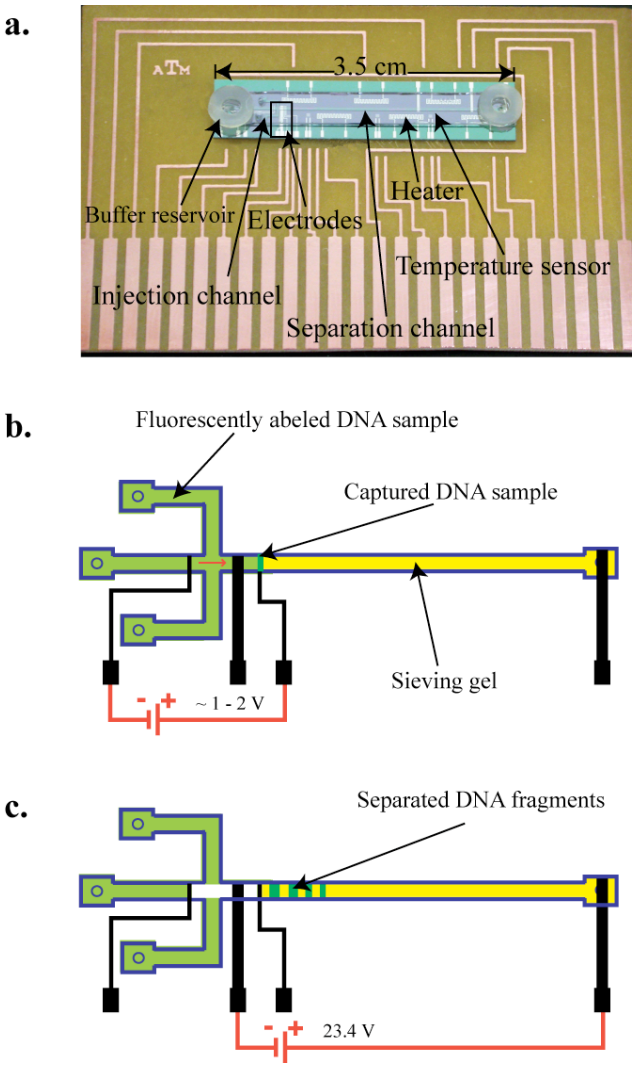

Figure I-5. (a) A photo of an assembled microfabricated gel electrophoresis device. This device has on-chip electrodes, heaters, and temperature sensors. The sieving gel is polymerized in the separation channel and DNA samples are loaded into the injection channel. Note that DNA migrates from left to right in this photo. (b) DNA compaction. A low voltage is applied between injection electrodes to concentrate the loaded DNA sample and define an injection plug. (c) DNA separation. After compaction, a voltage is applied between the separation electrodes to drive the DNA sample plug into the sieving gel for separation (E = 15 V/cm).

There are several channel designs used for sample injection: cross (T shaped), double-, or multi-T shaped [1]. Microfabricated gel electrophoresis devices have several advantages over convention gel electrophoresis technology. Firstly, the manufacturing costs for these devices are much lower when compared to that of conventional gel electrophoresis instruments. Using the photolithographic technology routinely employed in the microelectronics industry, the price of each device can be as low as $1 USD if produced in mass. Secondly, the microfabricated gel electrophoresis devices are suitable for deployment in remote fields for medical and biosensing applications. The microfabricated gel electrophoresis devices are very compact in size and are not dependent on pre-existing laboratory infrastructure. They have much lower power requirements than conventional electrophoresis instruments and could be integrated with other analytical components to make self-contained DNA analysis system. This feature makes it possible to eventually develop a hand-held DNA analysis device for use in doctors' clinics or battlefields far away from laboratories. Thirdly, these microfabricated gel electrophoresis devices can perform high-throughput DNA analysis, because the separation process is much faster (usually less than 20 minutes) than conventional electrophoresis technology. However, achieving high-resolution DNA separations in a few centimeters or less still posts a great challenge to the development of these devices, and the key is a sieving matrix that provides high-resolving power in an ultra-short distance.

1.4 Whole-gel scanning detection

Single-point detection is used in most DNA gel electrophoresis experiments. Here, a DNA sample containing fragments different in size is injected into one end of the separation channel filled with a pre-cast sieving matrix, driven through the gel by an electric field, and the separated fragments are detected at a point near the other end of the channel. The collected signal is recorded along with the corresponding time to generate an electropherogram for further analysis. However, in this detection scheme, the user cannot observe the evolution of the separation process during the run. All information on the separation process is obtained after the run is completed. This hinders more understanding of the physics of DNA migration in the sieving matrix during the separation process.

Whole-column imaging detection (WCID) was first proposed for capillary isoelectric focusing (CIEF) of proteins to solve problems of band distortion and loss in resolution [54] and was later applied to capillary electrophoresis (CE). There are two schemes of WCID used in CE (Figure I-6). The *scanning capillary method* involves moving either the whole separation capillary past a fixed detector [55, 56] or the excitation light source along the entire distance of a fixed capillary [57]. The scanning is performed by a mechanical movement, which requires some time (e.g. 12.5 s in [56] and 120 s in [57]) to complete. As a result, it is more difficult to capture details of a fast separation run. For the *expanded light-beam method*, the excitation light beam is projected all over the separation capillary through a combination of optical lens and filters [58-60]. There is no

mechanical movement required, but the length of the separation capillary is limited because of the difficulty for light projection over a very long distance.

WCID can offer improved performance over single-point detection used in conventional gel electrophoresis systems. First, the analysis time is much shorter because DNA fragments do not need to migrate along the entire length of the separation channel, so the run can be terminated as soon as the bands are sufficiently resolved. Second, due to a shorter separation length, the band broadening often encountered in conventional gel electrophoresis systems can be significantly reduced. This results in an increased separation resolution. Third, with careful design and optimization it is possible to observe DNA separations in real time and potentially use dispersion data (band broadening) to perform fragment sizing. More information on WCID and its applications can be found in a recent review by Wu *et al.* [61], and the references cited therein.

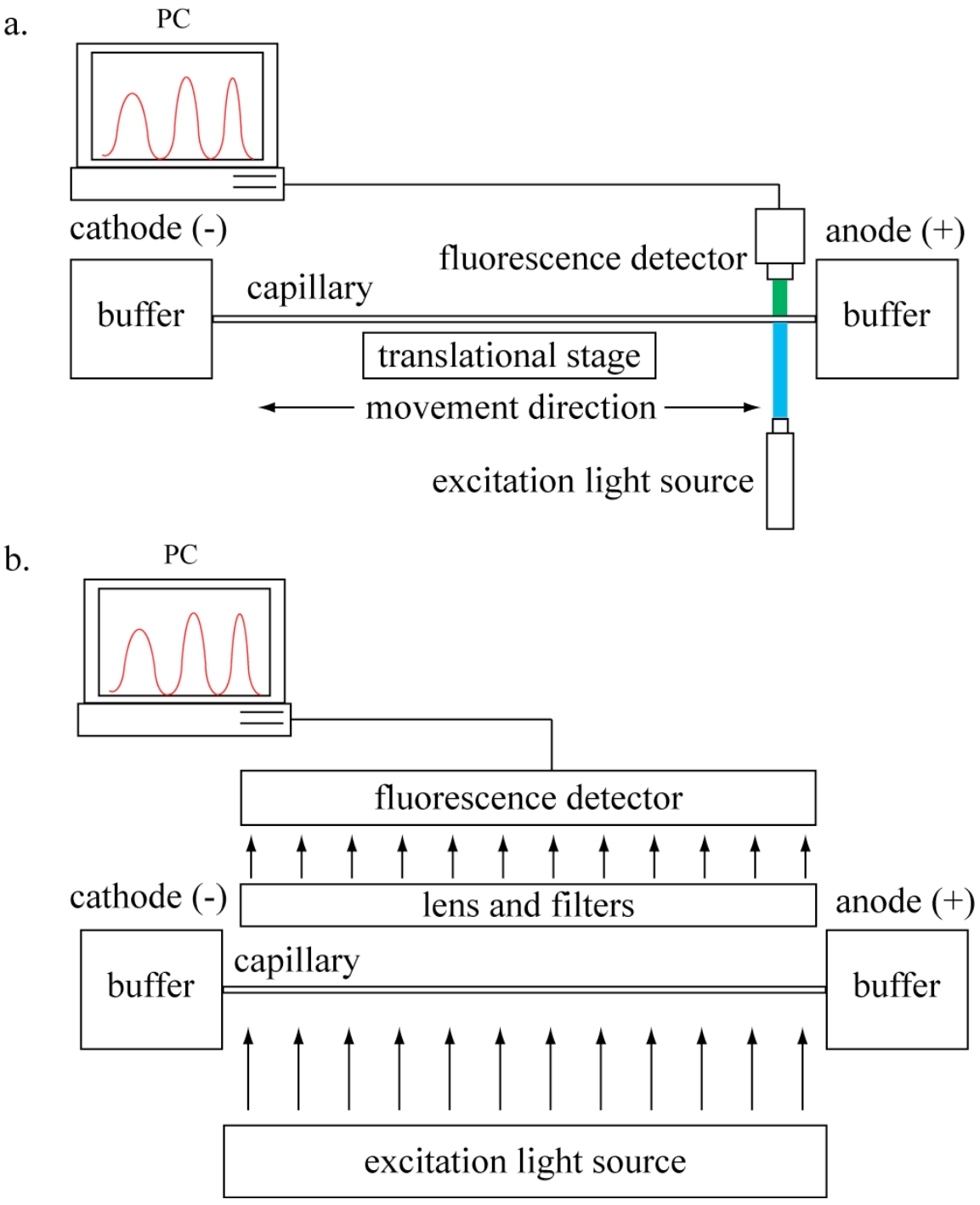

Figure I-6. A schematic presentation of WCID methods. (a) The scanning capillary method. (b) The expanded light-beam method.

1.5 Motivation and objectives

Gel electrophoresis is a critical analysis step in many genomic assays, and there is a strong demand for fast, low-cost, and high-throughout DNA gel electrophoresis technology. To design an optimized electrophoresis system, it is desirable to quantitatively determine the separation resolution directly from measurements of fundamental properties associated with the gel matrix instead of using the traditional trial and error process. Unfortunately, this predictive capability is currently lacking, due in large part to the need for a more detailed understanding of the fundamental parameters governing separation performance (mobility, diffusion, and dispersion), and acquisition of all the data needed for detailed gel characterization using conventional DNA sequencing instruments is very tedious and time-consuming.

In this study, we seek to address these issues by first characterizing ssDNA migrating in photopolymerized crosslinked polyacrylamide gels on a conventional slab gel DNA sequencer to establish the predicting capability of separation resolution. Secondly, we design and build an automated rapid whole-gel scanning detection system for microchip electrophoresis by integrating the scanning capillary method with our microfabricated gel electrophoresis device and perform fast, systematic measurements of the fundamental migration parameters on this system with a high level of spatial and temporal resolution. The ability to acquire both spatial and temporal data simultaneously provides a more detailed picture of the separation process that can potentially be used to improve separation performance over ultra-short distances. The specific objectives are as follows:

- **Establish the predicting capability for separation resolution on the benchtop slab gel sequencer.** The fundamental parameters (mobility, diffusion, and dispersion coefficient) of DNA migration in photopolymerized polyacrylamide gels are consistently measured under different gel and electric field conditions. These data are analyzed and compared with theoretical predictions for in-depth analysis of DNA migration physics (Chapter II).
- **Design and build an automated whole-gel scanning detection system for microchip gel electrophoresis.** This system will be tested by collecting mobility, diffusion, and dispersion data of DNA gel electrophoresis using both whole-gel scanning and single-point detection. The data collected with the two detection modes will be compared for system validation (Chapter III).
- **Measure dsDNA migration parameters with the whole-gel scanning detection system.** The dsDNA migration data will be measured under different dye and buffer conditions. These data will be compared to investigate the effects of these conditions on DNA migration behaviors (Chapter IV).
- **Test the Mercier-Slater dispersion model**. The dispersion coefficient data of ssDNA and dsDNA will be used to test the goodness of fitting (Chapter V).
- **Apply collected mobility, diffusion, and dispersion data for DNA sizing.** The dsDNA migration data will be used to test different mobility and dispersion models and investigate DNA sizing accuracy with dispersion data (Chapter VI).

CHAPTER II

MEASUREMENTS IN BENCHTOP SLAB GEL INSTRUMENT*

This chapter details the experiments for measurements of mobility, diffusion and dispersion coefficients of ssDNA migrating in photopolymerized polyacrylamide gels on a conventional slab gel DNA sequencer. Using the obtained data, we have successfully established a new predicting capability for separation resolution of DNA gel electrophoresis process.

2.1 Experimental setup

2.1.1 Reagents

All DNA separation runs were performed using Long Ranger® polyacrylamide sequencing gels (Cambrex Bio Science; Rockland, ME). Stock solutions at the desired concentrations were prepared by diluting the as-supplied 50 %T gel solution with an appropriate amount of deionized water. Crosslinking was performed using the photoinitiator supplied with ReproGel® sequencing gels (Amersham Biosciences Corp., Piscataway, NJ). Cy-5 labeled ssDNA sizing standards (MapMarker 400 and MapMarker 1000; BioVentures Inc.; Murfreesboro, TN) were used in all electrophoresis experiments. Formamide (99%, GC grade) was obtained from Sigma-Aldrich Corp (St. Louis, MO).

---

* Part of the data reported in this chapter is reprinted with permission from: Separation performance of single-stranded DNA electrophoresis in photopolymerized cross-linked polyacrylamide gels by Lo, R.C., Ugaz, V. M., *Electrophoresis* (2006) **27**, 373-386.

Tris-Borate-EDTA (TBE) running buffer was obtained as a 10x stock solution (Extended Range TBE Buffer, Catalog #161-0741; Bio-Rad Laboratories, Hercules, CA) and diluted to the desired final concentration with deionized water. Urea (electrophoresis purity), ammonium persulfate (APS), and TEMED were purchased from Bio-Rad Laboratories (Hercules, CA) for use in preparation of chemically crosslinked gels. All reagents were used as received.

2.1.2 Gel casting

Electrophoresis experiments were performed using an ALF Express II automated DNA sequencer (Amersham Biosciences Corp.; Piscataway, NJ), a 4 lane, single-color, slab gel-based electrophoresis instrument (Figure II-1). This system employs gel cassettes consisting of two glass plates: a lower thermoplate whose temperature is regulated with a circulating water bath, and a thinner upper cover plate. Two different gel cassette sizes were used in order to vary the separation length depending on conditions associated with a particular experiment. Gels are cast in the gap between the plates, which is defined by a pair of optically transparent 300 μm-thick spacers. During electrophoresis, the migrating Cy5 labeled ssDNA fragments are excited by a helium-neon laser (633 nm wavelength), and the corresponding fluorescence signal is recorded by a 40-lane array of photodetectors.

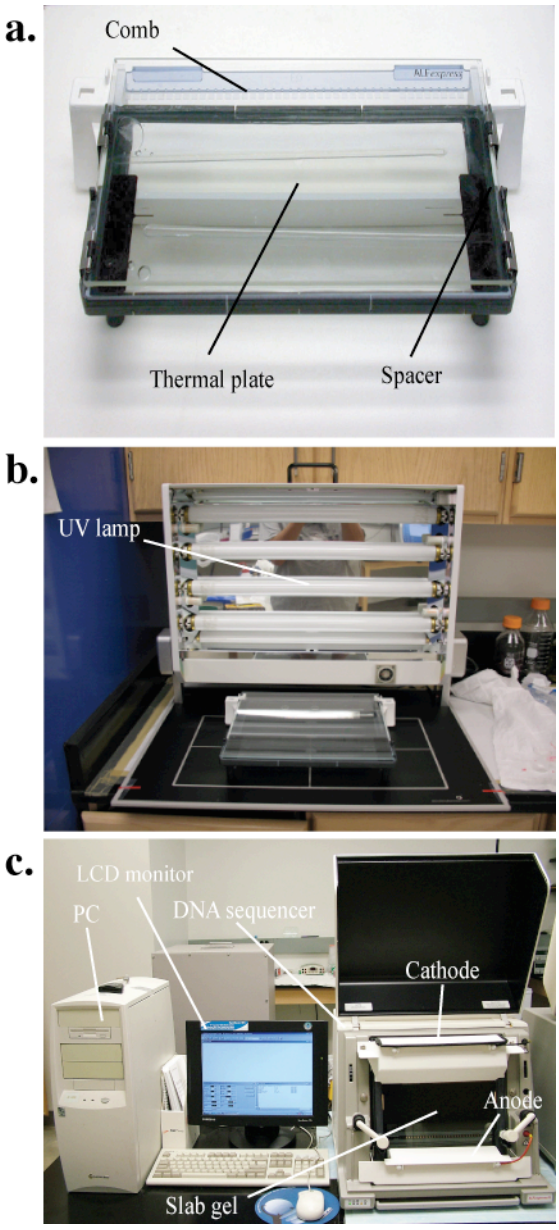

Figure II-1. Slab gel DNA sequencing system setup. (a) Gel cassette. (b) ReproSet UV illuminator. (c) ALFExpress II DNA sequencer.

Photopolymerized gels were prepared by adding two parts of the appropriate dilution of Long Ranger gel solution (prepared using deionized water) to one part of the ReproGel photoinitiator (Solution B) and gently mixing to obtain final gel concentrations of 6, 9, and 12 %T, respectively. The gel/photoinitiator mixture was loaded into the assembled gel cassette, and a standard 40-well comb was inserted. The gel cassette was then exposed to UV illumination (approximate flux ~ 5 W/cm^2) for 12 minutes using the ReproSet casting system supplied with the ALF Express instrument. Chemically polymerized gels were prepared by adding APS (10 % w/v solution; 6 µL/mL) and TEMED (0.6 µL/mL) to an appropriate mixture of urea, deionized water, and Long Ranger gel stock solution in order to obtain final desired urea (7 M) and gel concentrations (6 –12 %T). This mixture was loaded into the gel cassette and allowed to polymerize for one hour.

2.1.3 DNA sample preparation

A 7 µL sample volume consisting of 1 µL MapMarker standard ladder, 2 µL of loading dye (supplied with the MapMarker ladder), and 4 µL of formamide was loaded into each well of the gel cassette. Samples were prepared by making a master mix of the total volume needed to load all lanes used in a given run. Prior to loading, the master mix was pre-denatured by incubation in a dry bath at 92°C for 3 minutes, then snap-cooled on ice.

2.1.4 Electrophoresis procedure

After polymerization, the gel cassette was mounted in the sequencer and connected to the circulating water bath. Upper and lower buffer reservoirs were attached and filled with 0.5x TBE running buffer. The gel cassette was then heated to the 55 °C run temperature, and the comb was removed. All wells were flushed with running buffer prior to sample loading in order to eliminate contamination from particle debris and unpolymerized monomer residue. All electrophoresis runs were performed in constant voltage mode in order to maintain a uniform electric field strength. A further advantage sof the photopolymerized gel formulation is that it was not necessary to perform a lengthy prerun prior to loading the sample in order to maintain constant electric current conditions during the course of the separation experiments. We elaborate on this point in Section 2.3.1.

2.2 Measurements and analysis

The experimental procedures employed here follow the general protocol outlined by Brahmasandra *et al.* [38] in their studies of DNA migration in chemically polymerized crosslinked polyacrylamide gels.

2.2.1 Data analysis

After the conclusion of each electrophoresis experiment, the corresponding fluorescence intensity versus run time data were converted from the native ALF Express II file format (*.flx) to a text file using ImageMagick software (www.imagemagick.org). Once the

data was in a text file format, we used our own MATLAB (The MathWorks, Inc.) codes to calculate separation resolution, mobility, and coefficients of diffusion and dispersion using an Apple PowerMac Dual G4 workstation.

2.2.2 Mobility

Mobility experiments were performed using the MapMarker 1000 ladder (23 fragments ranging in size from 50 to 1000 bases) at three different gel concentrations (6, 9, and 12 %T). The migration time (t) of each eluted peak was recorded and used to calculate the migration velocity ($V = L/t$, where L is the separation length). The mobility of each DNA fragment was then computed by dividing the migration velocity by the electric field strength ($\mu = V/E$). Initially, runs were performed at three different separation lengths (3, 6, and 8.5 cm) in order to check for consistency. Since the difference in calculated mobilities was found to be within 10% in all cases, we selected a separation length of 8.5 cm (the standard short gel plate size) for all experiments. Similarly, less than 10% variation in the measured mobility values was observed for electric field strengths ranging from 15 – 40 V/cm (see discussion in Section 2.3.2). All reported mobility values represent the average of two independent separation runs.

2.2.3 Diffusion

Diffusion coefficients (D) were calculated by measuring the broadening of peaks associated with each separated band over time due to thermal motion alone. Samples were loaded and run for a sufficient time to allow all DNA fragments to migrate into the gel

(typically 30 – 40 minutes). The electric field was then switched off while the gel temperature was maintained at 55°C for a set time interval (the *delay time*). The electric field was then re-activated and the run was resumed until all separated peaks migrated past the detector. A moderate electric field strength (E = 30 V/cm) was used in order to provide consistent peak resolution while minimizing additional dispersion effects. Each peak was then fit to a Gaussian profile in order to determine the standard deviation σ. By performing a series of runs using different delay times (1 – 9 hours, depending on gel concentration), the following relationship could be used to compute the diffusion coefficient corresponding to each DNA fragment by performing a linear fit to the σ_{delay}^2 versus delay time data.

$$(\sigma^2 - \sigma_{elec}^2) = \sigma_{delay}^2 = 2Dt_{delay} \qquad \text{(II-1)}$$

Here, σ^2 is the overall peak variance, σ_{elec}^2 is the peak variance due to electrophoresis, σ_{delay}^2 is the peak variance due to delay, and t_{delay} is the delay time. Prior to performing the linear regression in equation (3), peak variances were converted from units of time (s) to units of length (cm) through multiplication of each peak variance by its corresponding migration velocity (cm/s) in the gel. The same conversion was also conducted in the computation of dispersion coefficients.

2.2.4 Dispersion

Dispersion coefficients (D^E) were calculated in a similar manner as the diffusion coefficients, except that the separation length was varied instead of the delay time. Experi-

ments were performed using separation lengths ranging from 3 – 20.5 cm, and the resulting peak variances were used to compute the dispersion coefficient of each DNA fragment using the following expression.

$$\sigma^2 = \sigma^2_{static} + 2D^E(L/V) \qquad \text{(II-2)}$$

where σ^2 is the overall peak variance, σ^2_{static} is the time-independent variance, L is the separation length, and V is the migration velocity. This expression is analogous to equation (II-1), except that the dispersion coefficient is determined from the slope of a linear fit to the overall variance versus migration time (L/V) data.

Finally, we note that all diffusion and dispersion experiments were performed using the MapMarker 400 ladder (20 fragments ranging in size from 70 to 400 bases). This sample was chosen because the MapMarker 1000 ladder required prohibitively long run times in order to allow all fragments to migrate through the gel, especially at high gel concentrations and low electric field strengths. Under these conditions (run times exceeding 20 hours) the fluorescence signals from the migrating fragments decayed to a level approaching that of the background noise, making it difficult to accurately fit the corresponding peaks and obtain consistent results. These problems were avoided by using the MapMarker 400 ladder.

2.3 Results and discussion

2.3.1 Comparison with chemically polymerized gels

An important issue when developing any experimental protocol to obtain reproducible quantitative measurements of mobility, diffusion, and dispersion involves ensuring that the electric current remains constant throughout the entire electrophoresis run. In chemically polymerized gels, this is accomplished by performing a *prerun* whereby an electric field is applied across the gel for a prescribed period of time prior to sample loading. Typically, preruns of several hours are necessary in order to completely expel charged residues associated with the chemical polymerization process and attain a stable current reading [13, 35, 42, 62, 63]. We performed a series of experiments under a representative set of operating conditions (E = 30 V/cm, T = 55 °C, 6 %T gel) in order to determine the optimal prerun duration for the photopolymerized gels employed here. Surprisingly, we found that the electric current remained stable (< 5% fluctuation) during the entire 5 hour prerun period, in contrast to the behavior observed in a comparable chemically polymerized gel (1.5x TBE concentration in the as-cast gel) where the current continually decreased and did not appear to stabilize during the same time interval. This behavior may be attributable to a combination of details associated with photoinitiation chemistry and buffer formulation. In any case, the ability to acquire and maintain a constant current without performing a lengthy prerun is a distinct advantage of the photopolymerized gel formulations employed here, especially for quantitative studies of DNA migration physics.

2.3.2 Mobility

We performed a series of experiments to measure mobility of ssDNA fragments at gel concentrations of 6, 9, and 12 %T. These data were then averaged over all electric field strengths and used to estimate pore sizes associated with each gel concentration using several different models, as well as for comparison with results of previous work reported in literature. We observed less than 10% variation in the measured mobility values over electric field strengths ranging from 15 – 40 V/cm (Figure II-2), in agreement with the observations of Brahmasandra *et. Al*. [38] but in contrast with other observations of an increase in mobility with electric field in single-stranded DNA electrophoresis [27]. Our results are consistent with the observation of a N^{-1} mobility scaling at the largest fragment sizes, with no signs of saturation that would be expected at fragment sizes approaching the threshold to begin experiencing orientation effects (see discussions for the reptation regime). Differences between our data and other studies may be due to the significant differences in gel formulations and running conditions employed.

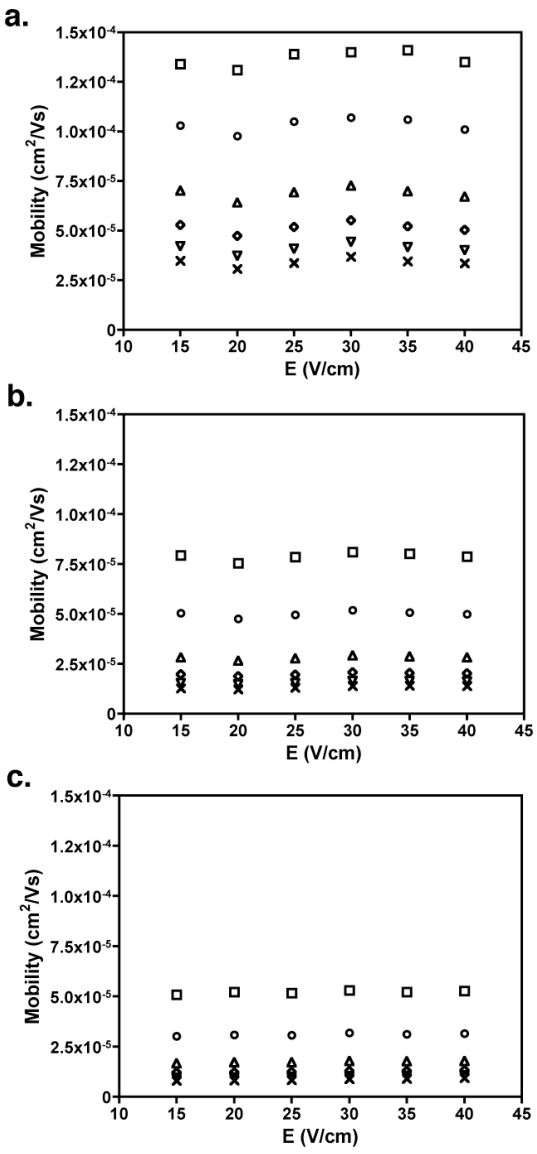

Figure II-2. Variation of electrophoretic mobility with electric field for (a) 6, (b) 9, and (c) 12 %T gel concentrations. Data are shown for 100 [□], 200 [○], 400[△], 600 [◇], 800 [▽], and 1000 [×] base fragment sizes. Run conditions: $T = 55°C$, and $L = 8.5$ cm.

2.3.2.1 Ogston sieving regime

The observed variation of mobility with fragment size can be broadly classified into two distinct regimes (Figure II-3a). For fragments smaller than the gel pore size ($R_g < a$, where R_g is the radius of gyration of a DNA fragment's equilibrium coil configuration and a is the mean gel pore size), the ssDNA molecules experience minimal perturbation to their equilibrium coil configurations as they travel through the matrix. This behavior is often modeled in terms of a sieving mechanism involving the migration of spherical particles through a network of rigid cylindrical fibers [7, 8]. In this framework (the *Ogston model*), an exponential dependence of mobility on fragment size and gel concentration is predicted. According to the Ogston model, a plot of $\log(\mu)$ versus gel concentration (i.e., a *Ferguson plot* [64]) is predicted to yield a straight line whose intercept with the ordinate (zero gel concentration) is equal to the log of the free solution mobility (μ_0). Using our mobility data for small DNA fragments (Figure II-3b), the series of linear fits in the corresponding Ferguson plot converge to an average value of $\mu_0 = 3.5 \pm 0.2 \times 10^{-4}$ cm^2/Vs. This result is in good agreement with literature values obtained under similar conditions when corrected to $T = 55$ °C by scaling with the ratio of water viscosity at the two temperatures [65] (Rousseau *et al.*: $\mu_0 = 3.8 \times 10^{-4}$ cm^2/Vs [13, 42], Pluen *et al.*: $\mu_0 = 3.3 \times 10^{-4}$ cm^2/Vs [27], and Brahmasandra *et al.*: $\mu_0 = 2.8 \times 10^{-4}$ cm^2/Vs [38]).

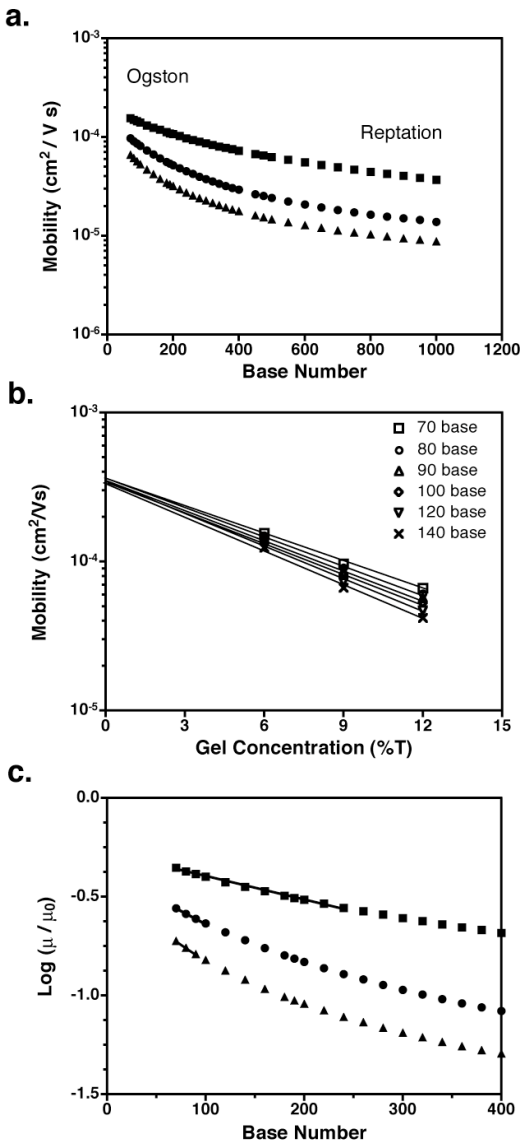

Figure II-3. (a) Variation of electrophoretic mobility with fragment size in 6 [■], 9 [●], and 12 [▲] %T photopolymerized gels. (b) Plot of mobility versus gel concentration (Ferguson plot) for fragment sizes in the Ogston regime. The average value of the y-intercept associated with linear fits to the data in this range yields the free solution mobility. (c) Plot of log (μ/μ_0) versus base number (Ogston plot) showing the range over which a linear relationship is observed for 6 [■], 9 [●], and 12 [▲] %T gels. This range corresponds to the Ogston migration regime, which was taken as the region in which $r^2 > 0.996$.

The exponential dependence of mobility on gel concentration associated with the Ogston sieving regime can be demonstrated with an *Ogston plot* construction [38]. That is, a plot of $\log(\mu/\mu_0)$ at a given gel concentration should scale linearly with DNA molecular size (expressed in terms of the fragment length M). As shown in Figure II-3c, this relationship holds for fragment lengths up to approximately 240 bases in the 6 %T gel, 100 bases in the 9 %T gel, and 90 bases in the 12 %T gels.

2.3.2.2 Reptation regime

When the DNA fragments are larger than the mean pore size of the gel ($R_g > a$), their migration can be described in terms of a reptation mechanism. In this picture, the migrating fragments adopt an extended configuration that deviates significantly from a random equilibrium coil in order to traverse the gel pore network in a head first or snake-like manner. The biased reptation with fluctuations (BRF) model provides refinements to standard reptation theory in order to account for electric field effects (biasing) on the migrating fragments. In general, BRF theories predict that electrophoretic mobility scales as [24, 38]

$$\mu = \mu_0 \left(\frac{1}{3N} + f(\varepsilon) \right) \tag{II-3}$$

where the term $f(\varepsilon)$ incorporates a dependence on the applied electric field strength. Thus, the $1/N$ term dominates for an intermediate range of fragment sizes (where N is proportional to the fragment length M by the relationship $N = M/M_a$), above which the mobility saturates and begins to exhibit an electric field dependence.

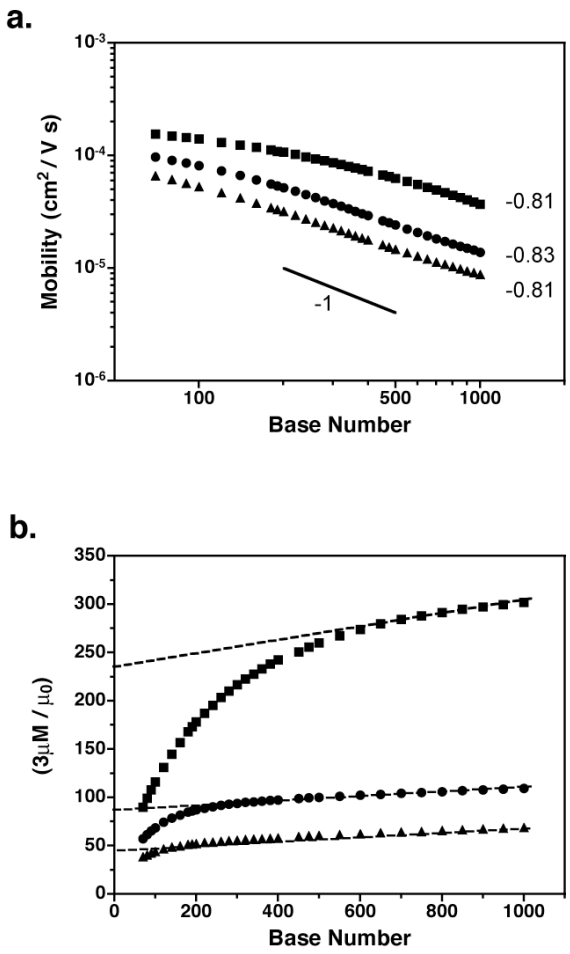

Figure II-4. (a) Log-log plot of mobility versus base number for 6 [■], 9 [●], and 12 [▲] %T gels. Slopes of linear fits to the data in the reptation regime are indicated on the plot. (b) Reptation plot construction in which the y-intercept of a linear fit to data in the reptation regime can be used to estimate the mean gel pore size in terms of an equivalent DNA fragment length (in units of bases) whose coil size (M_a) is the same as that of a single pore. The estimated M_a values are 235 bases for 6 %T [■], 80 bases for 9 %T [●], and 47 bases for 12 %T [▲] gels, respectively.

As discussed in Section 2.3.2, we observed minimal variation in the measured mobility values over the range of electric field strengths studied here. Consequently, the contribution of the *f(ε)* term can be ignored yielding a scaling of mobility with inverse fragment size ($\mu \sim M^{-1}$). As shown in Figure II-4a, we observe mobility scalings ranging from $M^{-0.81}$ to $M^{-0.83}$, in reasonable agreement with predictions of the reptation model.

2.3.2.3 Estimating the gel pore size

For single-stranded DNA, the Kratky-Porod equation [9] for semi-flexible polymers can be applied to compute the radius of gyration corresponding to a given fragment length. Using appropriate parameters (persistence length = 3 nm, contour length = 0.43 nm/base [10-12]), 240, 100, and 90 base fragments (Figure II-3c) are predicted to have R_g values of 9.73, 5.93, and 5.57 nm, respectively. Since the Ogston-reptation transition is representative of the limiting fragment size that can migrate through the gel in an unperturbed configuration, the value of R_g associated with this transition can be taken as a rough indication of the mean gel pore size. The corresponding equivalent pore sizes determined using this criterion are listed in Table II-1.

Table II-1. Comparison of gel pore size estimates based on mobility data.

Gel concen-tration (%T)	Ogston/reptation transition (bases) (Fig. II-4a)	Pore size (nm)					
		Ogston plot (Fig. II-3b)	Ogston function (Eq. (II-4))	Mercier-Slater model (Eq. (7))	vWBR model (Eq. (8))	Reptation plot (Fig. 3b)	Brahmasandra *et al.* [15]
6	240	9.73	20.09 (240 bases)/ 23.70 (1000 bases)	10.34 (240 bases)/ 8.65 (1000 bases)	11.75 (240 bases)/ 12.22 (1000 bases)	9.62 (*Ma* = 235)	7.04
9	100	5.93	13.76 (100 bases)/ 20.76 (1000 bases)	5.67 (100 bases)/ 4.41 (1000 bases)	6.41 (100 bases)/ 6.58 (1000 bases)	5.18 (*Ma* = 80)	5.18
12	90	5.57	11.99 (90 bases)/ 21.83 (1000 bases)	3.80 (90 bases)/ 3.50 (1000 bases)	4.22 (90 bases)/ 4.26 (1000 bases)	3.67 (*Ma* = 47)	3.73

Recently, Kopecka and co-workers [66] compared the pore size predictions of several different models using mobility data obtained in non-crosslinked sieving gels using a capillary electrophoresis instrument. First, a more rigorous adaptation of the standard Ogston model was applied, whereby deviations from the postulated linear relationship between $\log(\mu/\mu_0)$ and M employed in the Ogston sieving regime were compensated by employing the following equation

$$\sqrt{\ln\left(\frac{\mu_0}{\mu(M)}\right)} = \sqrt{\frac{\pi}{4}}\left(\frac{R+r}{a}\right) \qquad \text{(II-4)}$$

where R and r are the particle and fiber radii respectively. Thus, if R is expressed in terms of R_g, the pore size can be estimated from a plot of $[\ln(\mu_0/\mu)]^{1/2}$ versus R_g, which yields a straight line with slope $1/a$ and intercept r/a.

A second formulation proposed by Mercier and Slater provides a more realistic description of the geometric parameters that influence the fractional gel volume accessible to the migrating DNA [66, 67]. In this framework, the following relationship can be used to fit the mobility data.

$$\sqrt{\frac{\mu_0}{\mu(M)} - 1} \cong \frac{R_g + r}{a} \tag{II-5}$$

whereby a plot of $[(\mu_0/\mu) - 1]^{1/2}$ versus R_g is expected to yield a straight line with slope $1/a$ and intercept r/a. While strictly valid only within the Ogston regime, the Mercier-Slater model has been shown to effectively estimate pore sizes using mobility data over a much wider range of M.

Finally, the following empirical formulation proposed by van Winkle, Beheshti, and Rill (the vWBR model) [68, 69] can be used to predict pore sizes using mobility data spanning both the Ogston and reptation regimes.

$$\mu(M,C) = \frac{\mu(0,C)}{1 + \left(\frac{\mu(0,C)}{\mu(\inf,C)} - 1\right)\left(1 - e^{-M/m}\right)} \tag{II-6}$$

Here, a nonlinear curve fitting procedure must be applied to determine values of the adjustable parameters $\mu(0, C)$, $\mu(\inf, C)$, and m (note that $\mu(0, C)$ represents a *zero size* mobility, as opposed to the free solution mobility μ_0). The pore size can then be extracted by first computing M_a using the following expression [70]:

$$M_a = 3m\frac{\mu(\inf,C)}{\mu_0} \tag{II-7}$$

after which the Kratky-Porod model can be used to calculate R_g (and hence a). With the exception of the empirical vWBR model, the relationships between mobility and pore size discussed thus far have primarily focused on describing migration behavior in the Ogston regime. In the reptation regime, a measure of mean pore size can also be obtained by rearranging equation (II-3) into the following form [71].

$$\frac{3M\mu}{\mu_0} = M_a + 3f(\varepsilon)M \qquad \text{(II-8)}$$

Assuming $f(\varepsilon)$ remains essentially constant over the range of interest, a plot of $3M\mu/\mu_0$ versus M (often called a *reptation plot*) yields a straight line with intercept M_a, from which the Kratky-Porod model can be used to compute a from R_g (Figure II-4b).

We used our mobility data to compare the pore size predictions of these models for gel concentrations of 6, 9, and 12 %T (Table II-1). In addition, the Ogston function, Mercier-Slater, and vWBR models were evaluated both within the Ogston range (as determined in Figure II-3c) and over the entire range of fragment sizes. Several observations can be made from these results. First, the Mercier-Slater model provides the closest agreement with the pore sizes determined from the reptation plot (Figure II-4b). Despite the fact that the Mercier-Slater model is strictly valid only within the Ogston regime, good agreement is observed with the reptation plot results even when data from all fragment sizes (up to 1,000 bases) are used, consistent with the observations of Kopecka *et al*. (although closest agreement is obtained using data within the Ogston regime). This may be expected given this that $f(\varepsilon)$ is probably small within this range of conditions. It

is also notable that the assumed form of the shape factor employed by Kopecka *et al*. expressing the relationship between the analyte and pore geometries seems to provide good results despite the fact that it was chosen in the context of a non-crosslinked gel network.

Secondly, there appears to be a rather large discrepancy between the pore size estimates determined from fitting the linear region of the mobility versus fragment size data (Figure II-3c) and those computed by fitting the same data using equation (II-4). This seems surprising given that both approaches should reflect essentially equivalent formulations of the same basic model. Moreover, the pore sizes determined from the fits in Figure II-3c are actually closer to the values obtained from the reptation plot, despite the fact that use of the expression in equation (II-4) should provide a more rigorous analysis. In the case of the vWBR model, good agreement is also obtained with the reptation plot predictions in cases where the nonlinear fitting parameters could be accurately determined. Table II-2 shows that the best fits were obtained in the 12% T gel, while fitting parameters for the lower gel concentrations could only be determined with an unacceptably high level of uncertainty. Interestingly, our experiments were conducted at a temperature of 55 °C, close to the temperature range in which Kopecka *et al.* also encountered difficulties in generating accurate fits (although their experiments were performed in non-crosslinked gels). Finally, we note that pore sizes determined from the reptation plot analysis are close to the corresponding values obtained by Brahmasandra *et al* [38] using chemically polymerized gels at the same concentrations.

Table II-2. Fitting parameters for the vWBR model.

Parameters	6 %T (240 bases)	6 %T (1000 bases)	9 %T (100 bases)	9 %T (1000 bases)	12 %T (90 bases)	12 %T (1000 bases)
$\mu(0,C)$	$(1.96 \pm 0.009)\times10^{-4}$	$(1.96 \pm 0.027)\times10^{-4}$	$(1.77 \pm 0.18)\times10^{-4}$	$(2.12 \pm 0.08)\times10^{-4}$	$(1.69 \pm 0.25)\times10^{-4}$	$(1.83 \pm 0.04)\times10^{-4}$
$\mu(\infty, C)$	$(1.13 \pm 0.36)\times10^{-5}$	$(6.75 \pm 116)\times10^{-8}$	$(8.26 \pm 27.5)\times10^{-8}$	$(1.42 \pm 0.26)\times10^{-6}$	$(5.36 \pm 10.64)\times10^{-6}$	$(2.48 \pm 0.05)\times10^{-6}$
m	3511 ± 1251	$(6.36 \pm 109)\times10^{5}$	1604 ± 5925	8829 ± 1733	1262 ± 2781	2767 ± 69

2.3.3 Diffusion coefficients

In the case where the size of the migrating fragments is less than the mean pore size of the gel (the Ogston regime), it is reasonable to expect that the molecular diffusion process can be described in terms of the theoretical framework developed for dilute polymer solutions. The Zimm model, for example, incorporates the influence of hydrodynamic interactions on isolated polymer chains, yielding diffusivities that scale with molecular size according to $D \sim M^{-0.5}$ [30]. In the reptation regime, on the other hand, the translational diffusion process is related to the timescale required for an individual polymer chain to acquire sufficient displacement to escape a hypothetical tube representing the geometric constraints imposed by the surrounding gel network.

In this picture, a scaling of diffusivity as $D \sim M^{-2}$ is expected [15, 16]. It is difficult to identify a well-defined transition from one regime to the other based on the data in Figure II-5, perhaps due to the heterogeneous gel pore structure. When a linear fit is performed to a log-log plot of data over the entire range of fragment sizes, the measured diffusion coefficients are bracketed by these regimes, but appear to scale with base number in better agreement with the predictions of the reptation model (the slopes of the corresponding linear fits are –1.1 (6%T), –1.3 (9%T), and –1.8 (12%T), respectively). It is also notable that diffusion coefficients measured in the 9 %T UV gel are in good agreement with data obtained in a microfabricated gel electrophoresis device using the same gel under similar run conditions [72].

2.3.4 Dispersion coefficients

In addition to thermally driven motion of DNA molecules, the presence of an electric field also contributes to the band broadening process, whose effects can be expressed in terms of a *dispersion coefficient* (D^E).

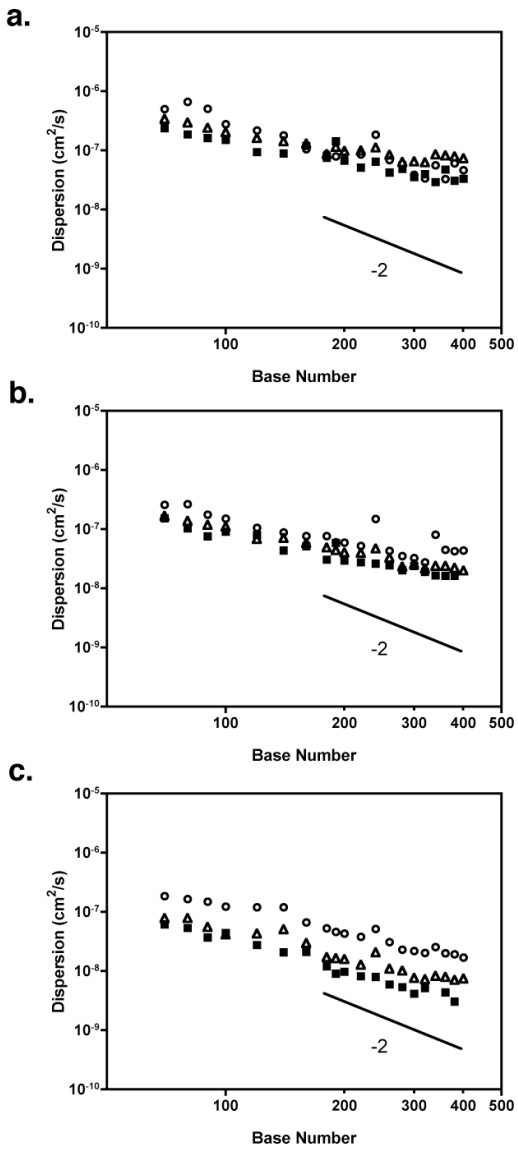

Figure II-5. Diffusion and dispersion coefficients as a function of fragment size for (a) 6, (b) 9, and (c) 12 %T gel concentrations. Data are shown for electric field strengths of 0 [■] (diffusion), 15 [△], and 30 [○] V/cm. A slope of –2 is indicated on the plot corresponding to the expected scaling in regime I of the BRF model.

Values of dispersion coefficients were measured in three gel concentrations (6 %T, 9 %T, and 12 %T, respectively) at six different electric field strengths ranging from 15 to 40 V/cm. We note that the measured values are actually "effective" dispersion coefficients, meaning that they include the cumulative effects of all band-broadening mechanisms (temperature gradients, inhomogeneities in buffer conductivity, etc.).

2.3.4.1 Fragment length dependence

The BRF model [36] predicts three scaling relationships for D^E

$$\text{Regime 1:} \quad D^E \sim N^{-2}\,\varepsilon^{0},\ N < \varepsilon^{-2/3} \tag{I-12a}$$
$$\text{Regime 2:} \quad D^E \sim N^{-0.5}\,\varepsilon^{1},\ \varepsilon^{-1} > N > \varepsilon^{-2/3} \tag{I-12b}$$
$$\text{Regime 3:} \quad D^E \sim N^{0}\,\varepsilon^{1.5},\ N > \varepsilon^{-1} \tag{I-12c}$$

where ε is the scaled electric field, a ratio of the applied electric field strength to the energy associated with thermally driven motion of a molecule of size M_a. Representative data illustrating the variation of D and D^E with base number are shown in Figure II-5. In 6 and 9 %T gels, the measured dispersion coefficients are close to their corresponding zero field values over the entire range of fragment sizes studied. In the 12 %T gel, both the diffusion and dispersion coefficients appear to approach a power law scaling close to M^{-2} at fragment sizes above approximately 200 bases (especially at E = 30 V/cm), suggesting behavior consistent with regime I of the BRF model (equation (I-12a).

Tinland *et al.* [73] experimentally observed the existence of the three reptation regimes in equation (I-12) with double-stranded DNA using several sieving matrices, while Brahmasandra *et al.* [38] reported a transition from scalings identified as $D^E \sim M^{-0.5}$ to

$D^E \sim M^{-2}$ with single-stranded DNA in chemically polymerized crosslinked gels (see Figure 8 of [38]). It is possible that the $M^{-0.5}$ regime reported by Brahmasandra *et al.* may have been a signature of the behavior exhibited by the 6 and 9%T gels. Close agreement with the D^E versus M behavior shown in Figures 4a-b, however, can be found in results obtained by Ugaz and co-workers using a microfabricated gel electrophoresis device. Under similar run conditions and using an identical photopolymerized gel formulation to that studied here (9 %T), a "plateau" in D^E values was observed for fragments in the 200 – 400 base range that is consistent with the scalings measured here (see Figure 2 in [44]).

2.3.4.2 Electric field dependence

We observed that, under the range of conditions studied here, DNA fragment mobility is essentially independent of electric field, consistent with regime I of the BRF model. As shown in Figure II-6, this is essentially what is observed over the entire range of electric field strengths studied, although a slight increase in the magnitude of D^E appears to occur at E = 20 – 25 V/cm. This behavior, however, deviates somewhat from the corresponding observations of Brahmasandra *et al*. [38] in chemically polymerized gels where values of D^E/D on the order of 10 – 20 that increased with increasing fragment size and electric field strength were reported, while we observe approximately constant values ($D^E/D < 5$) over a comparable range of conditions.

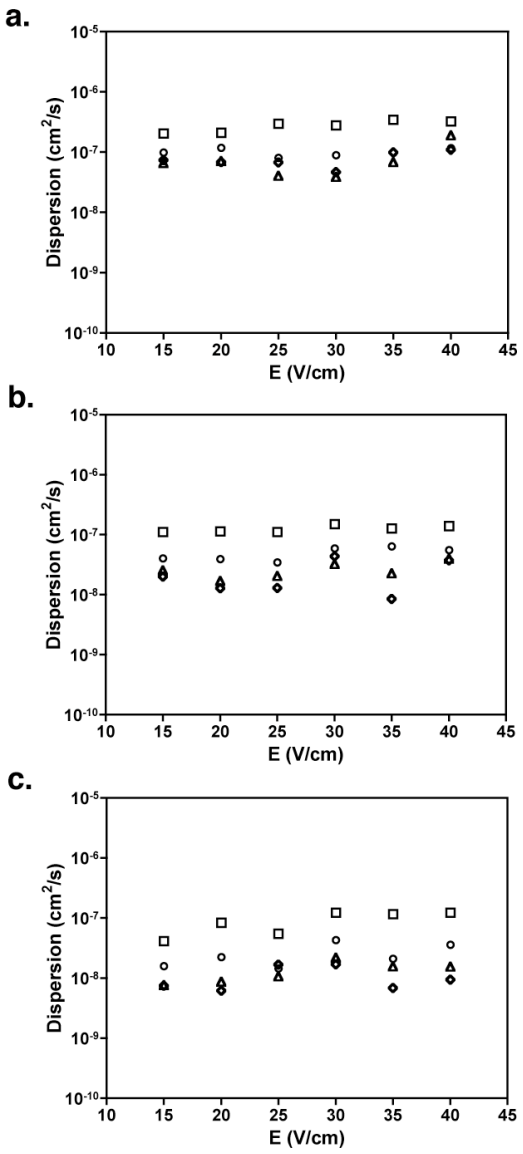

Figure II-6. Dispersion coefficients as a function of applied electric field strength for (a) 6, (b) 9, and (c) 12 %T gel concentrations. Data are shown for 100 [□], 200 [○], 300[△], and 400 [◇] base fragment sizes.

2.3.5 Separation resolution

The separation resolution between neighboring peaks was directly calculated using equation (1-13), where the peak half-widths (σ) were determined by fitting the fluorescence intensity traces to a Gaussian profile. Values were normalized to an equivalent single-base resolution by dividing them by the spacing between peaks in units of bases. For comparison, corresponding resolution predictions were made using equation (I-14) based on our measured data for fragment mobility, diffusion coefficient, and dispersion coefficient. For the purposes of making consistent resolution predictions, we employed a standard protocol for quantifying the fragment length dependence of these parameters. First, fits of the mobility versus base number data (averaged over all electric field strengths) were obtained at each gel concentration using the Mercier-Slater model. Next, linear regression was used to fit the $\log(D^E)$ versus $\log(M)$ data at each gel concentration and electric field strength, after which these fitting parameters were substituted into equation (I-14) along with the desired field strengths and separation lengths in order to calculate predicted resolution under specific run conditions. It should be noted that we initially attempted to employ a linear regression fit of the $\log(\mu)$ versus $\log(M)$ data, but found that resolution predictions obtained using this procedure did not accurately capture the measured behavior, especially at small fragment sizes. In general, we found that predicted resolution values were fairly sensitive to mobility, making it advisable to exercise caution in selecting an appropriate fitting procedure that accurately captures behavior over the *entire* fragment size range of interest. Results could also be improved by the

development of correlations for dispersion comparable to those described for mobility in the section of estimating gel pore size.

2.3.5.1 Fragment length dependence

Figure II-7 compares results of the resolution predictions with corresponding measured values. In general, the agreement between predicted and measured values is quite good. In the 6 %T gel, the resolution value remains relatively constant ($R \sim 0.2$) at all electric fields studied and predictions are close to the experimental data, both qualitatively and quantitatively. Increasing the gel concentration to 9 and 12 %T is accompanied by an increase in the magnitude of R, as well as a change in overall behavior such that R decreases with increasing fragment size. At these concentrations, agreement between predictions and observed data appears to diminish somewhat with increasing electric field. This is at least partially due to difficulties in representing the dispersion behavior over the entire fragment size range using a single fitting parameter (a piecewise approach, for example, may yield better results). Nevertheless, these results demonstrate the ability to characterize separation resolution behavior based solely on measurements of mobility and dispersion coefficients with a reasonable degree of accuracy.

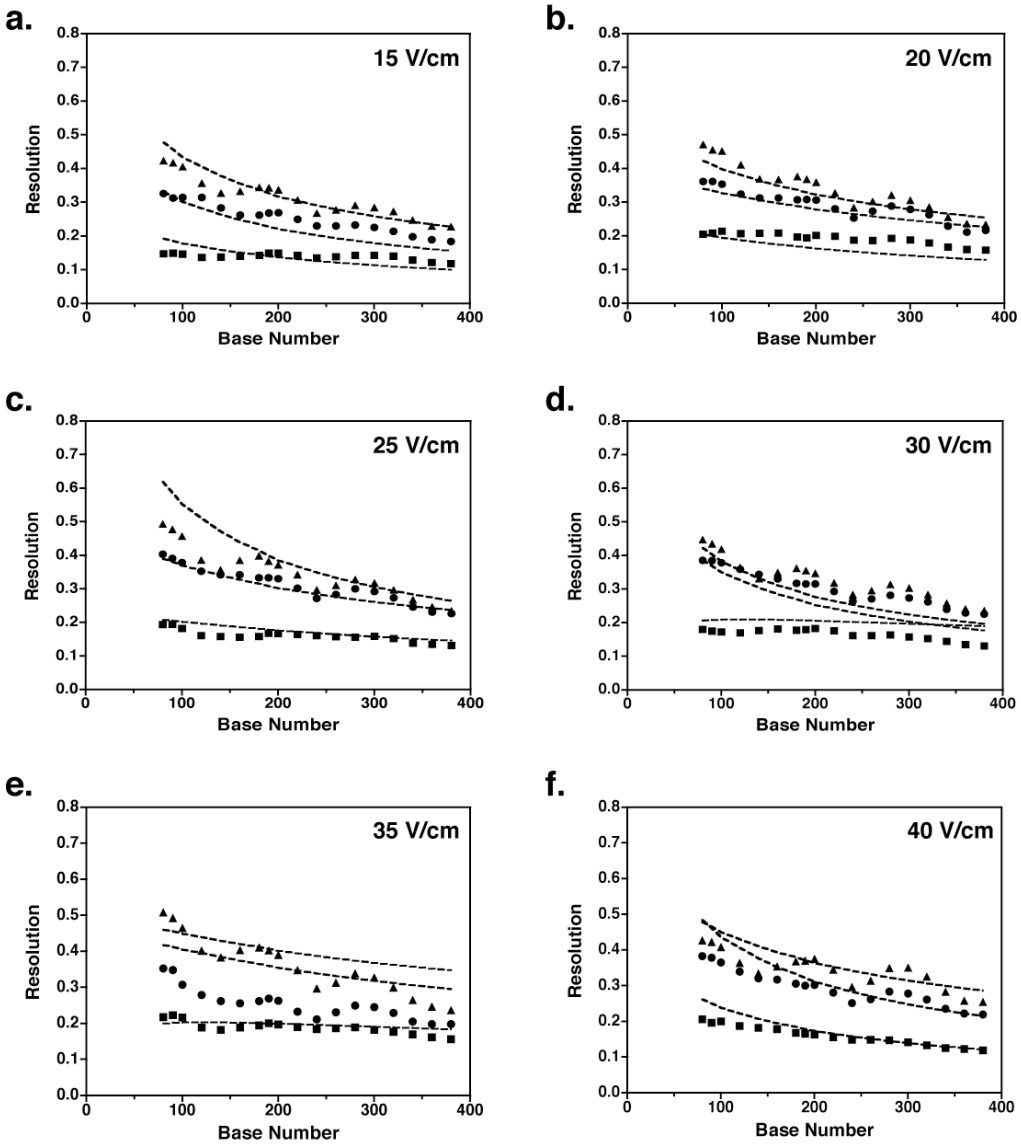

Figure II-7. Separation resolution as a function of base number, gel concentration, and electric field strength. Data are shown for 6 [■], 9 [●], and 12 [▲] %T gel concentrations at electric fields of (a) 15, (b) 20, (c) 25, (d), (e) 35, and (f) 40 V/cm. Dashed lines represent predictions using equation (2) based on the measured mobility and dispersion coefficients under each set of conditions. Run conditions: T = 55°C, and L = 8.5 cm.

2.3.5.2 Electric field dependence

As previously mentioned, our observations indicate that both fragment mobility and dispersion coefficient exhibit little variation with electric field strength over the range of conditions studied here. This behavior is reflected in the separation resolution data, which are also essentially independent of electric field (Figure II-8). This deviates from the results of Brahmasandra *et al*., where similar fits to their measured mobility and dispersion data as a function of electric field yielded a local maximum in resolution in the vicinity of 25 – 30 V/cm [38].

2.4 Concluding remarks

In this chapter, we have embarked on a comprehensive study aimed at measuring some of the key parameters (mobility, diffusion, and dispersion coefficients) associated with migration of single-stranded DNA in photoinitiated crosslinked polyacrylamide gels. These data can be used not only to extract information about the mean gel pore structure, but also to quantitatively predict the achievable separation resolution.

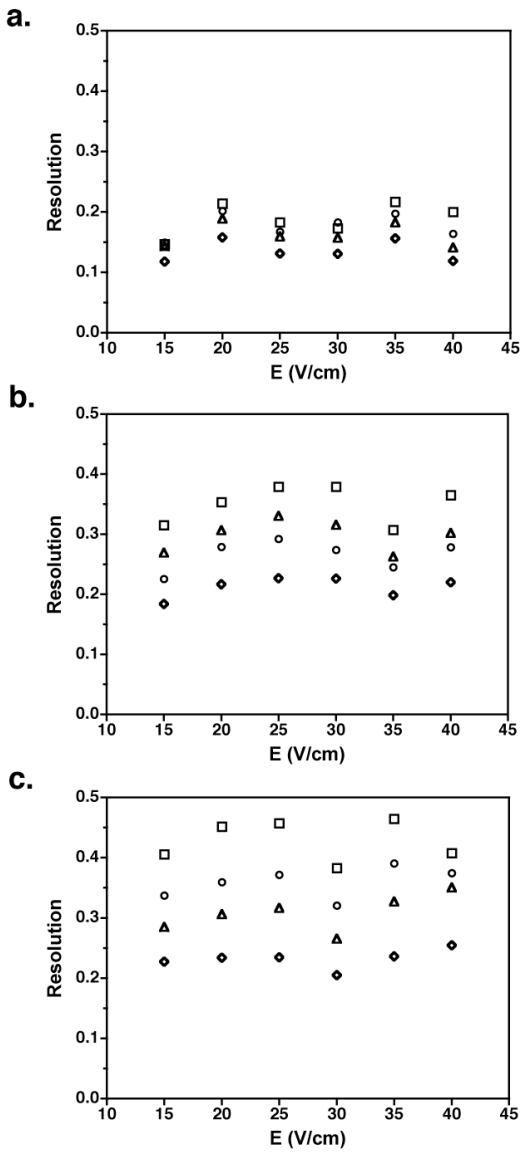

Figure II-8. Measured single-base separation resolution as a function of applied electric field strength for (a) 6, (b) 9, and (c) 12 %T gel concentrations. Data are shown for 100 [□], 200 [○], 300[△], and 380 [◇] base fragment sizes. Run conditions: T = 55°C, and L = 8.5 cm.

This information is valuable to support the design of advanced electrophoresis technology, especially in miniaturized systems where it is essential to optimize separation performance over ultra-short distances. Moreover, these data are badly needed in order to allow the predictions of theoretical models of electrophoretic DNA migration phenomena to be tested and improved.

Unfortunately, acquisition of all the data needed to perform a detailed gel characterization study such as this using conventional DNA sequencing instrumentation is an extremely tedious and time-consuming undertaking, almost prohibitively so. As an example, consider that depending on the gel concentrations and run conditions used, average experiment times ranged from 1 – 9 hours to collect mobility data, 14 – 30 hours to collect diffusion coefficient data, and 4 – 20 hours to collect dispersion coefficient data. Accounting for repeats to ensure run-to-run consistency, a total timescale on the order of 2,000 hours was required to obtain all the data presented in this paper (not including data processing and analysis time). This is equivalent to over 250 conventional 8-hour workdays! Clearly, there is a critical need for a next-generation rapid gel-screening platform capable of collecting all the data required for gel characterization in hours instead of months. Microfabricated gel electrophoresis devices have proven to be a feasible platform for such studies [44, 53, 74, 75]. We hope that the results of this work will stimulate further such studies, which have the potential to greatly advance our understanding of the physics of DNA electrophoresis.

CHAPTER III

AUTOMATED WHOLE-GEL SCANNING DETECTION SYSTEM FOR DATA COLLECTION IN MICROFLUIDIC GEL ELECTROPHORESIS DEVICES

This chapter details the configuration of the automated whole-gel scanning detection system for microchip electrophoresis and the experiments for measurements of mobility and dispersion coefficients of dsDNA migrating in photopolymerized polyacrylamide gels on a microfabricated gel electrophoresis. Using obtained migration data, we have successfully demonstrated the capability of our system to rapidly characterize the evolution of the DNA separation process.

3.1 Experimental setup

3.1.1 System configuration

The automated whole-gel scanning detection system (Figure III-1) is composed of a PowerBook G4 laptop computer (Apple Inc., Cupertino, CA), X-Y translation stage (Ludl Electronic Products Ltd., Hawthorne, NY), Hamamatsu ORCA-ER CCD camera (Hamamatsu Photonics, Bridgewater, NJ), Zeiss Axioskop 2 microscope (Carl Zeiss MicroImaging, Inc, Thornwood, NY, Thornwood, NY), electronic shutter (Part# 99A360; Ludl Electronic Products Ltd., Hawthorne, NY), and power supply (Model E3612A; Agilent Technologies Inc, Santa Clara, CA).

a.

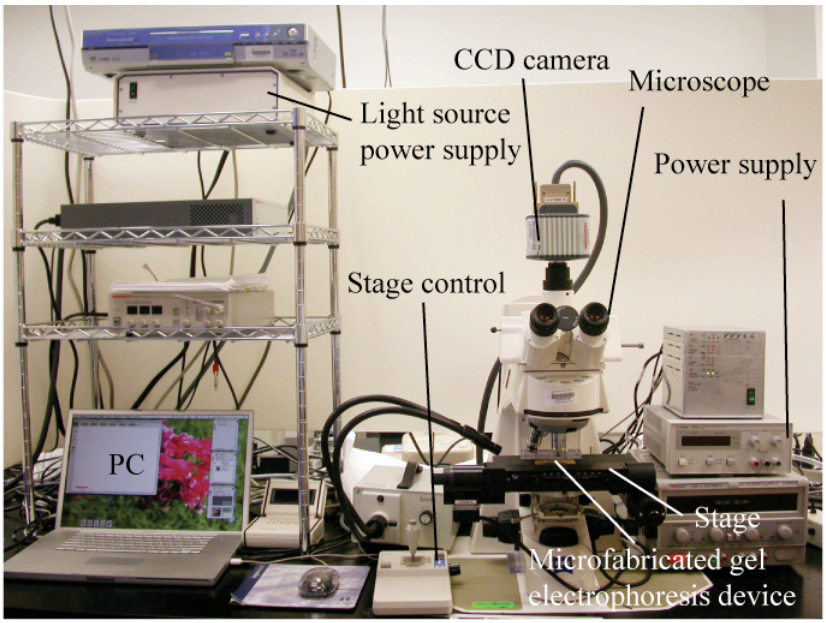

b.

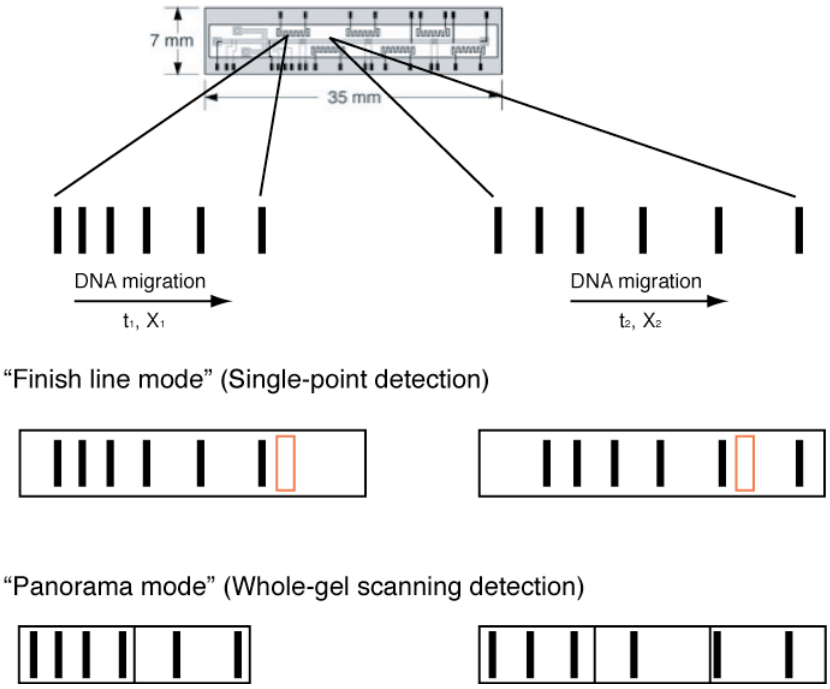

Figure III-1. (a) Setup of the whole-gel scanning detection system. The Hamamatsu ORCA-ER camera has a resolution of 1344 x 1024 pixels and a 12-bit (4096 levels) grayscale intensity response range. (b) Detection schemes for microchip gel electrophoresis.

The CCD camera was connected to the laptop computer via an IEEE1394 port, and the precision translation stage was linked to the computer via a Mac 5000 automation controller (Ludl Electronic Products Ltd., Hawthorne, NY). To assemble the microfluidic gel electrophoresis device, the glass separation channel (300 x 50 μm in cross section) and the silicon substrate were first cleaned and then bonded using a UV-cured optical glue (SK-9 Lens Bond, Summers Laboratories, Fort Washington, PA, USA). The assembly was mounted on a PC board using a Scotch Double Sided tape (3M Corporate Headquarters, St. Paul, MN, USA), and two buffer reservoirs were attached with Devcon 5-min epoxy (ITW Performance Polymers Consumer Dvision, Riviera Beach, FL). Figure III-2 depicts assembly of the major components for the microfluidic gel electrophoresis device. All electrodes on the silicon substrate were bonded to the PC board with aluminum wires (1 mil in diameter) using a wire bonder (Model 4523AD; Kulicke & Soffa Industries Inc., Fort Washington, PA).

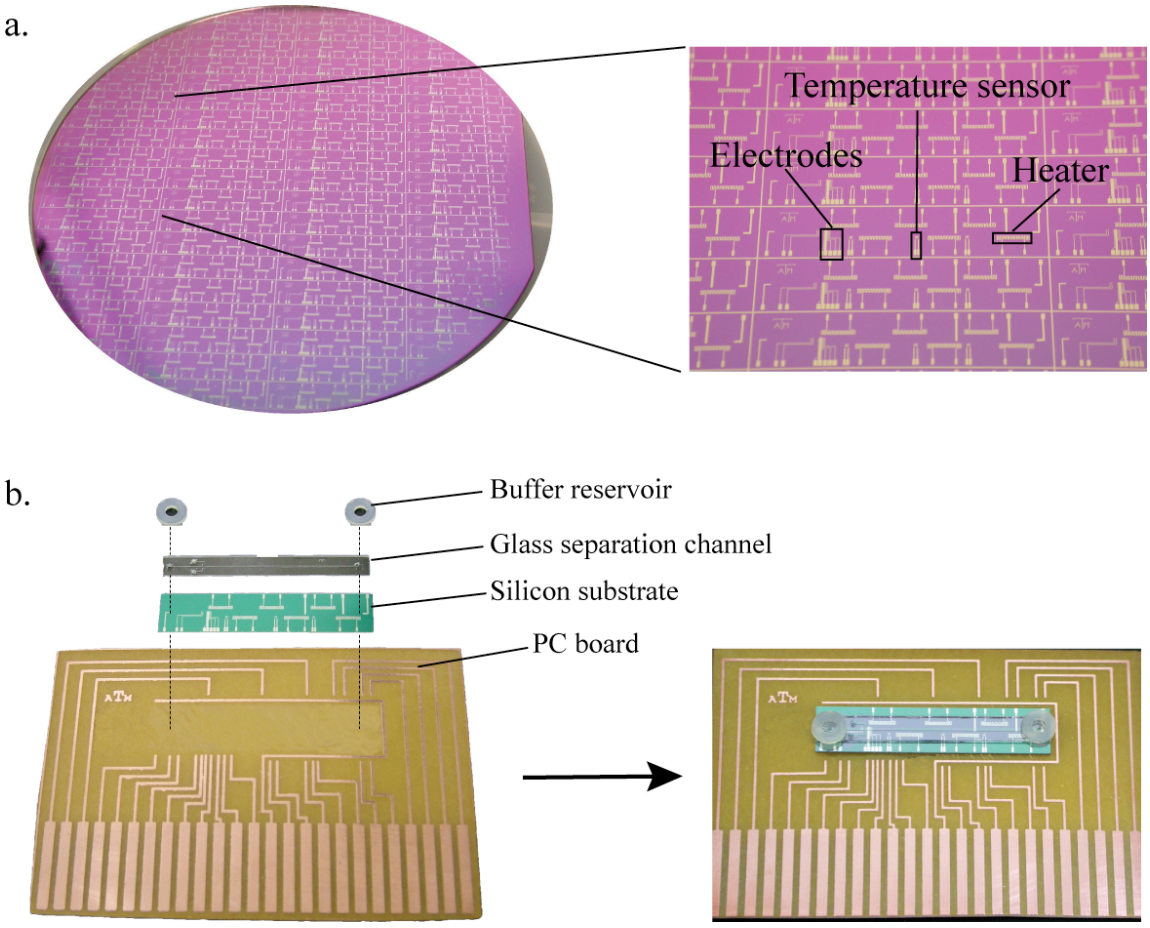

Figure III-2. (a) Photograph of a 6" silicon wafer with on-chip electrodes, heaters, and temperature sensors for electrophoresis and sample injection. (b) Assembly of the microfluidic gel electrophoresis device.

The assembled microfluidic gel electrophoresis device was mounted onto the translation stage and connected to a CB-50 I/O connector block (National Instruments Corp., Austin, TX, USA) by a 50-pin cable. DNA sample injection and separation were performed by applying electric voltages between on-chip electrodes through the cable. The laptop computer controls actions of the translational stage, CCD camera, and shutter to syn-

chronize image acquisition during the entire DNA separation runs. A mercury arc lamp (HBO100; Carl Zeiss MicroImaging, Inc, Thornwood, NY) provided excitation light (480 nm) through a fluorescein isothiocyanate (FITC) filter set (Part# F44-001; AHF analysentechnik AG, Tubingen, Germany).

3.1.2 Reagents

Duracryl® polyacrylamide sequencing gels (Proteomic Research Services, Inc.) were used in all DNA separations as the sieving matrix. Gel solutions at desired concentrations were prepared by diluting the 30% T, 2.6% C gel stock solution with a proper amount of deionized water and were mixed with Rhinohide® gel strengthener (Invitrogen Corporation, Carlsbad, CA) and photoinitiator (Solution B) from ReproGel® sequencing gel kits (GE Healthcare Bio-Sciences Corp., Piscataway, NJ) for UV cross-linking. Double-stranded DNA (dsDNA) sizing standards (customized MapMarker; 100 ng/μL; Bioventures, Murfreesboro, TN) were labeled with the YOYO-1 dye (Y3601; Invitrogen Corp., Carlsbad, CA). Fluorescein-labeled double-stranded DNA (dsDNA) sizing standards (customized MapMarker; 100 ng/μL; Bioventures, Murfreesboro, TN) were prelabeled with fluorescein by the vendor. Formamide (99%, GC grade) was obtained from Sigma-Aldrich Corp (St. Louis, MO). 2-mercaptoethanol (M6250; Sigma-Aldrich Corp, St. Louis, MO) was added to DNA samples to minimize dye photobleaching [44, 76]. The running buffer was prepared by diluting a 10X stock solution (Extended Range TBE buffer, Catalog number: 161-0741; BioRad, Hercules, CA) to the desired final concentration (0.5X) with deionized water. All reagents were used as received.

3.1.3 Gel casting

The glass microchannel was rinsed with a detergent solution (Alconox, Inc., White Plains, NY) and deionized water to remove particles. After this cleaning, the glass microchannel was rinsed with RainX Anti-Fog solution (SOPUS products, Houston, TX) to promote uniform wetting inside the microchannel by the gel monomer mixture. The UV-crosslinked gels were prepared by gently mixing the gel monomer stock solution (diluted with a proper amount of deionized water), gel strengthener, and photoinitiator to obtain a final concentration of 6%T and 12% v/v Rhinohide. This mixture was loaded into the microchannel with a syringe, and the gel interface was defined by masking the injection channels with an opaque electrical tape. The loaded device was first exposed to UV illumination (6 mw/cm^2) for 2 minutes in the UV crosslinker (XL-1500; Spectrolinker Corp., Westbury, NY). The tape was then removed, and the unpolymerized residue was vacuumed out of the injection channel and replaced with the running buffer. The reloaded device was again exposed to UV light for 10 minutes to finish the gel polymerization process.

3.1.4 DNA sample preparation

DNA samples were prepared in a total volume of $10\,\mu$L for runs under the same conditions. The dsDNA sample was composed of $1\,\mu$L of unlabeled MapMarker standard ladder, $4\,\mu$L of YOYO-1 dye, $4\,\mu$L of deionized water, and $1\,\mu$L of 2-mercaptoethanol. The ssDNA sample was prepared by mixing $1\,\mu$L of fluorescein-labled MapMarker standard ladder and $1\,\mu$L of formamide. The mixture was pre-denatured at 95°C on a thermal cy-

cler (Tgradient; Biometra biomedizinische Analytik GmbH, Goettingen, Germany) for 2 minutes and then snap-cooled on ice. 8 μL of 0.5X TBE buffer were added to make the final volume 10 μL. For each gel separation experiment, 0.2 μL of the sample was loaded into the injection channel, while 1 μL to fill up the whole microchannel for each free solution mobility measurement.

3.1.5 Electrophoresis procedure

After UV gel polymerization, the microfluidic gel electrophoresis device was plugged into the control cable socket on the X-Y translation stage. A low voltage (1 V) was applied for 1 to 2 minutes to concentrate the DNA sample and to form a well-defined injection plug at the gel interface. Once the sample focusing was complete, excess DNA sample was removed from the injection channel and replaced with the running buffer (0.5X TBE). A constant voltage (23.4 V) was applied over a distance of 1.56 cm (E = 15 V/cm) to perform DNA separation. For free solution electrophoresis, the DNA sample was loaded to fill up an empty microchannel and then concentrated in the same way as in gel electrophoresis. The electric field was 5 V/cm (7.8 V over 1.56 cm). Electrophoresis experiments for dsDNA were performed at the room temperature (22°C), and those for ssDNA at 55°C. For temperature control of ssDNA electrophoresis runs, calibration was performed by placing the assembled device in an oven and monitoring the resistance of the temperatures sensors at five different temperatures (20 to 65 ºC). For each resistance measurement, the oven was allowed to reach equilibrium for 30 minutes, and the measured resistance values were linearly regressed against the corresponding tempature

points to determine the calibration line (Figure III-3). The temperature control was achieved by applying a potential to the heaters until the resistance readouts of the sensors reach those at the desired temperature (55 ºC). A stable temperature was usually reached within 5 minutes because of the thermal equilibration between the device and the surrounding air [74].

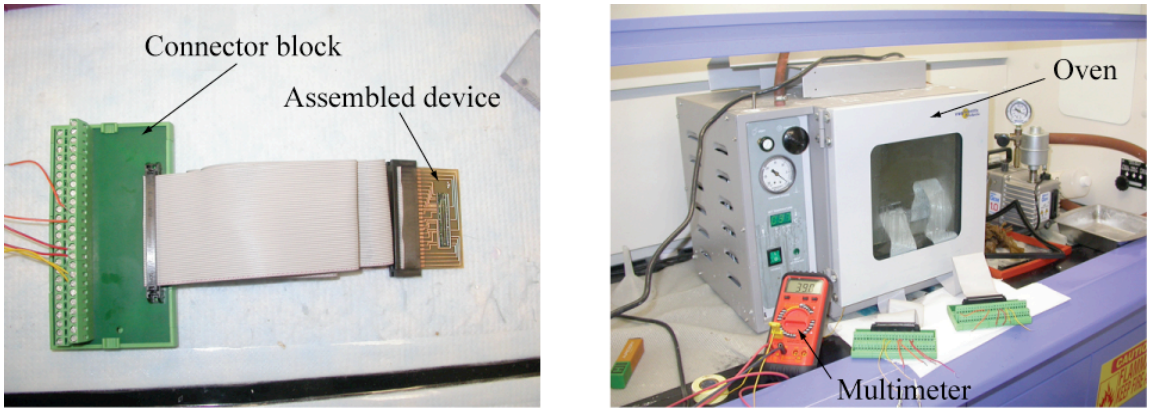

Figure III-3. Temperature calibration of assembled microfluidic gel electrophoresis devices.

3.2 Data collection and analysis

3.2.1 Image acquisition and joining

A new Openlab® (Improvision Inc., Lexington, MA) code was written to synchronize the microscope, CCD camera, and translation stage to acquire several series of 12-bit gray-scale images of DNA migrating in the photopolymerized crosslinked polyacrylamide gel along the separation channel during all electrophoresis experiments (Figure III-4). The corresponding frame time for each image was recorded when the image was taken. We then used our own MATLAB® (The Mathworks, Inc., Natick, MA) codes to perform background subtraction using images of the first scan as background layers. The background subtraction was performed by subtracting the background layer from the corresponding layer taken at the same position of the separation channel. Images after background subtraction were then joined with PanaVue ImageAssembler 3 (www.panavue.com) to form a composite view like those of conventional slab gels. Intensity data were extracted from these joined images with our own MATLAB® codes into a text file format for calculations of mobility and dispersion coefficients. The overall workflow for data collection is shown in Figure III-5.

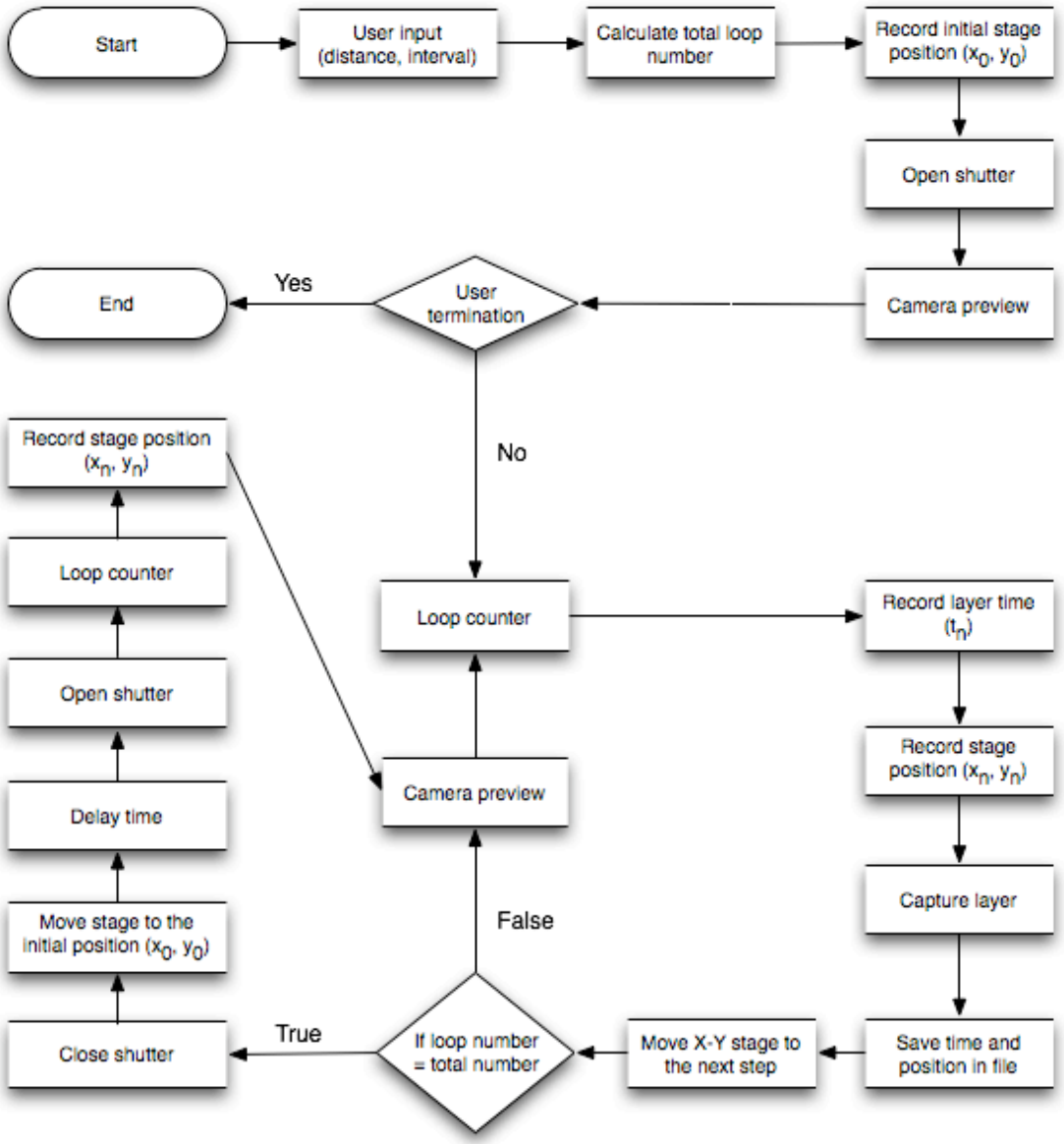

Figure III-4. Flow chart for automated image acquisition of DNA gel electrophoresis. The total loop number is the number of images needed to cover the whole scanning distance.

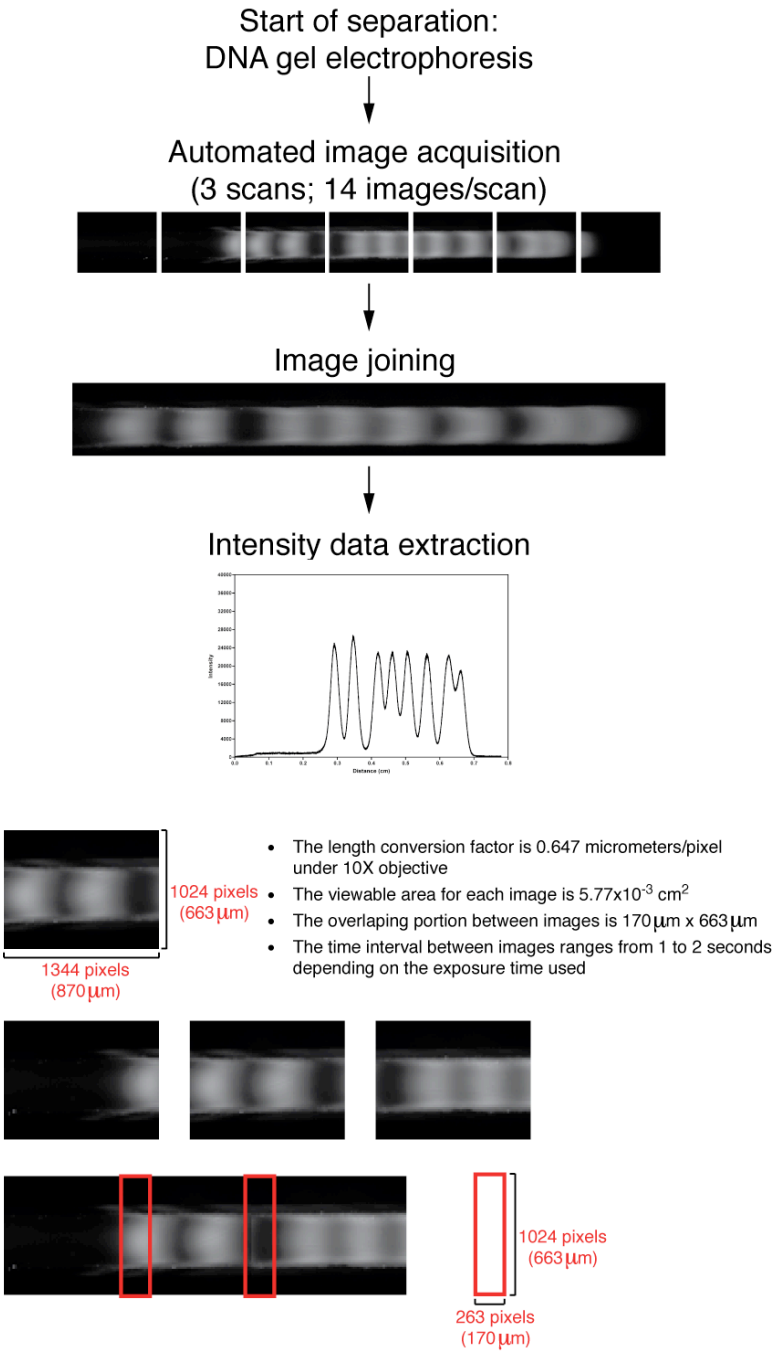

Figure III-5. Workflow for image acquisition and processing of whole-gel scanning detection. The number of images needed depends on the scanning distance.

3.2.2 Mobility

Mobility measurements were conducted with customized MapMarker ladders (8 fragments ranging in size from 75 to 500 bp) in 6%T Duracryl gels. For each set of mobility data, three composite images containing separated DNA fragments were selected for intensity extraction with in-house MATLAB programs. For each pair of composite images, differences in individual fragment positions and the corresponding frame times were used to calculate the migration velocity for each DNA fragment ($V = (x_2-x_1)/(t_2-t_1)$). The mobility for each fragment was then determined by dividing the migration velocity by the applied electric field strength ($\mu = V/E$). For each separation run, the average of mobility values calculated from two image pairs were taken as the representative values. The relative variation in mobility values calculated from two image pairs in the same run was found to be within 15% (see discussion in Section 3.3.2).

Free solution mobility measurements were performed in a similar manner except that there was no gel in the microchannel. The free solution mobility of dsDNA was measured at 22°C, while that of ssDNA at 55°C. All reported mobility values are the average of three independent runs.

3.2.3 Dispersion coefficients

Dispersion coefficients (D^E) were calculated by measuring the band broadening of each separated DNA fragment over time due to presence of the applied electric field. The same set of intensity data from mobility measurements was used to calculate dispersion

coefficients for each DNA fragments. Each peak was fitted to a Gaussian profile to obtain the standard deviation σ. The dispersion coefficient corresponding to each DNA fragment was determined using the following equation:

$$\sigma^2 = \sigma_{static}^2 + 2D^E(t_R) \qquad \text{(III-1)}$$

where σ^2 is the overall peak variance, σ_{static}^2 is the time-independent variance, and t_R is the corresponding retention time for each fragment. The data analysis process follows the general outlines in our previous work on the slab gel sequencer [77].

3.3 Results and discussion

3.3.1 Image acquisition and processing

In each DNA gel electrophoresis experiment, several scans were performed along the separation channel. To avoid photobleaching of the labeling dye, we made the exposure time as short as possible (10-30 ms) for image acquisition, and programmed the electronic shutter to close during the delay time between each scan. We visually checked the brightness of YOYO-labeled DNA under the microscope and found no rapid decay in the fluorescence intensity in the duration of our experiments. This was verified by integrating the fluorescence intensity extracted from the scanned images along the separation length. The integrated area for each individual peak remained roughly constant between scans, indicating no photobleaching in the course of our DNA separation experiments. The delay time was set as 60s for the run conditions used here. The length of the delay time depends on the desired number of scans and the velocity of DNA fragments

migrating in the sieving gel. A shorter delay time is needed for more scans and fast moving DNA fragments.

The composite view of each scan was generated by joining images taken along the separation channel. The number of images needed to cover the whole separation length depends on the microscope objective used and the size of the overlapping area for each individual image. After trial and error, a 10X objective and an overlapping area of 170 μm by 663 μm (~ 20%) on each side of an image were selected to generate composite views that require the least number of images but still provide best details of DNA fragments migrating in the gel (Figure III-4). With this combination, 14 images are needed to cover a separation distance of 1.0 cm. The time interval between each image ranges from 1 to 2 seconds, depending on the exposure time used. In general, each scan takes less than 30 seconds to cover the entire separation distance of 1.0 cm. For these scans, the time interval between each individual image in the same scan did not affect the measurement of mobility and dispersion coefficients, because these parameters were calculated by comparing the exact frame time and on-chip position/band width for the desired fragment between two separate scans.

Objectives with higher magnifying powers can be used to obtain more details, but the viewable area for each individual image decreases, and thus more images are needed to cover the same separation distance, which means longer scanning time and more computer system memory. For example, a 20X objective requires 28 images to cover a dis-

tance of 1.0 cm with the same overlapping area as mentioned previously. The scanning time and system memory demand are doubled for this setting.

The overlapping area of each individual image affects the number of images needed to generate a composite view of migrating DNA fragments and also the quality of these joined images. For the setting we selected, the total overlapping area accounts for about 40 percent of the total viewable area. Smaller overlapping areas were tested, but the images were not properly joined, especially when DNA bands fell on the image edges. The resulting band was properly joined, which makes it difficult to correctly determine mobility and dispersion coefficients. If a larger overlapping area is used, more images are needed to build a composite image because of less viewable area.

A single exposure time (10-30 ms) was used for image acquisition throughout the duration of each separation run to ensure a smooth baseline after joining. It is important to select an appropriate value so that the fluorescence intensity of all labeled DNA fragments does not overshoot the 12-bit grayscale values (0-4095). However, larger DNA fragments are always brighter than smaller ones as they migrate more slowly and thus undergo less dispersion phenomena. This may be a problem for very small fragments because they become very dim when all bands are resolved in the gel. To address this issue, we tried automated exposure for each individual image in the scanning process, but this resulted in an uneven baseline and longer scanning time. Therefore, we still used one single exposure time for best results.

Shown in Figure III-6 is a representative set of images and intensity data. The baseline and peak shape of the extracted intensity data are very smooth. All the eight bands of the dsDNA sample can be resolved and observed within 1 cm. The 75-bp fragment experienced the most dispersion because it migrated farthest in the gel, and thus resulted in the widest peak on the electropherogram. Using this detection scheme, the whole separation run completed within 10 minutes instead of 30 minutes for runs under the same conditions using the finish line mode. In the whole-gel scanning mode, we can observe the progress of DNA separation during experiment and also obtain both spatial and temporal migration data with high accuracy in nearly real time.

Figure III-7 is a typical electropherogram obtained using the finish line mode. Unlike the whole-gel scanning mode, the peak of the 500-bp fragment is the widest instead of that of the 75-bp fragment. This difference resulted from the two detection modes used for data collection. In the finish line mode, all the peaks had to migrate over the entire separation length (0.5 cm in this case). The largest fragment (500 bp) experienced the most dispersion because of its long migration time and therefore gave the widest peak on the resulting electropherogram. In this scheme, we can only see the peaks after the completion of the separation run and obtain the intensity data as a function of time.

In addition to gel electrophoresis, our system is also capable of monitoring DNA fragments migrating in the running buffer and thus makes it possible to directly measure free solution mobility in one simple experiment. As shown in Figure III-8, the measurement of the free solution mobility can be completed within 90 seconds and 0.1 cm. The free solution mobility of both dsDNA and ssDNA can be measured with our system.

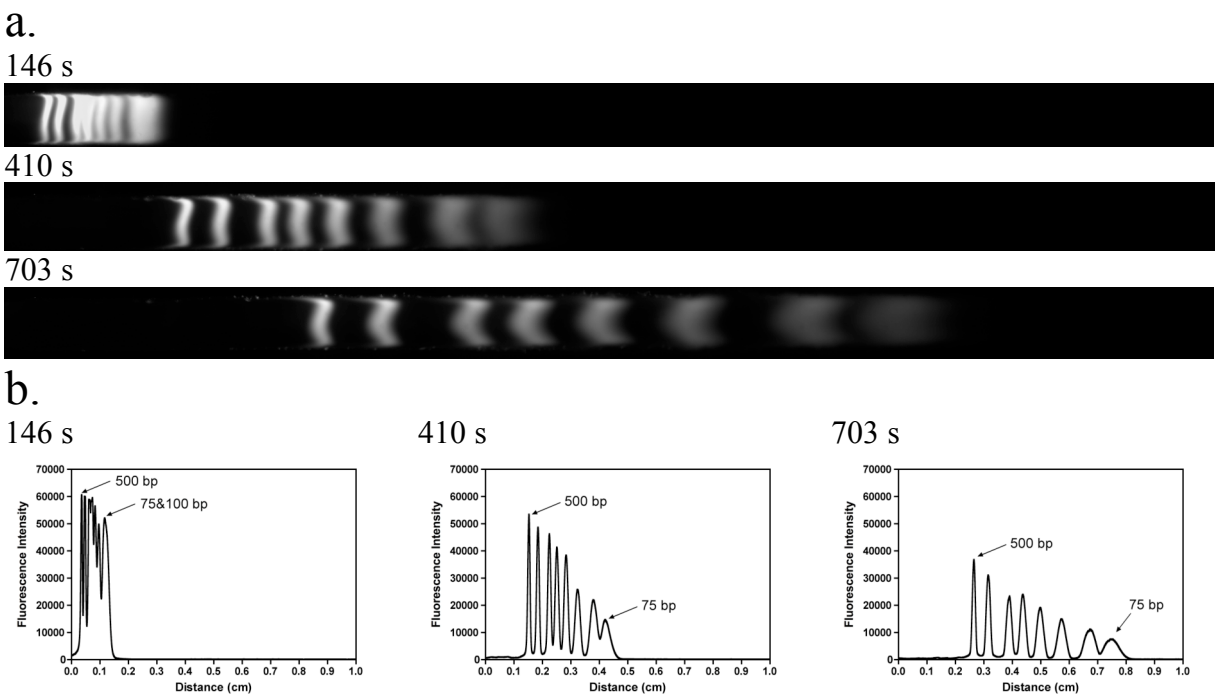

Figure III-6. A representative separation run of DNA fragments labeled with YOYO-1 in 6%T Duracryl gel with 12% Rhinohide gel strengthener in the panorama mode. (a) Composite view at (i) 146 s, (ii) 410 s, and (iii) 703 s. (b) Extracted intensity data for the three scans. Run conditions: $T = 22°C$, and $E = 15$ V/cm.

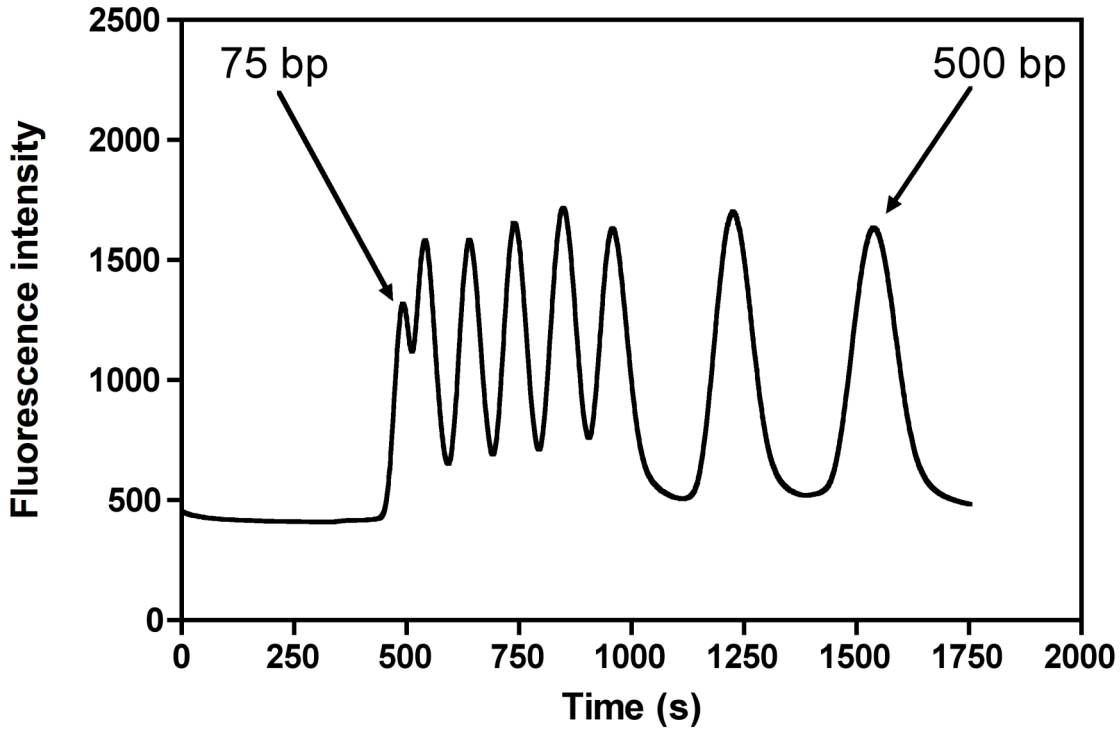

Figure III-7. A typical finish-line electropherogram for separation of dsDNA fragments labeled with YOYO-1 in 6%T Duracryl gel with 12% Rhinohide gel strengthener. Run conditions: L = 0.5 cm, T = 22°C, and E = 15 V/cm.

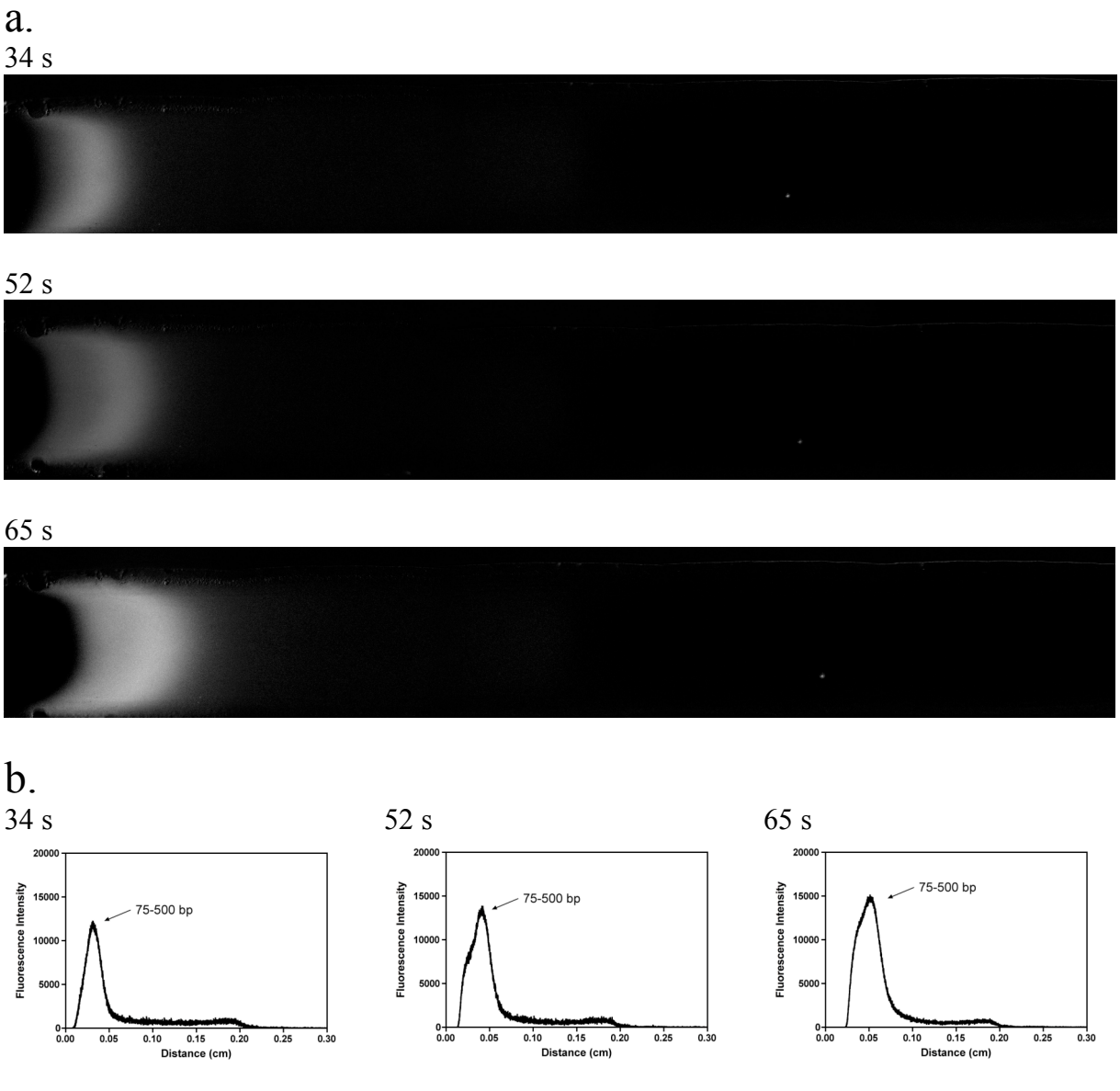

Figure III-8. A representative experiment for free solution mobility measurement of dsDNA fragments labeled with YOYO-1 in 0.5X TBE buffer. (a) Composite view at (i) 34 s, (ii) 52 s, and (iii) 65 s. (b) Extracted intensity data for the three scans. Run conditions: T = 22°C, and E = 5 V/cm.

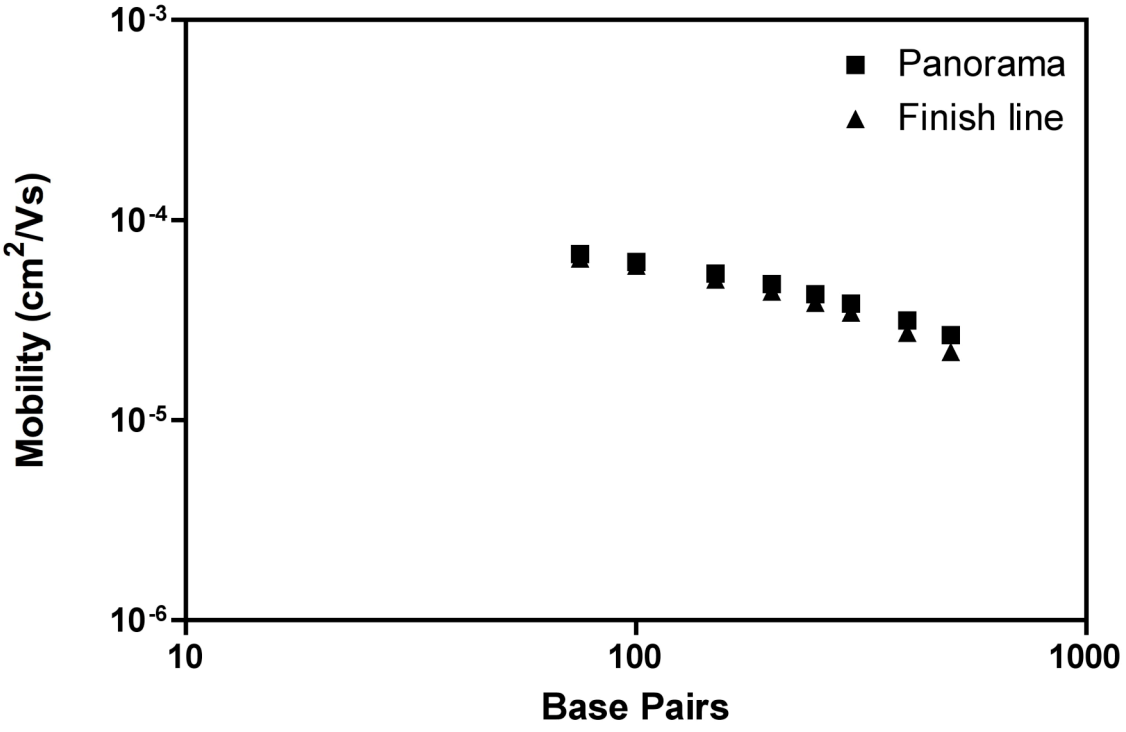

Figure III-9. Mobility data for 6%T Duracryl gel with 12% Rhinohide gel strengthener. Run conditions: $T = 22°C$, and $E = 15$ V/cm.

3.3.2 Mobility

We performed a series of experiments to measure mobility of dsDNA fragments at 6%T in both whole-gel scanning and single-point detection modes under the same conditions. As shown in Figure III-9, mobility data obtained with both detection modes are in good agreement. For the finish line mode, the relative variation in measured mobility for each DNA fragment ranges from 5 to 18% and is more obvious for fragments larger than 100 bp. The lower measured mobility for the finish line mode may result from ionic depletion within the gel, because each fragment in the injected sample has to migrate over the whole separation distance (typically 0.5 cm) to be detected.

In the panorama mode, we found that the migration velocities of DNA fragments were not uniform throughout the whole separation process. The measured mobility for each fragment randomly fluctuated during the separation run. The variation in mobilities determined from two consecutive scans ranged from 1 to 13% in the mobility data reported here. Similar behaviors were also observed in separation of ssDNA in chemically polymerized crosslinked polyacrylamide slab gels [78]. This inconsistency in measured mobilities may be caused by irregularities in gel structures.

More variation was observed in the free solution mobility calculated from two consecutive scans, ranging from 8 to 63% for dsDNA and 13 to 61% for ssDNA, respectively. The average free solution mobility (μ_0) was determined to be $1.9 \pm 0.4 \times 10^{-4}$ and $3.6 \pm 0.1 \times 10^{-4}$ cm^2/Vs for dsDNA and ssDNA, respectively. These results are in agreement

with literature values (Table III-1) determined under similar conditions when corrected to T = 22 and 55 °C for dsDNA and ssDNA, respectively, by scaling the ratio of water viscosity at two different temperatures [46].

Table III-1. Summary of measured free solution mobility

Reference	Free Solution Mobility (cm^2/Vs)	DNA Sample
Nkodo *et al.* [45]	4.0×10^{-4}	dsDNA
Rhee *et al.* [79]	3.3×10^{-4}	dsDNA
Fabrizio *et al.* [39]	1.1×10^{-4}	dsDNA
Rousseau *et al.* [13, 42]	3.8×10^{-4}	ssDNA
Pluen *et al.* [27]	3.3×10^{-4}	ssDNA
Brahmasandra *et al.* [38]	2.8×10^{-4}	ssDNA
Lo *et al.* [77]	3.5×10^{-4}	ssDNA

3.3.3 Dispersion coefficients

As shown in Figure III-10, the dispersion coefficients measured in the finish line mode are larger than those in the panorama mode, and the difference is more obvious with increasing fragment sizes. This trend is consistent with observations in the mobility data from the two detection modes. A "plateau" in D^E values from the finish line mode was observed for fragments size ranging from 250 to 500 bp. Similar phenomena were also observed in separation of ssDNA in UV polymerized polyacrylamide gels on both a desktop sequencer [77] and a microfluidic electrophoresis chip [44].

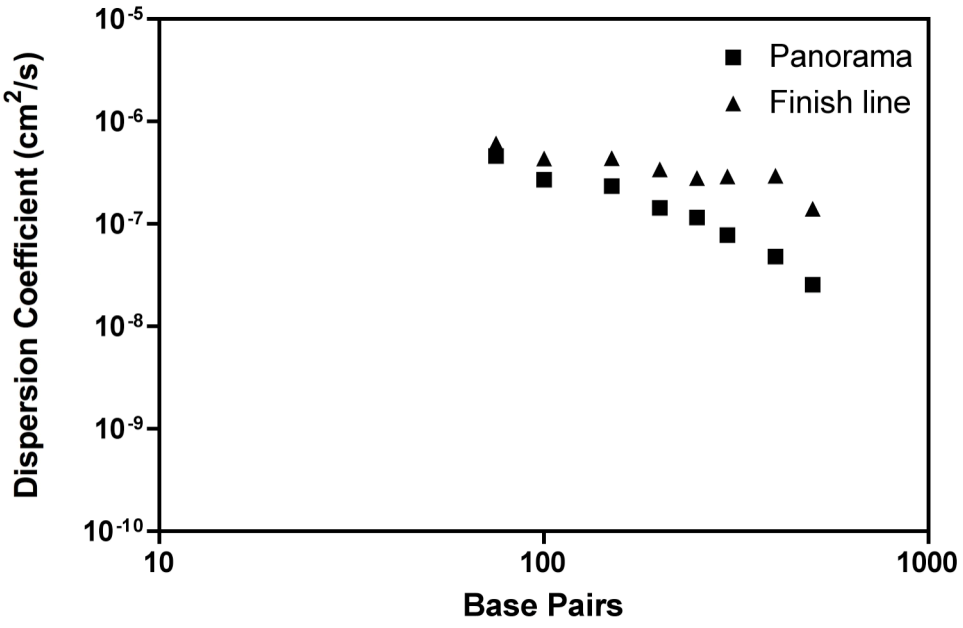

Figure III-10. Dispersion data for 6%T Duracryl gel with 12% Rhinohide gel strengthener. Run conditions: $T = 22°C$, and $E = 15$ V/cm.

The D^E values collected in the panorama mode do not show a tapering-off trend for fragments larger than 200 bp. The scaling relationship between the dispersion coefficients and fragment size (M) approaches to a power law of M^{-2} (slope = -1.42) instead of a slope of -0.60 in the same size range of dispersion data collected in the finish line mode. This is consistent with the first regime of the BRF model.

The discrepancy in dispersion coefficient scaling may result from the different detection schemes used in data collection. For the finish line mode, three individual runs with different separation lengths (e.g. 0.4, 0.5, and 0.6 cm, respectively) are needed to determine

one set of D^E data. However, there are run-to-run variations for this scheme, even with the same gel formulation and operating conditions. For example, the gel structure and fluorescence signal baseline would not be exactly the same for all the three individual runs. In addition, the fluorescence signals from fragments migrating in a long separation distance decays sometimes to a level approaching that of the background noise, which makes it difficult to accurately fit the corresponding peaks and obtain consistent results.

These issues are eliminated in the panorama mode, because each set of D^E data is determined within one single run by taking series of images at several time intervals during the separation process. This not only significantly reduces the experiment time but also ensures consistent run conditions for data collection.

3.3.4 Separation resolution

In Section 2.3.5, we demonstrated the separation resolution could be well predicted with measured mobility and dispersion data. Using equation (I-14), the single-base separation resolution for both detection schemes was calculated and shown in Figure III- 11.

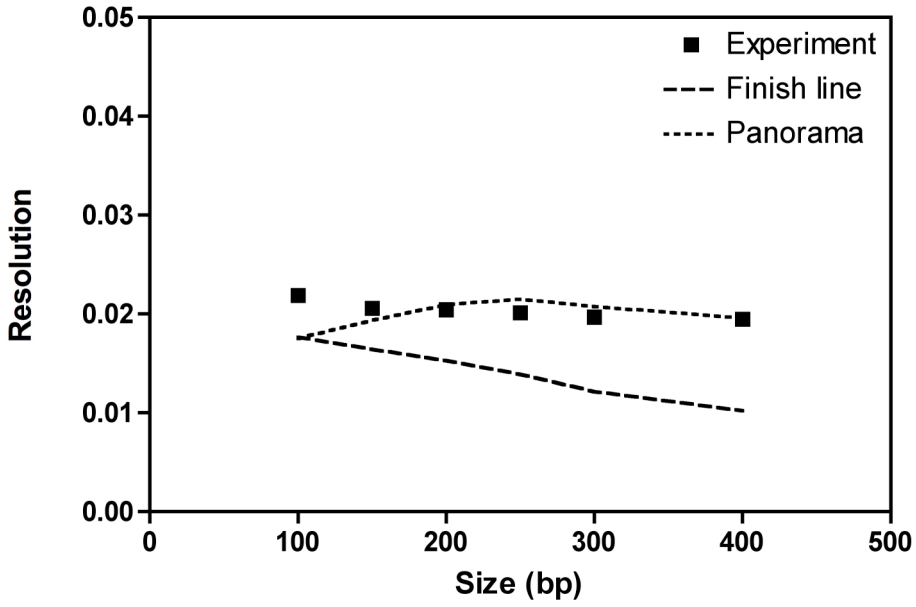

Figure III-11. Separation resolution vs. DNA fragment size. Dotted lines represent predictions using equation (2) based on mobility and dispersion coefficients measured in the finish line and panorama modes. Run conditions: 6 %T Duracryl gel, 15 V/cm, 0.5X TBE, YOYO-1 dye, T = 22°C, and L = 0.5 cm.

The measured separation resolution remained relatively constant (R ~ 0.020) over the size range studied here. The predicted R values from the panorama mode were in good agreement with the experimental values, while those from the finish line mode showed a decreasing trend ranging from ~0.017 to ~ 0.011 under the same run conditions. The decreased separation resolution resulted from the extended residence time in the gel for each DNA fragment migrating to the detection window in the finish line mode, which caused more band broadening because each fragment had to migrate over the entire

separation length. This effect was more obvious for larger fragments. For example, the residence time was 703 s for the 400-bp fragment in the panorama mode and 1224 s for the same fragment in the finish line mode with a separation length of 0.5 cm. The resulting separation resolution was ~ 0.020 for the panorama mode and ~ 0.011 for the finish line mode. The separation resolution decreased with an increasing residence time.

3.4 Concluding remarks

We designed and built a new automated rapid whole-gel scanning detection system for DNA microchip electrophoresis and had demonstrated its capability to collect a complete set of mobility and dispersion data in one separation run within an hour instead of multiple runs for hours or even days on the conventional platform using single-point detection. In addition to much shorter analysis time, our system also enables the user to observe in nearly real time throughout the entire gel the evolution of separation process with a high temporal and spatial resolution by rapid acquisition of gel images during the separation run. This ability provides a more detailed picture of the separation process that can be used to refine theoretical models and improve the separation performance of the next-generation electrophoresis technology.

In this study, we performed single-color, single-lane whole-gel scanning detection for microchip electrophoresis. With further automation and design, it is potential to develop a multiple-color, multiple-lane whole-gel scanning detection system for not only DNA but also other analytes such as RNA and proteins. We hope that the results from this

work can identify a more powerful tool for the whole electrophoresis community to get more insight into the fundamental physics of DNA electrophoresis and thus be able to rapidly design and screen potential materials as sieving matrices.

CHAPTER IV

MEASUREMENTS OF dsDNA MIGRATION PARAMETERS IN MICROCHIP GEL ELECTROPHORESIS

This chapter details measurements of the mobility and dispersion coefficient for dsDNA under different dye and buffer conditions. After comparing these migration data, we found that the dispersion coefficients measured in the Clark-Mathies buffer were more consistent with predictions of the BRF model. We speculate that this resulted from the more stabilized dye-DNA complex in the CM buffer.

4.1 Introduction

DNA labeling is a technique used in DNA gel electrophoresis for sample detection. There are three types of DNA labeling, including radioisotopes, chemiluminescent detection, and fluorescent dyes. Conventionally, several radioisotopes (usually ^{32}P, ^{33}P, ^{35}S or ^{3}H) are incorporated into DNA fragments for labeling [80]. These markers are now less popular because of health and environmental issues. The chemiluminescent detection relies on a biotin-streptavidin marker emitting photons after an enzymatic reaction [81]. There are no radioactivity issues with this method. However, it requires both chemically attaching the biotin-streptavidin marker and an enzyme-catalyzed reaction to work. Fluorescent dyes were first used in DNA sequencing [82]. There are two methods of fluorescence labeling, covalent attachment [82] and intercalation [83]. The covalent attachment of a fluorescent dye to DNA fragments requires synthesis of fluorescent oli-

gonucleotide primers. The intercalation of a fluorescent dye is the insertion of the planar aromatic component of the dye molecule between two base pairs of dsDNA [84]. This process does not involve any primer synthesis or covalent bonding and is therefore a simple alternative for DNA fluorescence labeling. The labeling can be performed before separation by simply mixing the DNA sample with the dye solution. Several dimeric intercalating dyes, e.g. Ethidium homodimer (EthD), YOYO, and TOTO, have been demonstrated to form stable, highly fluorescent complexes with dsDNA molecules under slab gel electrophoresis conditions [83, 85]. However, several cases of band splitting, smearing, and low fluorescence signal have been reported in separations using TAE and TBE buffers [86-88]. Clark *et al.* found that the cation in the running buffer greatly affects the quality of these DNA separations and that tetrapentylammonium (NPe_4^+) can significantly improve the quality of the separation runs by making cationic dyes, such as TOTO and YOYO, bind more tightly to dsDNA molecules [89].

In this chapter, we investigated the effects of labeling dyes and running buffers on behaviors of dsDNA migrating in the sieving gel by measuring mobility and dispersion coefficients using our whole-gel scanning detection system.

4.2 Experimental setup

The collection of mobility and dispersion data of dsDNA under different dye and buffer conditions followed the general procedure outlined in Chapter III.

4.2.1 Running buffers

The TBE buffer was prepared by diluting a 10X stock solution (Extended Range TBE buffer, Catalog number: 161-0741; BioRad, Hercules, CA) to the desired final concentration (0.5X) with deionized water. The Clark-Mathies buffer ("1X CM buffer") [89] was prepared by adding proper amounts of 3-[[tris(hydroxymethyl)-methyl]amino]propanesulfonic acid (catalog# T5316; Sigma-Aldrich, St. Louis, MO) and EDTA salt (catalog# 161-0728; Bio-Rad Laboraories, Hercules, CA) to deionized water. This mixture was then titrated with NPe_4OH solution (catalog# 88005; Sigma-Aldrich, St. Louis, MO) until pH reaches 8.4. The final solution contained 80 mM taps-NPe_4 and 1 mM H_2EDTA.

4.2.2 DNA sample preparation

DNA samples were prepared in a total volume of $10\,\mu L$ for runs under the same conditions. The dsDNA sample labeled with intercalating dyes was composed of $1\,\mu L$ of unlabeled MapMarker standard ladder, $4\,\mu L$ of labeling dye, $4\,\mu L$ of deionized water, and $1\,\mu L$ of 2-mercaptoethanol. The intercalating dyes, YOYO-1 and SYBR Green I, were purchased from Invitrogen Corporation (Carlsbad, CA). The fluorescein-labeled dsDNA sample was prepared by mixing $1\,\mu L$ of pre-labeled MapMarker standard ladder, $8\,\mu L$ of

deionized water, and 1 μL of 2-mercaptoethanol. For each gel separation experiment, 0.2 μL of the sample was loaded into the injection channel.

4.3 Results and discussion

4.3.1 Mobility

We performed a series of experiments to measure mobility of dsDNA fragments labeled with three different dyes in both 0.5X TBE and 1X CM buffers. In the TBE buffer (Figure IV-1a), we observed the measured mobilities of dsDNA fragments labeled with intercalating dyes (YOYO-1 and SYBR Green I) are lower than those of fluorescein end-labeled fragments. YOYO-1 and SYBR Green I are positively charged intercalating dyes (+2 and +1, respectively). They reduce the mobility of DNA by increasing the contour length of the DNA molecule and canceling the negative charge carried by the DNA backbone [90]. Fluorescein is negatively charged (-2) and covalently attached to DNA with one dye molecule on one strand of the dsDNA fragment. It does not significantly change the contour length or affect the charge of the labeled DNA fragment. As a result, measured mobilities of YOYO-1 labeled dsDNA fragments are expected to be lower than those labeled with the other two dyes.

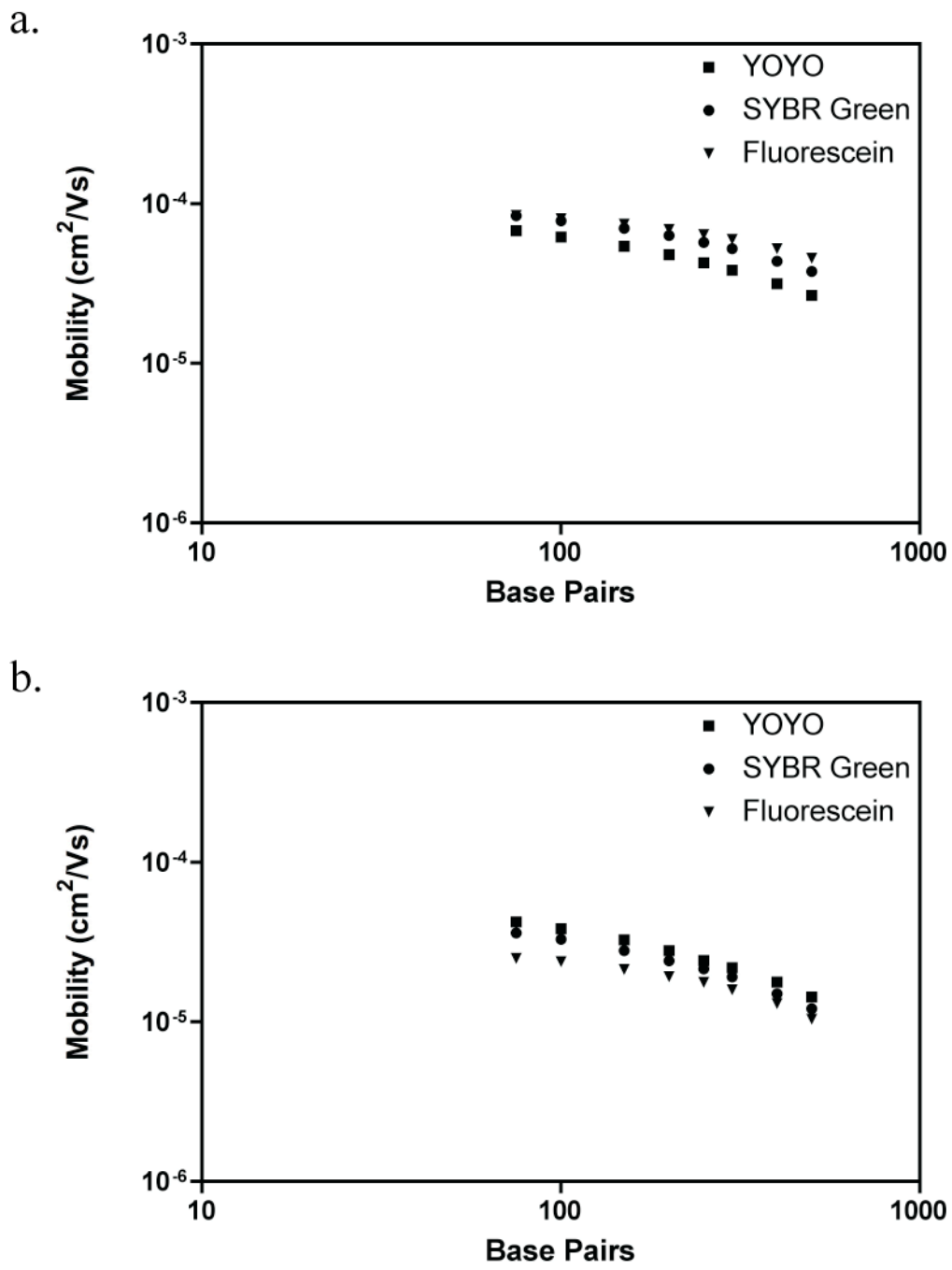

Figure IV-1. Measured mobility of dsDNA fragments labeled with different fluorescent dyes in (a) 0.5 X TBE and (b) 1X CM buffer. Run conditions: 6%T Duracryl gel, T = 22°C, and E = 15 V/cm.

In the CM buffer, the large cation, NPe_4^+, disrupts the dynamic dissociation of the intercalating dye molecule from the DNA fragment and thus makes the dye-DNA complex more stable during the electrophoresis process [89]. The intercalating dyes are more tightly bound to the DNA molecule. The reduced mobility values may result from the counterion atmosphere around the DNA molecule formed by the NPe_4^+ ions, which shields the repulsion force from the applied electric field [89, 91].

Under the dye and buffer conditions used here, the base lines for extracted intensity data were all very smooth (Figures IV-2 and IV-3). All the peaks were in a symmetric shape. Generally, the fluorescence traces of DNA fragments labeled with YOYO-1 and SYBR Green I were smoother in the CM buffer than in TBE (see (a) and (b) in Figures IV-2 and IV-3), but there was no obvious difference observed for fluorescein-labeled fragments. The rougher peaks for 75-bp fragments may result from lower fluorescence signal-to-noise ratio after migration and dispersion in the gel.

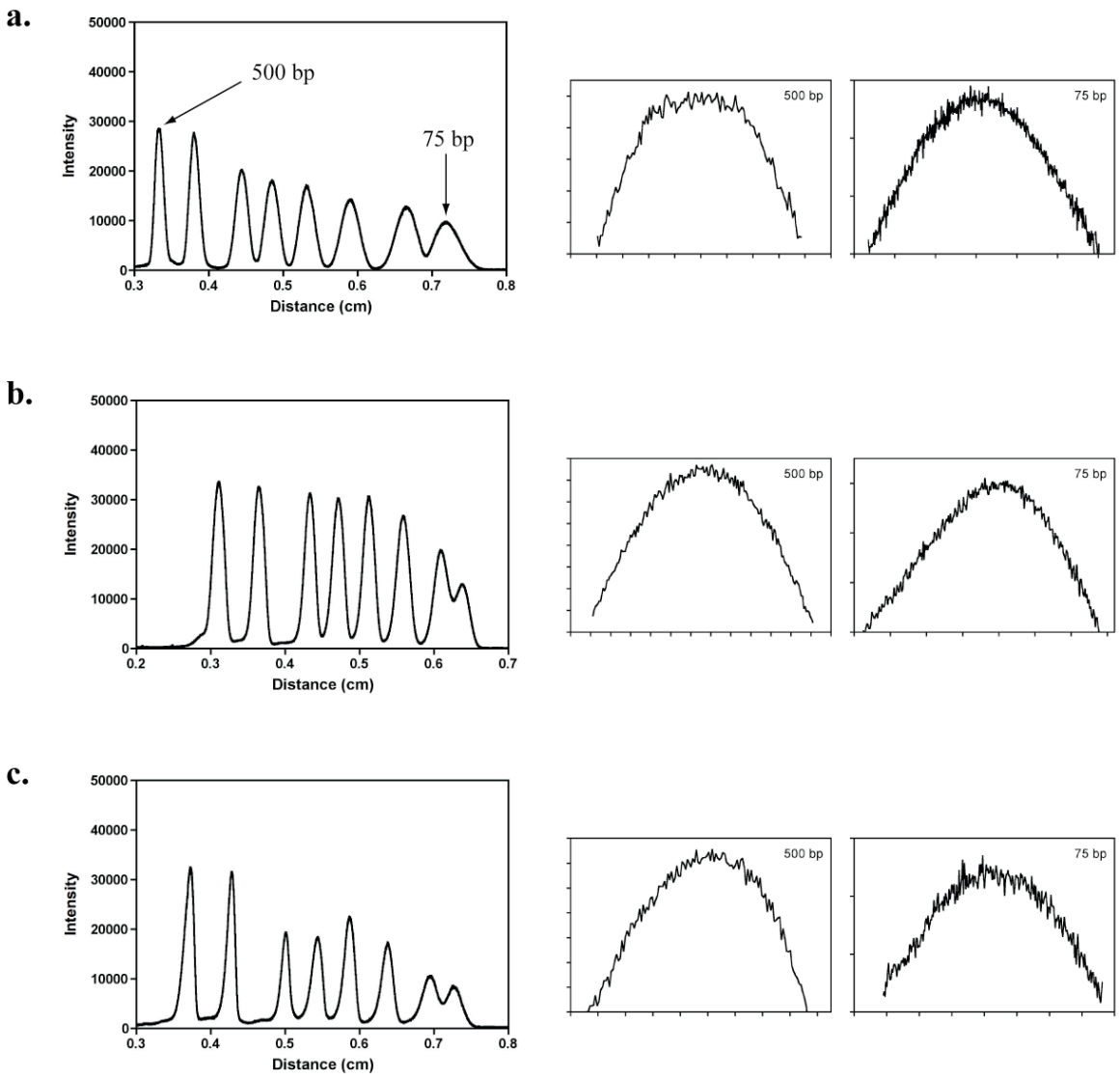

Figure IV-2. Intensity data for dsDNA fragments labeled with (a) YOYO-1, (b) SYBR Green I, and (c) fluorescein. Run conditions: 6%T Duracryl gel, 0.5X TBE, T = 22°C, and E = 15 V/cm.

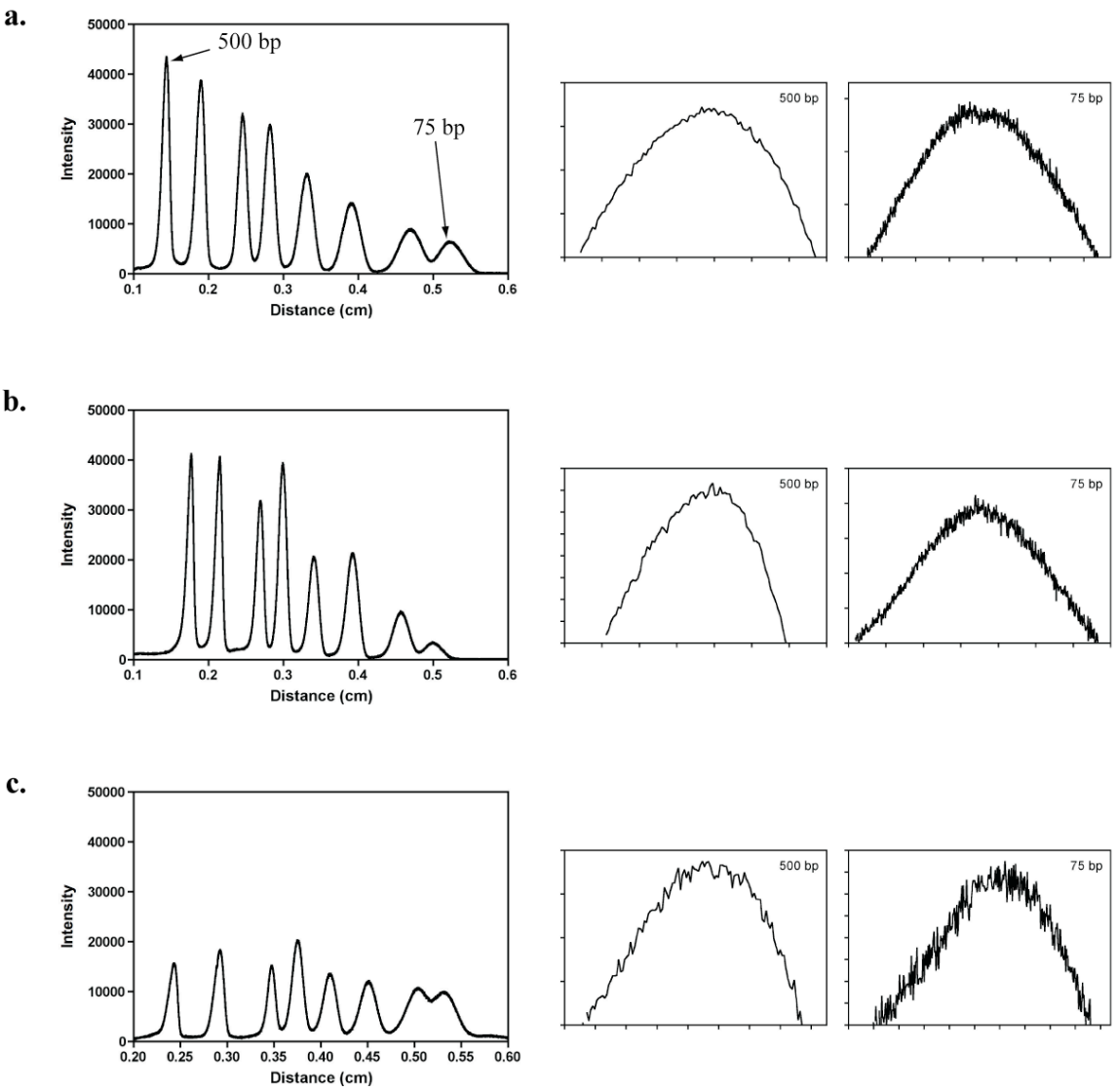

Figure IV-3. Intensity data for dsDNA fragments labeled with (a) YOYO-1, (b) SYBR Green I, and (c) fluorescein. Run conditions: 6%T Duracryl gel, 1X CM buffer, T = 22°C, and E = 15 V/cm.

The free solution mobility of both dsDNA and ssDNA was directly measured in TBE and CM buffers. The measured values are in reasonable agreement with those in the literature (see Section 3.3.2).

Table IV-1. Free solution mobility of fluorescently labeled dsDNA and ssDNA

Labeling dye	Mobility (cm2/Vs)	
	0.5X TBE	1X CM
Fluorescein[a]	$3.59 \pm 0.10 \times 10^{-4}$	$2.09 \pm 0.42 \times 10^{-4}$
YOYO-1[b]	$1.89 \pm 0.42 \times 10^{-4}$	$1.91 \pm 0.57 \times 10^{-4}$
SYBR Green I[b]	$1.44 \pm 0.14 \times 10^{-4}$	$1.27 \pm 0.02 \times 10^{-4}$
Fluorescein[b]	$1.94 \pm 0.50 \times 10^{-4}$	$1.28 \pm 0.34 \times 10^{-4}$

a) ssDNA. $T = 55°C$, and $E = 5$ V/cm.
b) dSDNA. $T = 22°C$, and $E = 5$ V/cm.

4.3.2 Dispersion coefficients

In the TBE buffer (Figure IV-4a), the measured dispersion coefficients of YOYO-labeled dsDNA fragments scales as the prediction of the first regime of the BRF model (slope = -1.42), but those of SYBR Green- and fluorescein- labled fragments show a rapid decreasing trend for smaller fragments and taper off beyond 200 bp with slopes of -0.83 and -0.75, respectively. Similar behaviors were observed in dispersion data of ssDNA separated in similar photopolyacrylamide gels and TBE buffer on the same microfluidic gel electrophoresis device [44].

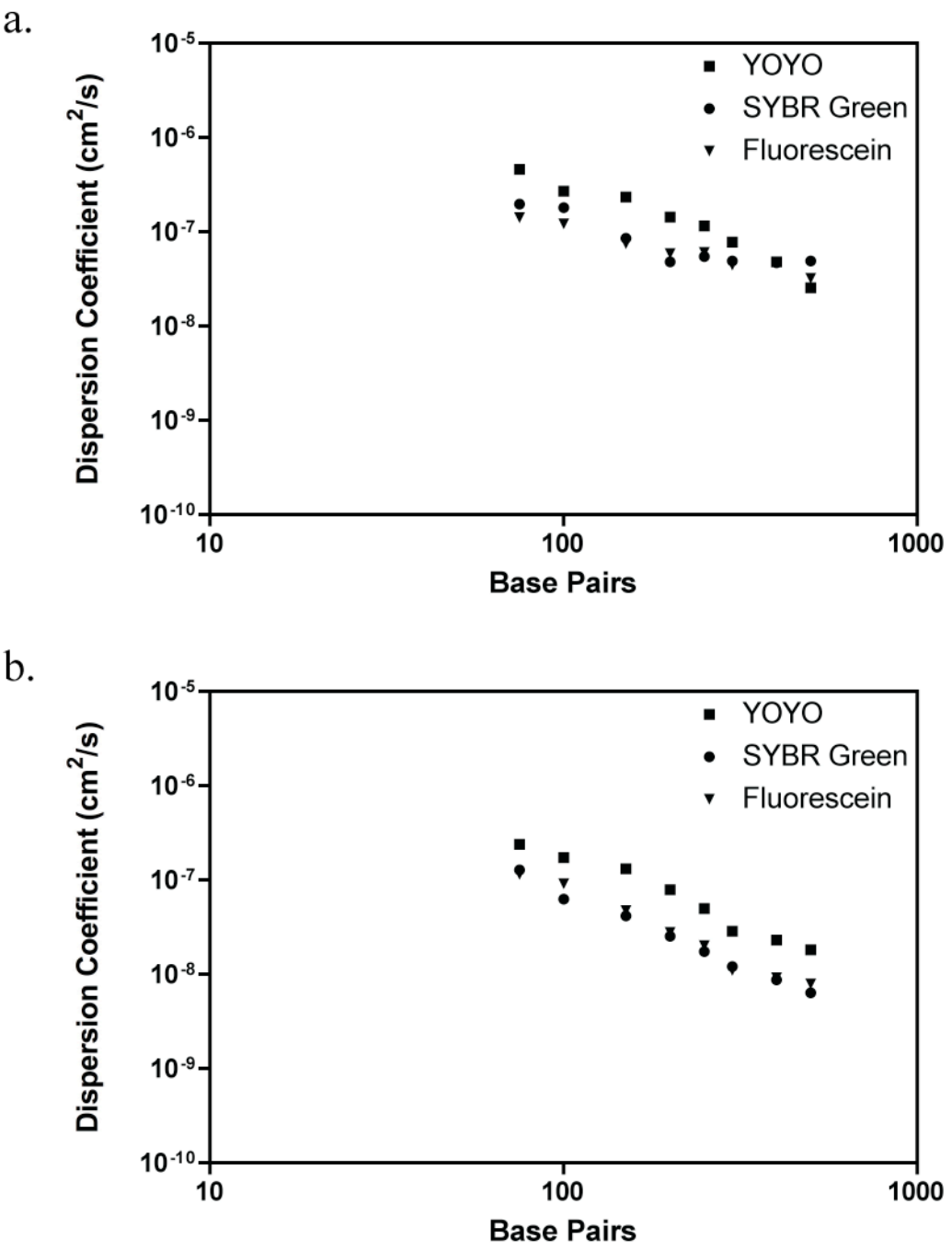

Figure IV-4. Measured dispersion coefficients of dsDNA fragments labeled with different fluorescent dyes in (a) 0.5 X TBE and (b) 1X CM buffer. Run conditions: T = 22°C, and E = 15 V/cm.

As shown in Figure IV-4b, the measured dispersion coefficients are lower in the CM buffer. It is interesting to note that measured D^E values scale consistently with fragment size in good agreement with the first regime of the BRF model for all the three labeling dyes (slope = ~ -1.5). There is no "plateau" region observed for fragments larger than 200 bp as in the TBE buffer. However, the details of this behavior are still not fully understood.

4.3.3 Separation resolution

The single-base separation resolution (R) for DNA gel electrophoresis was calculated using mobility and dispersion data measured under different dye and buffer conditions. In 0.5X TBE buffer (Figure IV-5a), the predicted separation resolution of DNA fragments labeled with SYBR Green and fluorescein remained relatively constant over the whole size range. For YOYO-labeled fragments, R first increased with size between 100 and 200 bp and remained constant thereafter.

In the 1X CM buffer (Figure IV-5b), the separation resolution for DNA labeled with the three dyes became higher than in 0.5X TBE especially for SYBR Green-labeled fragments. The R values for DNA labeled with these three dyes showed an increasing trend with fragment size and then remained roughly constant thereafter.

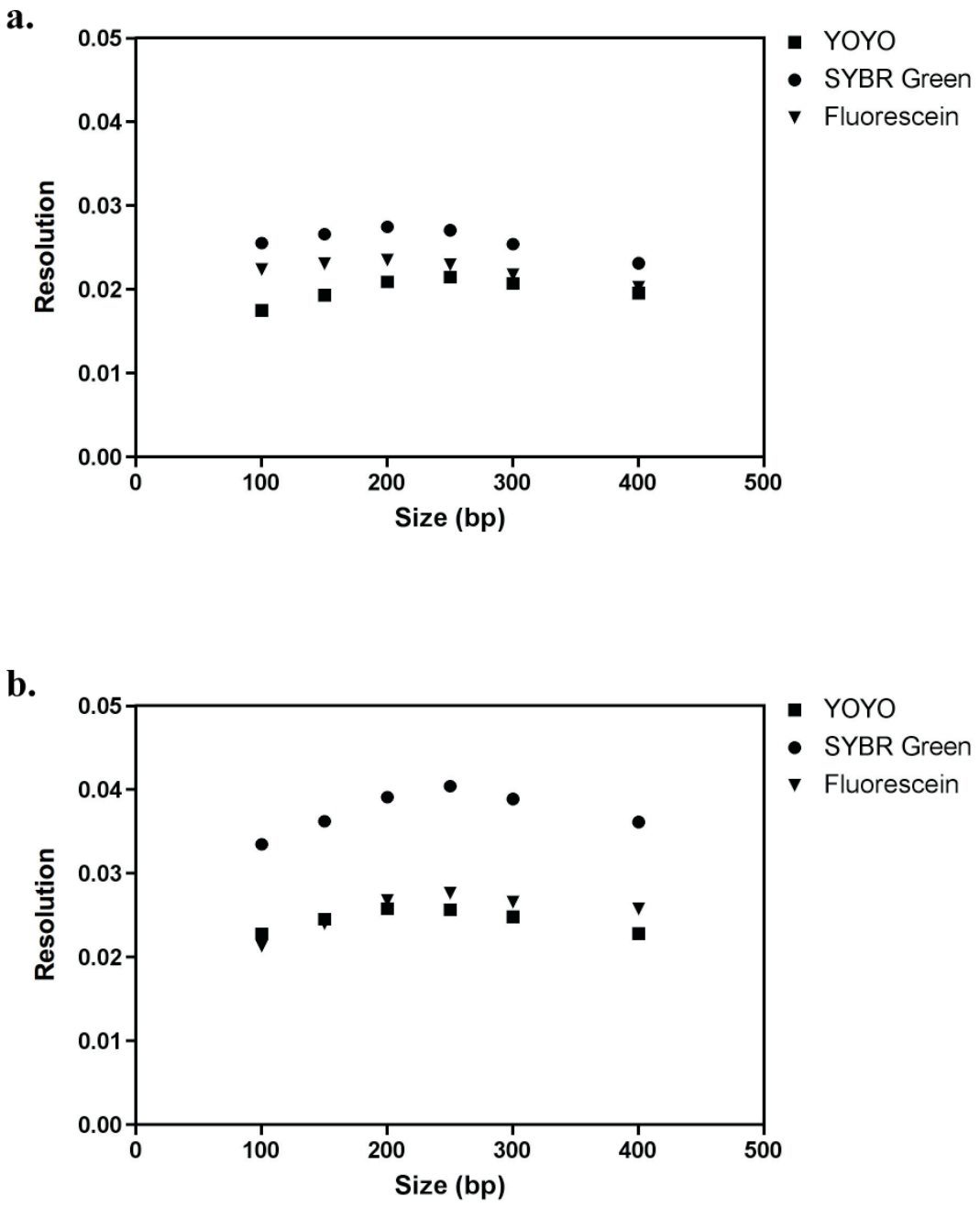

Figiure IV-5. Predicted single-base separation resolution in (a) 0.5X TBE and (b) 1X CM buffer. Run conditions: 6 %T Duracryl gel, 15 V/cm, and $T = 22°C$. $L = 0.5$ cm was used to calculate separation resolution.

4.4 Concluding remarks

We have collected migration parameters (mobility and dispersion coefficient) of dsDNA separation in photopolymerized crosslinked polyacrylamide gels with both TBE and CM buffers on our automated whole-gel scanning detection system. These data can be obtained within 10 minutes instead of hours or even days on conventional electrophoresis systems.

The CM buffer has proven to be a good running buffer for capillary electrophoresis separation of dsDNA labeled with intercalating dyes, because it stabilizes the dye-DNA complex and there is no mobility shift for a wide range of dye to DNA ratio [89, 91]. After analysis and comparison of migration data acquired in both TBE and CM buffer, we found that the CM buffer can also serve as a good running buffer for such separations on the microfluidic gel electrophoresis chip, because the mobility and dispersion data are more consist, especially the D^E scaling. There is no flat section for larger fragments (200 bp and beyond) as observed in the TBE buffer. However, the details of how this buffer affects the dispersion behaviors of the DNA are still not very clear. More work will be needed to investigate its effects.

CHAPTER V

TEST OF MERCIER-SLATER DISPERSION MODEL

This chapter details tests of the Mercier-Slater dispersion model for its goodness of fitting for dispersion coefficients. We tested this model with our mobility and dispersion data of both ssDNA and dsDNA under different run conditions, and also proposed an alternative model for comparison.

5.1 Introduction

Mobility (μ) and dispersion coefficient (D^E) are two important parameters for characterization of the separation performance of DNA gel electrophoresis. These parameters have been studied both theoretically [20, 36, 92, 93] and experimentally [38, 44, 73, 77, 94]. Different scaling regimes (i.e. Ogston regime, the reptation regime, and the reptation with orientation regime) for both mobility and dispersion coefficient versus DNA fragment size have been proposed and experimentally verified. However, they work separately instead of jointly as a uniform function with smooth transitions between different regimes. There are currently no theories unifying these scaling relationships for both μ and D^E as single general equations. Van Winkle *et al.* [68, 69] proposed an empirical equation that provides good mobility fit for dsDNA fragments migrating in these scaling schemes. Based on this empirical model, Mercier *et al.* [95] proposed a universal interpolating equation for D^E of DNA fragments migrating in sieving gels (referred to as the M-S dispersion model thereafter).

In this chapter, we tested the M-S dispersion model with our mobility and dispersion data of both ssDNA and dsDNA for its goodness of fitting. For comparison, we applied the same model to the data from Brahmasandra *et al* at a similar electric field strength. We also proposed an alternative model and tested its goodness of fitting.

5.2 Mobility fitting

The vWBR model was used to fit mobility data of both ssDNA and dsDNA fragments migrating in photopolymerized and chemically polymerized polyacrylamide gels.

$$\mu(M,C) = \frac{\mu(0,C)}{1 + \left(\frac{\mu(0,C)}{\mu(\inf,C)} - 1 \right) \left(1 - e^{-M/m} \right)} \qquad \text{(II-6)}$$

where m is a fitting parameter in bases/base pairs, C is the gel concentration, and $\mu(0, C)$ and $\mu(inf, C)$ are the zero- and infinite- size mobilities, respectively. With determined fitting parameters, this model was then included in the M-S dispersion model to fit the dispersion data.

5.3 Dispersion coefficient fitting

There are at least three major regimes for both μ and D^E, depending on the relative sizes between the DNA molecule and the gel pore. In the Ogston regime (Regime I), the DNA molecule is smaller than the mean gel pore size and easily sieved through the gel. In the reptation regime (Regime II), the DNA molecule remains in a random coil conformation larger than the mean gel pore size and threads head first through the gel. In the the reptation with orientation regime (Regime III), the large DNA molecule is oriented in the

direction of the applied electric field and migrates through the gel in an elongated conformation. There is no separation possible in this regime. Among these regimes, the reptation regime is of most interest from researchers, because it is where the DNA mobility scales linearly with its size ($\mu \propto M^{-1}$), which makes it possible to perform DNA separation in a sieving gel matrix.

The M-S dispersion model was developed based on an empirical universal interpolating function for DNA mobility (vWBR model). The scaling relationships for these three major regimes for D^E were mathematically joined to generate a universal function that makes smooth transitions between different regimes [95].

$$D^E(M,C,E) = [(D_I^E)^x + (D_{II}^E)^x + (D_{III}^E)^x]^{1/x} \tag{V-1}$$

$$D^E(M,C,E) = ([\frac{k_B T}{q_{eff}} vWBR(M,C,E)]^2 \frac{1}{M^2 + M_0(C,E) * M} + \frac{D_R^2(C,E)}{M} + D_\infty^2(C,E))^{1/2}$$

where k_B is the Boltzmann constant, T is the Kelvin temperature, q_{eff} is the effective charge per monomer, and $vWBR$ is the mobility determined by the vWBR model. M_0, D_R, and D_∞ are fitting parameters. M_0 is the DNA molecular size that is comparable to the mean gel pore size. D_R is the dispersion coefficient of the DNA molecule whose relative size is close to the transition between the regimes of reptation and reptation with orientation. D_∞ is the dispersion coefficient of the DNA molecule whose relative size reaches the reptation with orientation regime. It is independent of the fragment size.

Here, we used the first two regimes of the M-S dispersion model to fit our dispersion data, because we did not observed the reptaion plateau regime, which is associated with the term D_∞. To see the individual contribution of the terms associated with Regimes I and II, we plotted them separately with the measured D^E data.

$$D_I^E(M,C,E) = ([\frac{k_B T}{q_{eff}} vWBR(M,C,E)]^2 \frac{1}{M^2 + M_0(C,E) * M})^{1/2} \quad \text{(V-2)}$$

$$D_{II}^E(M,C,E) = [\frac{D_R^2(C,E)}{M}]^{1/2} \quad \text{(V-3)}$$

In the course of testing the M-S dispersion model, we always got large M_0 values, usually more than the whole size range studied. To investigate how M_0 values would change in a different expression, we decided to change the denominator in Regime I from

$$\frac{1}{M^2 + M_0(C,E) * M} \quad \text{to} \quad \frac{1}{(M + \sqrt{M_0(C,E) * M})^2}$$

This change was chosen because the M_0 values were generally reduced by half or more when using this relationship, and it had a similar form to that of equation (V-1). The revised model was referred to as the "modified denominator model" thereafter and was evaluated for its goodness of dispersion data fitting.

$$D^E(M,C,E) = ([\frac{k_B T}{q_{eff}} vWBR(M,C,E)]^2 \frac{1}{(M + \sqrt{M_0(C,E) * M})^2} + \frac{D_R^2(C,E)}{M})^{1/2} \quad \text{(V-4)}$$

$$D_I^E(M,C,E) = ([\frac{k_B T}{q_{eff}} vWBR(M,C,E)]^2 \frac{1}{(M + \sqrt{M_0(C,E) * M})^2})^{1/2} \quad \text{(V-5)}$$

$$D_{II}^E(M,C,E) = [\frac{D_R^2(C,E)}{M}]^{1/2} \quad \text{(V-6)}$$

The effective charge per monomer, q_{eff}, for both ssDNA and dsDNA is summarized in Table V-1.

Table V-1. Summary of effective charge per monomer for ssDNA and dsDNA

Reference	Effective charge per monomer (e/monmer)	
	ssDNA	dsDNA
Ross *et al.* [96]	-0.18[a]	-0.36
Smith *et al.* [97]	-0.05/-0.03[a]	-0.1[b]/-0.06[c]
Pluen *et al.* [27]	-0.2	-0.4[d]

a) Half of the measured value of dsDNA
b) Calculated with a persistence length of 50 nm
c) Calculated with a persistence length of 82.5 nm
d) Two times of the measured value of ssDNA

In our test, we used -0.05e and -0.1e as the effective charge per monomer for ssDNA and dsDNA, respectively. The temperature, T, was 328.15 and 295.15 K for ssDNA and dsDNA, respectively. Prism 4 (GraphPad Software, San Diego, CA) was used to perform all nonlinear fitting processes. The steps of dispersion fitting are described below, and the initial guess for each fitting parameter is shown in Table V-2.

1. Fit the measured mobility data into the vWBR model to determine the fitting parameters, $\mu(0, C)$, $\mu(inf, C)$, and m.
2. Place the determined parameters in the vWBR model and combine it with the M-S dispersion model.
3. Use the M-S dispersion model to fit the measured dispersion data to determine the fitting parameters, M_0 and D_R.

Table V-2. Initial guesses for fitting parameters

Model	Initial Guess		
vWBR	$\mu(0, C)$ (cm^2/Vs)	$\mu(inf, C)$ (cm^2/Vs)	m (bp)
	1.0×10^{-5}	1.0×10^{-5}	100
M-S dispersion	M_0 (bp)		D_R (cm^2/s)
	100		1.0×10^{-10}

5.4 Results and discussion

5.4.1 Mobility fitting

We used the vWBR model to fit the mobility data collected in both photopolymerized and chemically polymerized polyacrylamide gels. For ssDNA (Figure V-1), the fit well captured both qualitatively and quantitatively the trend of scaling between mobility and DNA fragment size. However, values of standard deviation for the fitting parameter *m* were very large, indicating large uncertainty. We further verified this by comparing with ssDNA mobility data from Brahmasandra *et al*. This may result from the run temperature (55ºC) used in our separation experiments, because Kopecka *et al.* had similar issues with their mobility data collected at 60ºC. For dsDNA mobility data (Figure V-2), the fit was good qualitatively and quantitatively, but large values of standard deviation for *m* were also observed in these fits.

a.

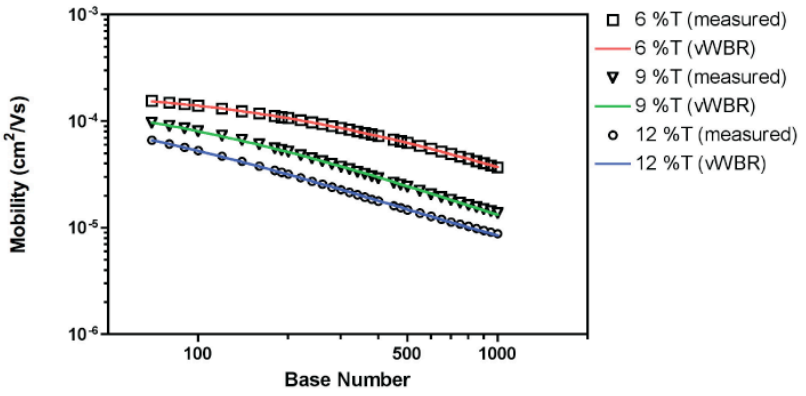

Parameters	6%T	9%T	12%T
μ(0, C)	$(2.03 \pm 0.005) \times 10^{-4}$	$(1.89 \pm 0.03) \times 10^{-4}$	$(1.73 \pm 0.03) \times 10^{-4}$
μ(∞, C)	$(1.25 \pm 0.62) \times 10^{-6}$	$(3.69 \pm 6.57) \times 10^{-7}$	$(2.66 \pm 0.20) \times 10^{-6}$
m	35624 ± 17738	38039 ± 67961	2770 ± 239

b.

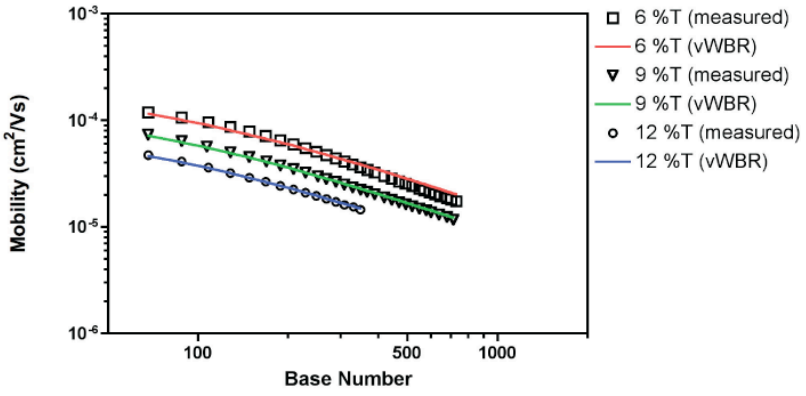

Parameters	6%T	9%T	12%T
μ(0, C)	$(2.25 \pm 0.09) \times 10^{-4}$	$(1.50 \pm 0.02) \times 10^{-4}$	$(9.70 \pm 0.13) \times 10^{-5}$
μ(∞, C)	$(8.48 \pm 440) \times 10^{-8}$	$(6.10 \pm 96.5) \times 10^{-8}$	$(7.78 \pm 96.8) \times 10^{-8}$
m	$(1.91 \pm 96.5) \times 10^{5}$	$(1.54 \pm 24.2) \times 10^{5}$	$(7.84 \pm 97.2) \times 10^{4}$

Figure V-1. Mobility fits for ssDNA. (a) measured in photopolymerized polyacrylamide gels. (b) measured in chemically polymerized polyacrylamide gels at E = 20 V/cm. Run condition: T = 55ºC in Long Ranger® polyacrylamide sequencing gels.

a.

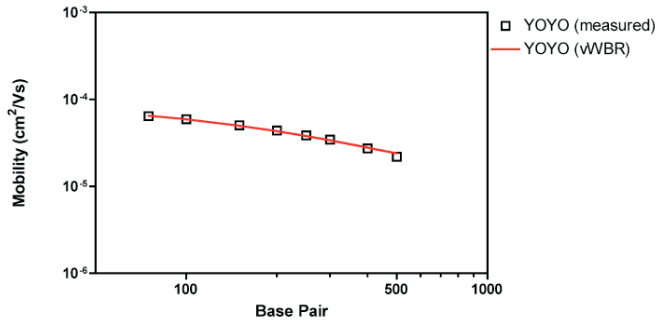

Parameters	YOYO
μ(0, C)	(9.40 ± 0.58) X 10^{-5}
μ(∞, C)	(1.57 ± 91.9) X 10^{-7}
m	(1.02 ± 59.1) X 10^{5}

b.

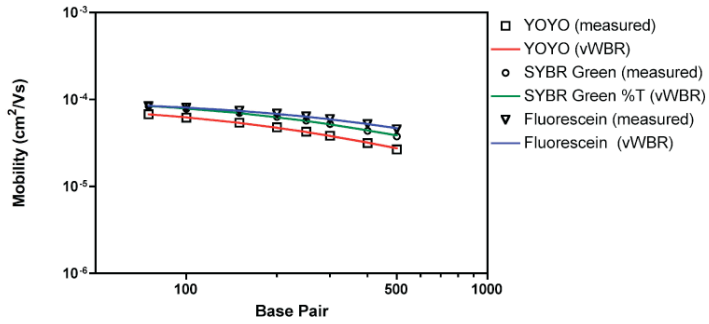

Parameters	YOYO	SYBR Green	Fluorescein
μ(0, C)	(9.17 ± 0.25) X 10^{-5}	(1.07 ± 0.03) X 10^{-4}	(9.91 ± 0.19) X 10^{-5}
μ(∞, C)	(2.18 ± 58.6) X 10^{-7}	(3.27 ± 95.9)X 10^{-7}	(4.28 ± 158) X 10^{-7}
m	(8.95 ± 240) X 10^{4}	(9.21 ± 270) X 10^{4}	(1.03 ± 37.9) X 10^{5}

c.

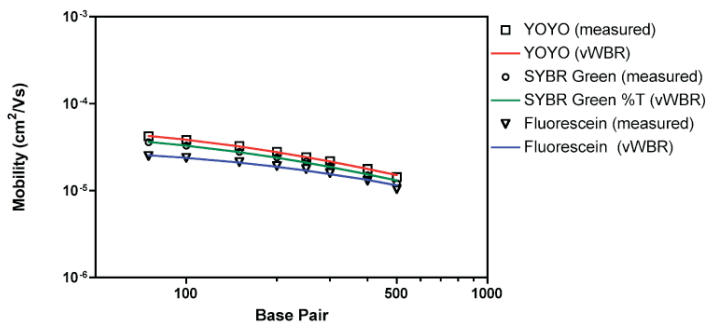

Parameters	YOYO	SYBR Green	Fluorescein
μ(0, C)	(6.28 ± 0.24) X 10^{-5}	(5.31 ± 0.32) X 10^{-5}	(3.25 ± 0.24) X 10^{-5}
μ(∞, C)	(1.14 ± 34) X 10^{-7}	(8.98 ± 481) X 10^{-8}	(8.36 ± 876) X 10^{-8}
m	(8.67 ± 257) X 10^{4}	(9.63 ± 512) X 10^{4}	(1.07 ±110) X 10^{5}

Figure V-2. Mobility fits for dsDNA. (a) Finish line mode. Run conditions: 0.5X TBE, L = 0.5 cm, E = 15 V/cm, and T = 22 ºC. (b) Panorama mode. Run conditions: 0.5X TBE, E = 15 V/cm, and T = 22 ºC. (c) Panorama mode. Run conditions: 1X CM buffer, E = 15 V/cm, and T = 22 ºC. All experiments were performed in 6%T Duracryl gels.

5.4.2 Dispersion fitting

With fitting parameters from the mobility data, we proceeded to implement the dispersion data via both the original M-S dispersion model and the modified denominator model. We used nonlinear fitting to determine the parameters M_0 and D_R. During the analysis process, we found that the fit was sensitive to the data used, e.g. the degree of scattering and/or the presence of outliers. In order to minimize these effects, we chose data from electric field strengths that appeared to give the cleanest data trends.

5.4.2.1 ssDNA

As shown in the figures (Figures V-3 ~ V-8), the magnitude of the term associated with Regime I is dominating over the range of fragment sizes studied here (M = 70 – 400 bases), while D_R is always much smaller, so its contribution to overall fitting is minimal. The difference is especially pronounced in 12%T gels. The value of M_0 is generally much larger than reasonable based on the meaning of M_0, the point where the fragment and gel pore sizes are comparable (Table V-3).

In the M-S dispersion model, M_0 is comparable to the gel pore size, and therefore it is expected to decrease with increasing gel concentrations. However, we observed that the value of M_0 generally increases with increasing gel concentrations, which appears to be the opposite of what we expected. In the beginning, we thought that the sensitivity of the fit was responsible for this observation, so we selected the cleanest data sets, but later we found that this seems to hold over most of our data.

In addition to the original M-S dispersion data, we also explored a modified model. The fit results were similar to those using the original model. D_I^E still dominates all over the range of fragment sizes studies. However, the values of M_0 obtained in this model generally decreased to half or less those from the original M-S dispersion model. We are not sure if this manipulation has any physical or mathematical basis, but this may provide another way of constructing such universal interpolating functions.

Table V-3. Summary of fitting parameters for ssDNA.

Original model:

$$D(M,C,E) = \left(\left|\frac{k_B T}{q_{eff}} vBR(M,C,E)\right|^2 \frac{1}{M^2 + (M_0(C,E) * M)} + \frac{D_R^2(C,E)}{M}\right)^{1/2}$$

Modified denominator:

$$D(M,C,E) = \left(\left|\frac{k_B T}{q_{eff}} vBR(M,C,E)\right|^2 \frac{1}{\left(M + \sqrt{M_0(C,E) * M}\right)^2} + \frac{D_R^2(C,E)}{M}\right)^{1/2}$$

Lo and Ugaz

Original model

E = 15 V/cm	6%T	9%T	12%T
M_0	1152	2086	3537
D_R	8.93 X 10^{-9}	3.93 X 10^{-9}	1.91 X 10^{-9}
R^2	0.9318	0.9783	0.9488

E = 20 V/cm	6%T	9%T	12%T
M_0	1093	1351	1330
D_R	8.37 X 10^{-9}	1.00 X 10^{-7}	1.00 X 10^{-7}
R^2	0.9347	0.9468	0.9267

Modified denominator

E = 15 V/cm	6%T	9%T	12%T
M_0	679	1099	2507
D_R	4.64 X 10^{-7}	9.04 X 10^{-8}	1.27 X 10^{-9}
R^2	0.9461	0.9855	0.9598

E = 20 V/cm	6%T	9%T	12%T
M_0	608	796	788
D_R	2.27 X 10^{-7}	1.70 X 10^{-9}	1.00 X 10^{-7}
R^2	0.9372	0.9698	0.9406

Brahmasandra *et al.*

Original model

E = 20 V/cm	6%T	9%T	12%T
M_0	2719	4409	5962
D_R	2.90 X 10^{-9}	2.42 X 10^{-10}	2.18 X 10^{-10}
R^2	0.9978	0.9985	0.9644

Modified denominator

E = 20 V/cm	6%T	9%T	12%T
M_0	2084	3601	4236
D_R	2.11 X 10^{-7}	8.50 X 10^{-8}	9.92 X 10^{-11}
R^2	0.9981	0.9987	0.9653

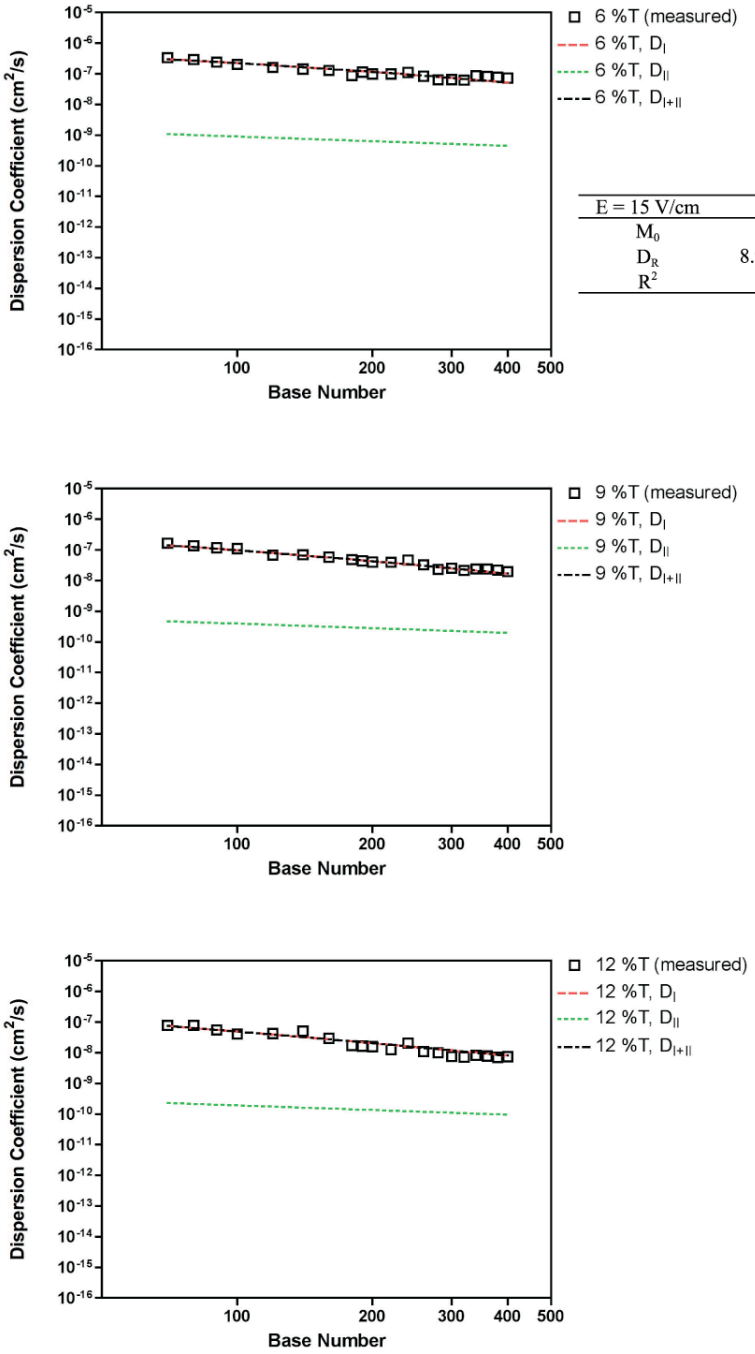

E = 15 V/cm	6%T	9%T	12%T
M_0	1152	2086	3537
D_R	8.93×10^{-9}	3.93×10^{-9}	1.91×10^{-9}
R^2	0.9318	0.9783	0.9488

Figure V-3. Dispersion coefficient versus fragment size for ssDNA. Original M-S dispersion model; E = 15 V/cm.

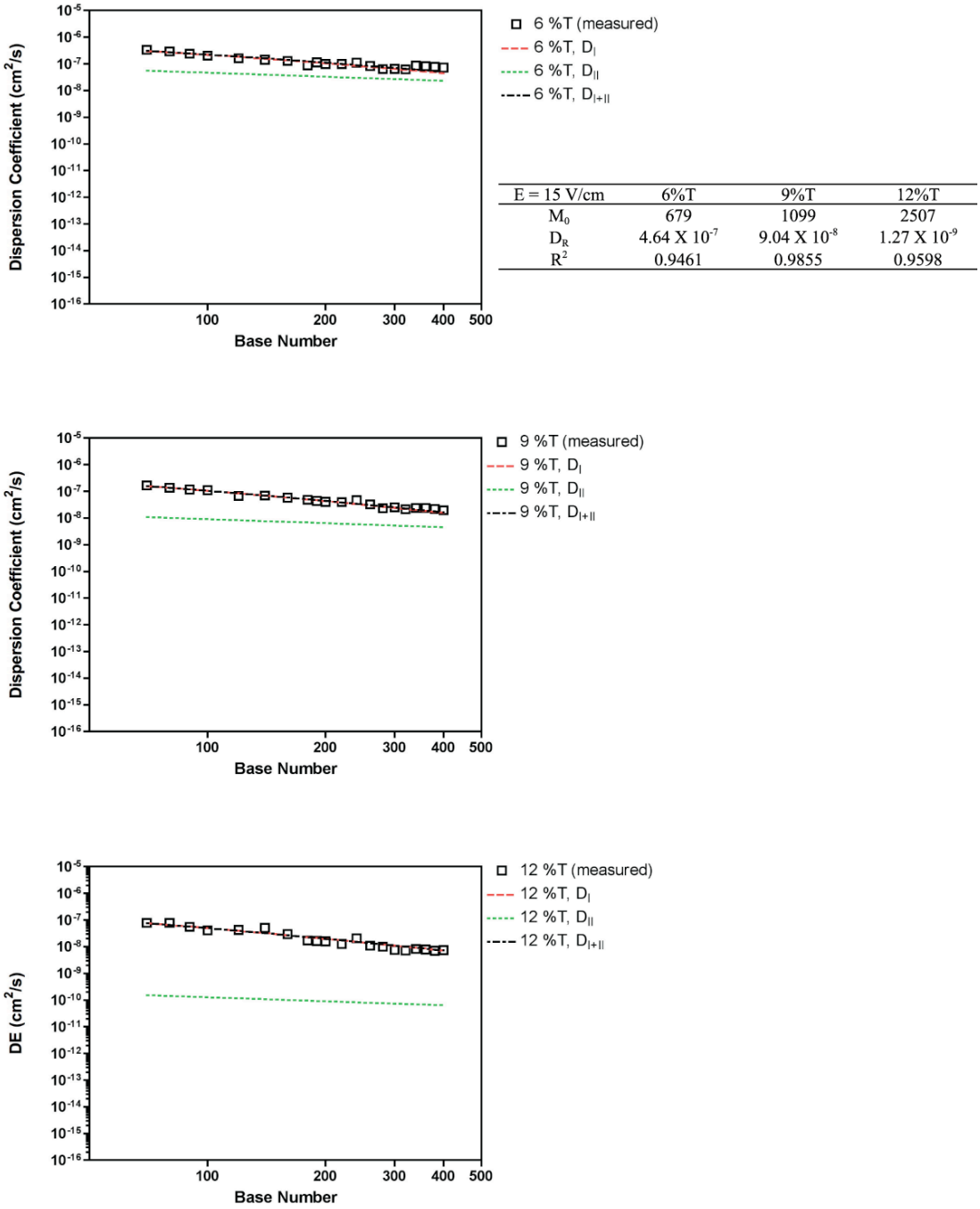

E = 15 V/cm	6%T	9%T	12%T
M_0	679	1099	2507
D_R	4.64×10^{-7}	9.04×10^{-8}	1.27×10^{-9}
R^2	0.9461	0.9855	0.9598

Figure V-4. Dispersion coefficient versus fragment size for ssDNA. Modified denominator model; $E = 15$ V/cm.

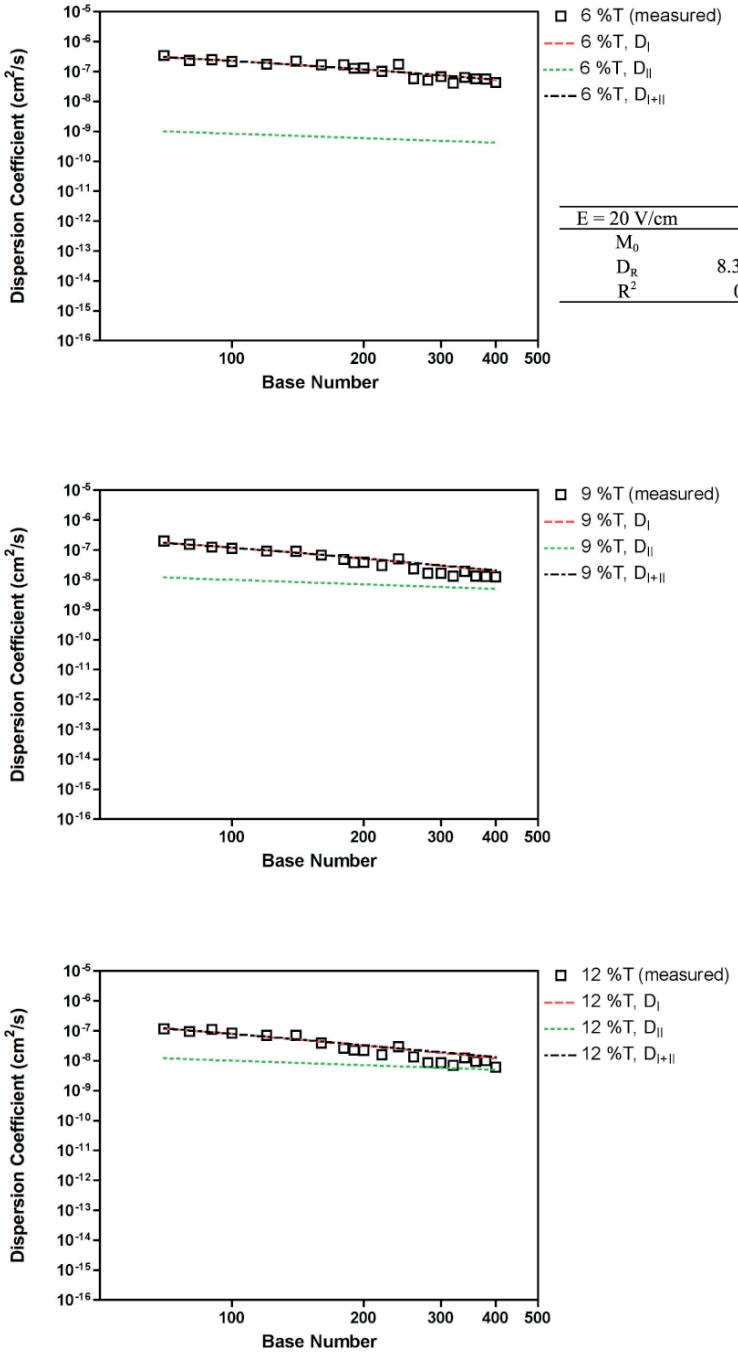

E = 20 V/cm	6%T	9%T	12%T
M_0	1093	1351	1330
D_R	8.37 X 10^{-9}	1.00 X 10^{-7}	1.00 X 10^{-7}
R^2	0.9347	0.9468	0.9267

Figure V-5. Dispersion coefficient versus fragment size for ssDNA. Original M-S dispersion model; E = 20 V/cm.

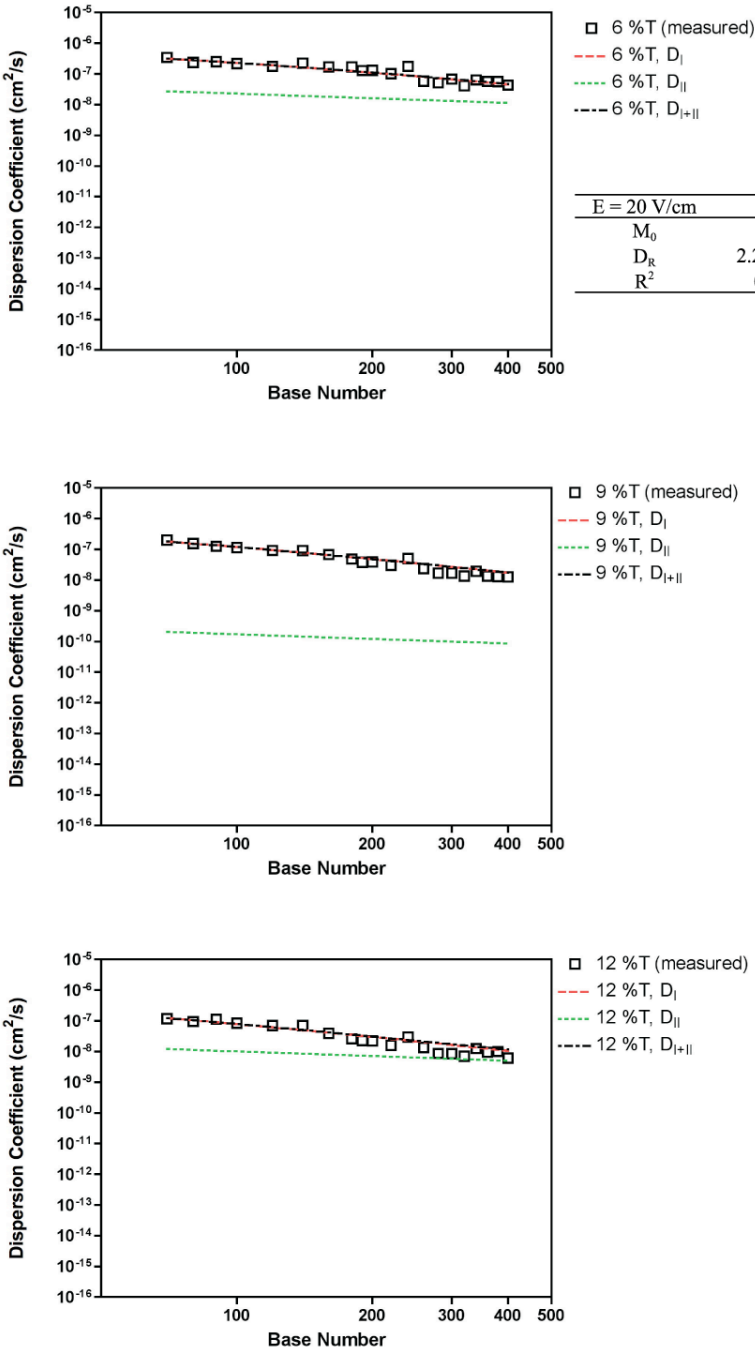

E = 20 V/cm	6%T	9%T	12%T
M_0	608	796	788
D_R	2.27×10^{-7}	1.70×10^{-9}	1.00×10^{-7}
R^2	0.9372	0.9698	0.9406

Figure V-6. Dispersion coefficient versus fragment size for ssDNA. Modified denominator model; $E = 20$ V/cm.

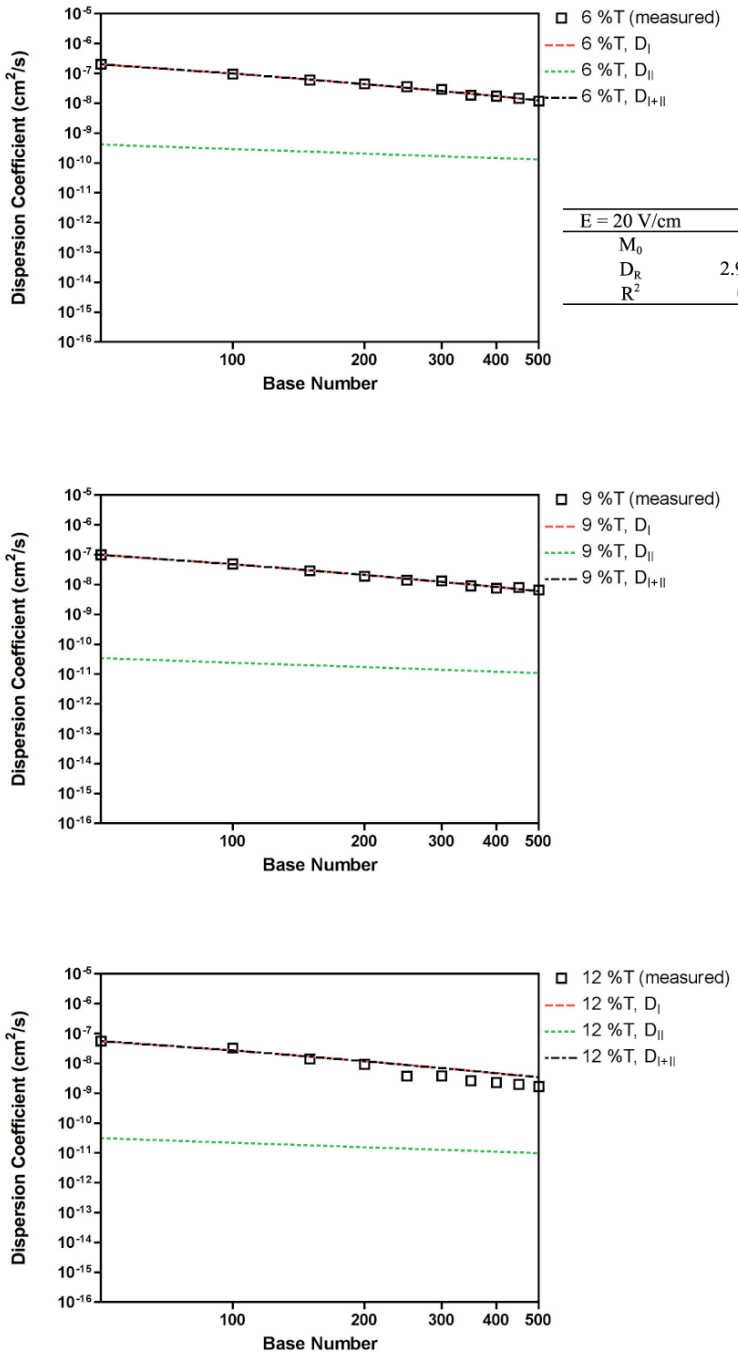

E = 20 V/cm	6%T	9%T	12%T
M_0	2719	4409	5962
D_R	2.90×10^{-9}	2.42×10^{-10}	2.18×10^{-10}
R^2	0.9978	0.9985	0.9644

Figure V-7. Dispersion coefficient versus fragment size for ssDNA (Brahmasandra *et al.*). Original M-S dispersion model; $E = 20$ V/cm.

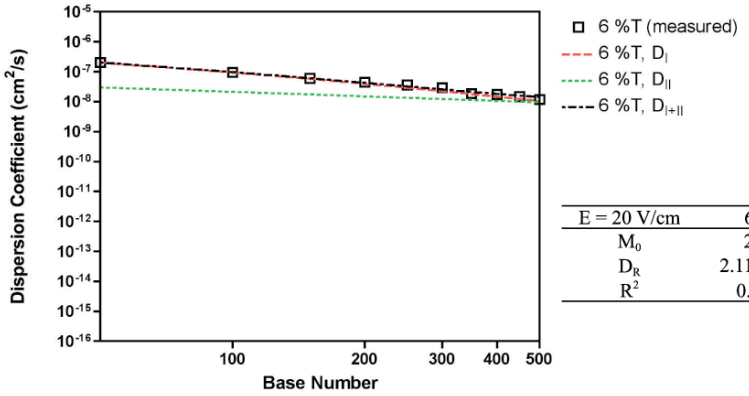

E = 20 V/cm	6%T	9%T	12%T
M_0	2084	3601	4236
D_R	2.11×10^{-7}	8.50×10^{-8}	9.92×10^{-11}
R^2	0.9981	0.9987	0.9653

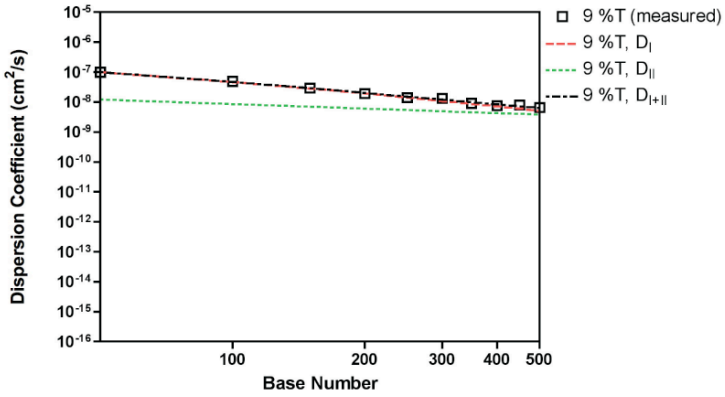

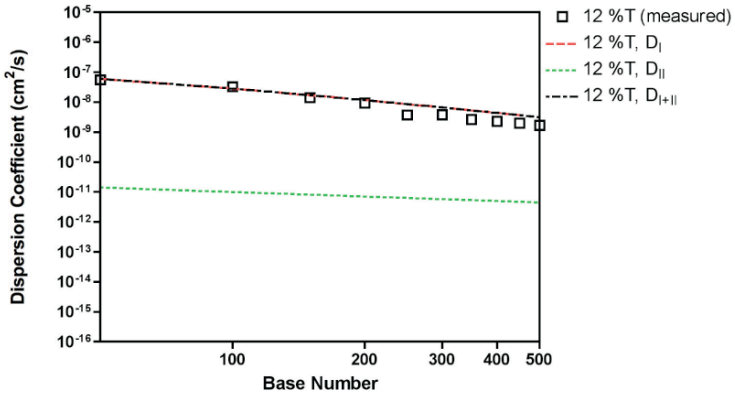

Figure V-8. Dispersion coefficient versus fragment size for ssDNA (Brahmasandra *et al.*). Modified denominator model; $E = 20$ V/cm.

5.4.2.2 dsDNA

We applied the M-S dispersion model to fit the dispersion coefficient data for dsDNA fragments migrating in photopolymerized polyacrylamide gels under different dye and buffer conditions (Figures V-9 to V-13). In contrast to the results from ssDNA, the values of M_0 were generally much smaller than reasonable (Table V-4), and the magnitude of D_R for YOYO-labeled dsDNA fragments was mostly dominant over the size range we studied. This is opposite to what we observed in the ssDNA data fitting. There were no significant differences observed in the fitting results of the dispersion data from experiments conducted in both TBE and CM buffers. In general, the M-S dispersion model provides a decent fit for dispersion coefficients of dsDNA qualitatively and quantitatively.

Table V-4. Summary of fitting parameters for dsDNA.

Original M-S dispersion model

a.

E = 15 V/cm	YOYO
M_0	1.00×10^{-7}
D_R	4.72×10^{-6}
R^2	0.891

b.

E = 15 V/cm	YOYO	SYBR Green	Fluorescein
M_0	1.00×10^{-7}	87	322
D_R	2.18×10^{-6}	2.18×10^{-7}	5.71×10^{-7}
R^2	0.8017	0.9186	0.9693

c.

E = 15 V/cm	YOYO	SYBR Green	Fluorescein
M_0	1.00×10^{-7}	10	1.00×10^{-7}
D_R	1.12×10^{-6}	8.85×10^{-11}	3.36×10^{-7}
R^2	0.8321	0.9586	0.8889

Modified denominator model

a.

E = 15 V/cm	YOYO
M_0	1.00×10^{-7}
D_R	4.72×10^{-6}
R^2	0.891

b.

E = 15 V/cm	YOYO	SYBR Green	Fluorescein
M_0	1.00×10^{-7}	17	138
D_R	2.07×10^{-6}	5.89×10^{-7}	6.48×10^{-7}
R^2	0.798	0.9234	0.9737

c.

E = 15 V/cm	YOYO	SYBR Green	Fluorescein
M_0	1.00×10^{-7}	1	1.00×10^{-7}
D_R	1.11×10^{-6}	2.42×10^{-9}	3.00×10^{-7}
R^2	0.832	0.961	0.8866

a) Finish line mode. Run conditions: 0.5X TBE, L = 0.5 cm, E = 15 V/cm, and T = 22 ºC.
b) Panorama mode. Run conditions: 0.5X TBE, E = 15 V/cm, and T = 22 ºC.
c) Panorama mode. Run conditions: 1X CM buffer, E = 15 V/cm, and T = 22 ºC.

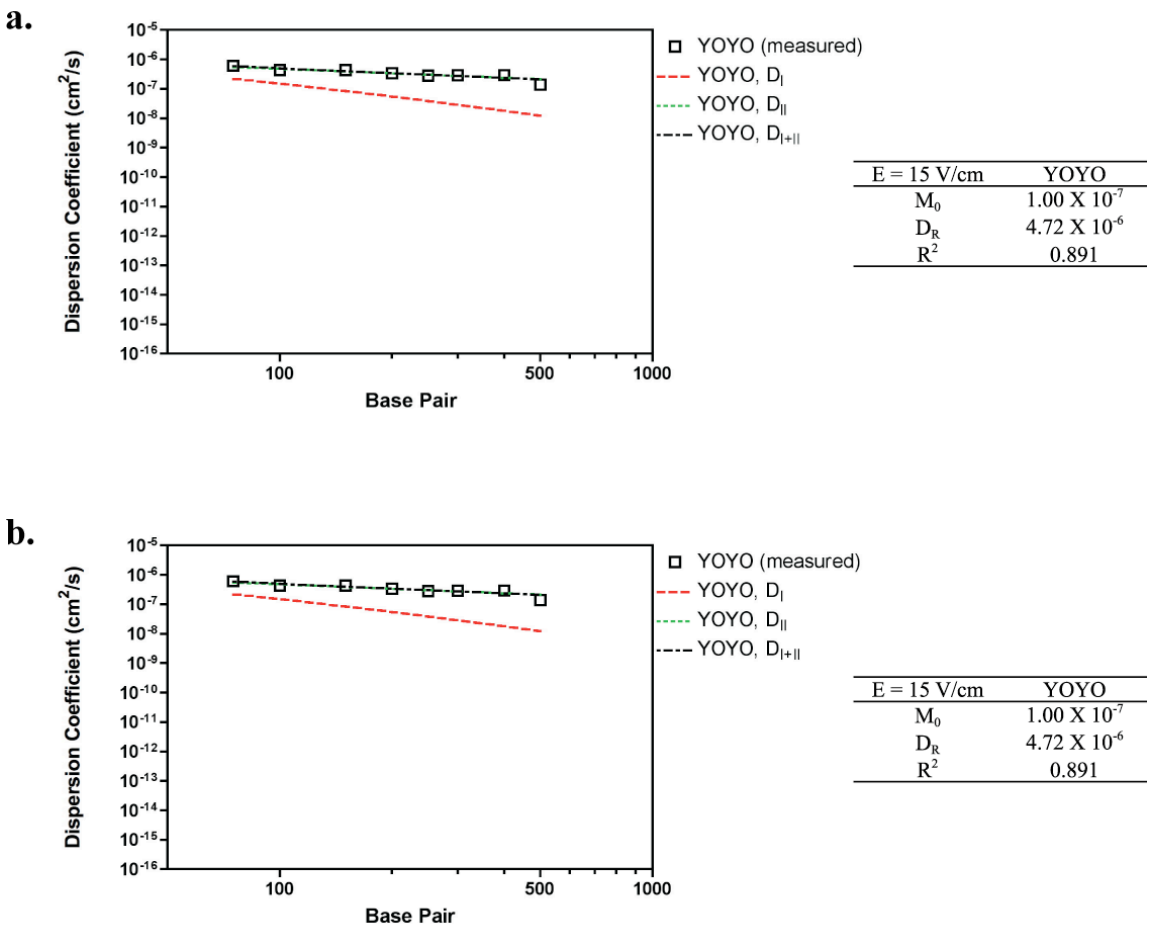

Figure V-9. Dispersion coefficient versus fragment size for dsDNA. (a) Original M-S dispersion model. (b) Modified denominator model. The dispersion coefficients were measured in the finish line mode.

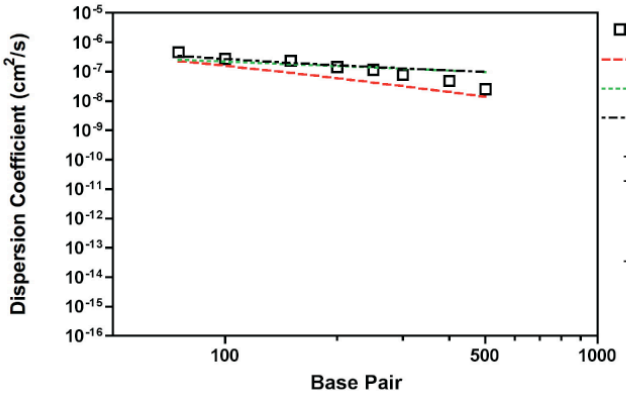

E = 15 V/cm	YOYO	SYBR Green	Fluorescein
M_0	1.00×10^{-7}	87	322
D_R	2.18×10^{-6}	2.18×10^{-7}	5.71×10^{-7}
R^2	0.8017	0.9186	0.9693

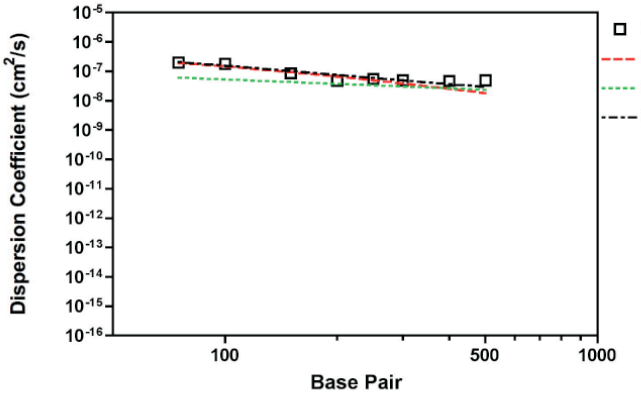

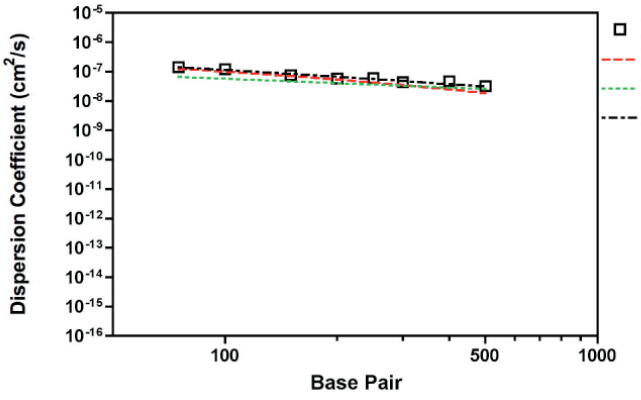

Figure V-10. Dispersion coefficient versus fragment size for dsDNA. Original M-S dispersion model; 0.5X TBE.

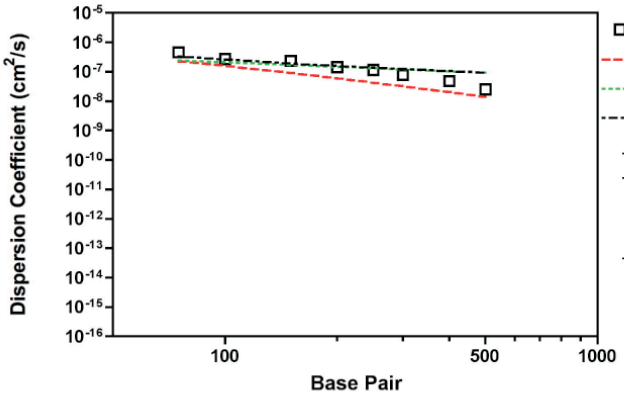

E = 15 V/cm	YOYO	SYBR Green	Fluorescein
M_0	1.00×10^{-7}	17	138
D_R	2.07×10^{-6}	5.89×10^{-7}	6.48×10^{-7}
R^2	0.798	0.9234	0.9737

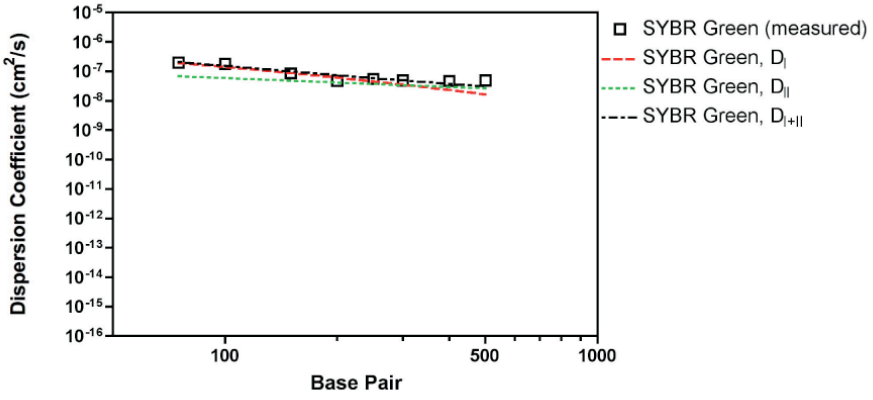

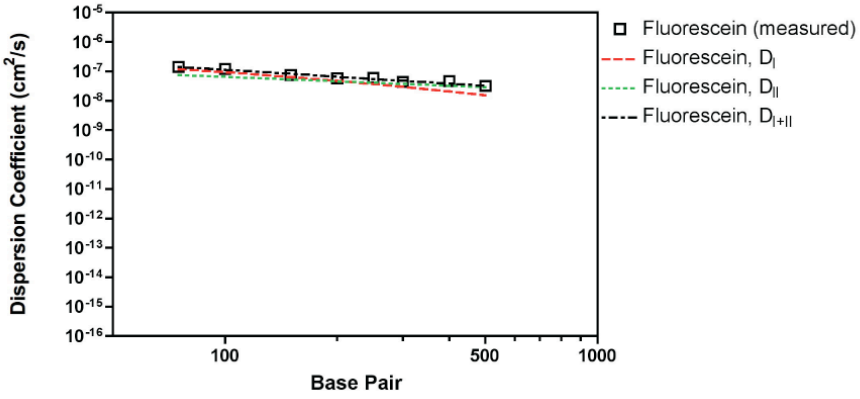

Figure V-11. Dispersion coefficient versus fragment size for dsDNA. Modified denominator model; 0.5X TBE.

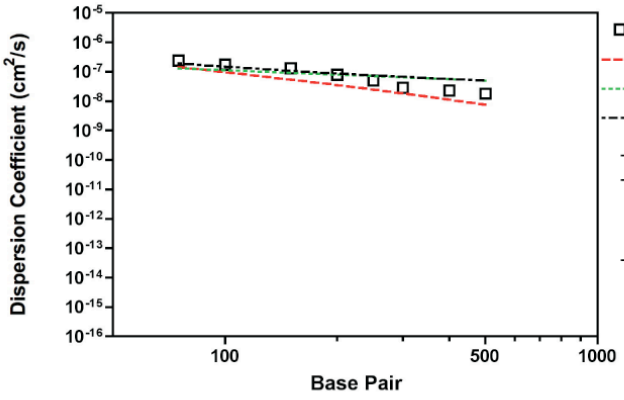

E = 15 V/cm	YOYO	SYBR Green	Fluorescein
M_0	1.00×10^{-7}	10	1.00×10^{-7}
D_R	1.12×10^{-6}	8.85×10^{-11}	3.36×10^{-7}
R^2	0.8321	0.9586	0.8889

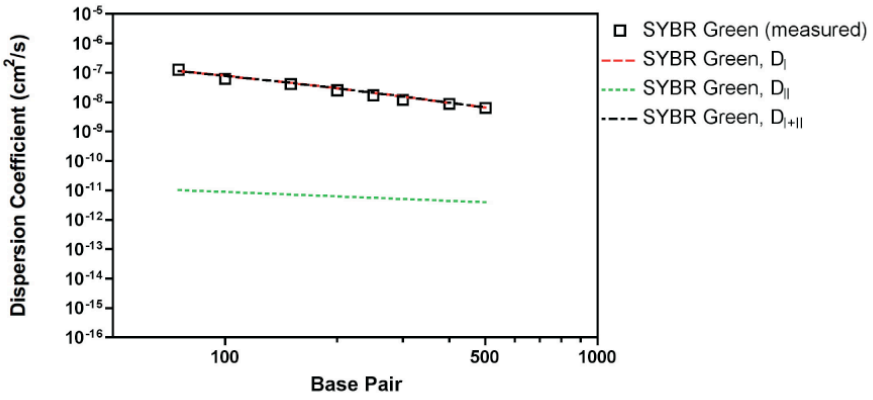

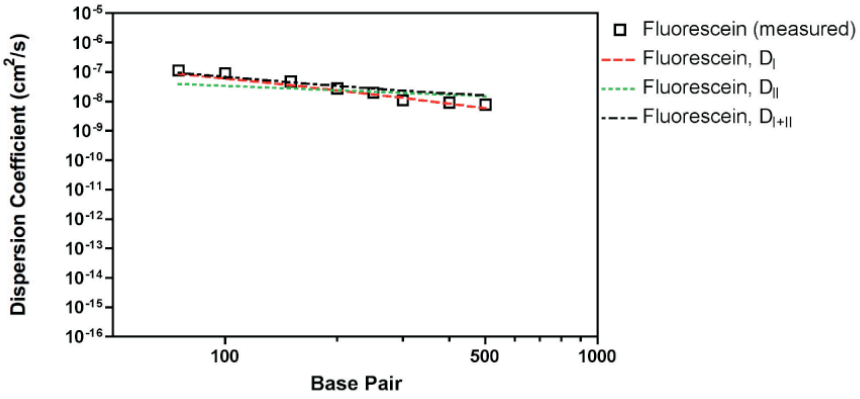

Figure V-12. Dispersion coefficient versus fragment size for dsDNA. Original M-S dispersion model; 1X CM buffer.

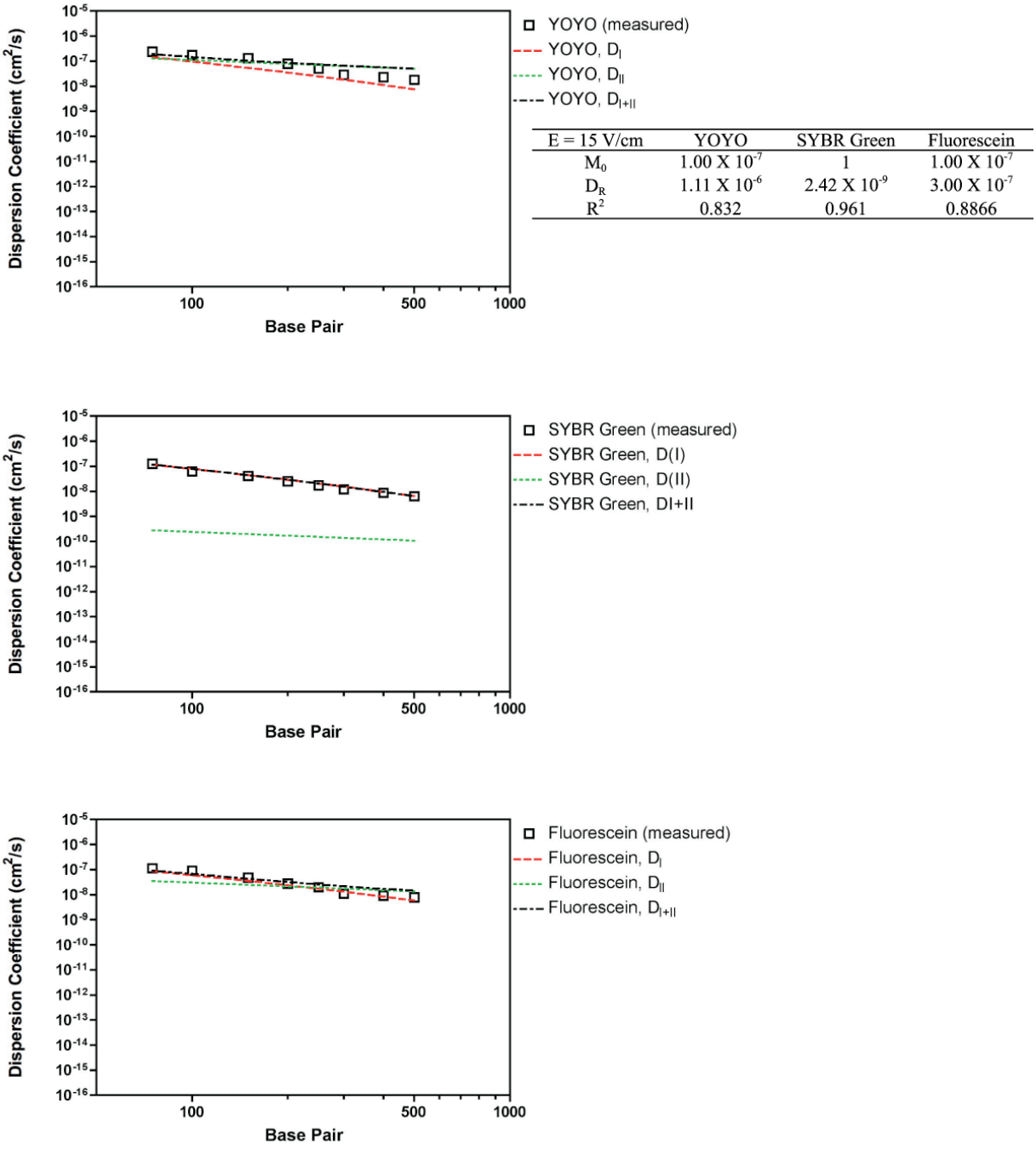

E = 15 V/cm	YOYO	SYBR Green	Fluorescein
M_0	1.00×10^{-7}	1	1.00×10^{-7}
D_R	1.11×10^{-6}	2.42×10^{-9}	3.00×10^{-7}
R^2	0.832	0.961	0.8866

Figure V-13. Dispersion coefficient versus fragment size for dsDNA. Modified denominator model; 1X CM buffer.

5.5 Concluding remarks

In this chapter, we tested the goodness of the universal interpolation function for dispersion coefficients of DNA fragments migrating in the sieving gel and found that it generally gives good fit results for ssDNA and dsDNA fragments within the size range we studied. It is possible to use this function to perform DNA sizing by measuring the dispersion coefficients of DNA fragments migrating in the sieving gel. However, we need to point out that the fitting parameters seem to be fairly sensitive to the data, and therefore it is important to obtain dispersion data with little amount of scattering. This is difficult to achieve, especially for a wide range of DNA fragment sizes. More work on our integrated microchip electrophoresis system could generate such data for further testing and refinement of this function.

CHAPTER VI

APPLICATION OF MIGRATION DATA TO DNA SIZING

This chapter details our efforts to evaluate the accuracy of several mobility-based methods for DNA size calling under different buffer and dye conditions. We also tried to size DNA fragments using the dispersion data collected on our whole-gel scanning detection system. To our knowledge, this is the first attempt to use dispersion data for DNA sizing.

6.1 Introduction

Gel electrophoresis has been used in many genomic analysis assays such as restriction fragment length polymorphism (RFLP) [98], variable number of tandem repeats (VNTR) [99], and short tandem repeats (STR) [100], to detect DNA polymorphisms that vary in DNA contour length. For proper assay results, it is critical to obtain correct DNA size information. In a typical DNA sizing experiment, the DNA fragment of an unknown size is electrophoresed in the same run with those in a size standard of known sizes. The migration parameter (such as migration distance, migration time, or mobility) of the unknown fragment is compared with those of the size standard, and this information is then converted to a relative DNA size. Several methods are used to perform this sizing calling, e.g. plots of migration time versus fragment size [101], migration distance versus 1/size [102], and mobility versus 1/log(size) [103], with either linear regression or polynomial fitting. However, these size-calling methods are usually arbitrarily chosen by different research groups for electrophoresis data collected under various run conditions,

e.g. gel formulations, buffers, and labeling dyes. To our knowledge, there is no such evaluation of the accuracy of these size-calling methods using electrophoresis data consistently collected with different buffers and labeling dyes.

In this chapter, we used the migration data from Chapter IV to evaluate several mobility-based size-calling methods and also try to perform DNA sizing with measured dispersion coefficients.

6.2 Size estimation

Three DNA fragments (75, 150, and 250 bp, respectively) were designated as "unknowns" for sizing in all methods evaluated, while all other fragments (100, 200, 300, 400, and 500 bp, respectively) were used as size standards to prepare a calibration curve. The estimated size for each unknown fragment was then determined from the calibration curve of the standards.

For each evaluated size-calling methods, mobility/dispersion coefficients from three independent runs were used. The general steps are described below.

1. Use the mobility/dispersion data of the size standards to determine the fitting parameters of each model by linear or nonlinear regression.
2. Enter the mobility/dispersion coefficient data of the "unknowns" into the completed model to determine corresponding fragment size.

6.2.1 log-log plot

A log-log plot of mobility versus fragment size is frequently used in the study of DNA migration behaviors. We linearly regressed log(mobility) on log(fragment size) for size estimation of "unknown" fragments.

$$\log(\mu) = a\log(M) + b$$

$$M = 10^{(\log(\mu)-b)/a} \qquad \text{(VI-1)}$$

where a and b are fitting parameters, and M is the estimated fragment size.

6.2.2 μ versus 1/ln(M) plot

Rye *et al.* [103] plotted mobilities versus 1/ln(M) and performed a least-squares fit for size estimation in their study of stability of dye-DNA complexes.

$$\mu = c(1/\ln(M)) + d$$

$$M = e^{\frac{c}{(\mu-d)}} \qquad \text{(VI-2)}$$

where c and$d$ d are fitting parameters.

6.2.3 Mercier-Slater model

Mercier and Slater proposed a more realistic description of the geometric parameters that influence the fractional gel volume accessible to the migrating DNA [66, 67]. In this framework, the following relationship can be used to fit the mobility data.

$$\sqrt{\frac{\mu_0}{\mu(M)} - 1} \cong \frac{R_g + r}{a} \qquad \text{(II-5)}$$

whereby a plot of $[(\mu_0/\mu) - 1]^{1/2}$ versus R_g is expected to yield a straight line with slope $1/a$ and intercept r/a. Here r is the gel fiber radius, and a is the pore size, both in nm.

We first fitted the mobility data of the size standards (100-500 bp) to determine the values of r and a and then entered these values into eq. (II-5) for size calling. The mobilities of those "unknowns" were used to calculate R_g values in nm, and they were put in the the Kratky-Porod equation [9] to determine the corresponding size in base pairs.

$$R_g^2 = \frac{pL_c}{3}[1 - 3(\frac{p}{L_c}) + 6(\frac{p}{L_c})^2 - 6(\frac{p}{L_c})^3(1 - e^{-\frac{L_c}{p}})] \qquad \text{(I-5)}$$

where L_c is the contour length of the DNA molecule, and p is the persistence length (L_c = 0.34 (nm/base pair) X DNA molecular size (M), and p = 50 nm for dsDNA [97]).

6.2.4 Mercier-Slater dispersion model

In Chapter V, we tested the Mercier-Slater dispersion model for its goodness in fitting dispersion data collected on our microfludic gel electrophoresis device. Here we tried to perform DNA size calling with this model, because D^E is more sensitive to changes in fragment size.

$$D^E(M,C,E) = ([\frac{k_B T}{q_{eff}}\mu(M,C,E)]^2 \frac{1}{M^2 + (M_0(C,E) * M)} + \frac{D_R^2(C,E)}{M})^{1/2} \qquad \text{(V-1)}$$

where k_B is Boltzmann constant, T is the Kelvin temperature, q_{eff} is the effective charge per base pair, and M_0 and D_R are fitting parameters. In this equation, the mobility was fitted with the empirical formulation proposed by van Winkle *et al.* (the vWBR model) [68, 69].

$$\mu(M,C) = \frac{\mu(0,C)}{1 + \left(\frac{\mu(0,C)}{\mu(\inf,C)} - 1 \right) \left(1 - e^{-M/m} \right)} \qquad \text{(II-6)}$$

The dispersion data of the size standards were put into eq. (V-4) to determine the fitting parameters, M_0 and D_R. The dispersion coefficients of the "unknowns" were then placed in the equation to estimate corresponding fragment size in base pairs.

6.3 Results and discussion

6.3.1 Effect of different detection modes

We compared the sizing accuracy of these four methods using migration data collected in both the panorama and finish line detection modes with 0.5X TBE buffer and YOYO-labeled DNA fragments (Figure VI-1).

The plots of *log-log* and *μ versus 1/ln(M)* give similar sizing results for both detection modes. There is more variation (> 10 bp) in the size estimation for the 75-bp fragment, because this fragment is outside the range of the sizing standards (100-500 bp), and, therefore, the size estimation was performed by an extrapolation.

The *Mercier-Slater model* gives the best sizing results for all three "unknowns", especially for mobility data collected in the panorama mode, because this model captures very well the scaling trend of the mobility data both qualitatively and quantitatively.

The *Mercier-Slater dispersion model* has the worst sizing accuracy when compared to other mobility-based methods.

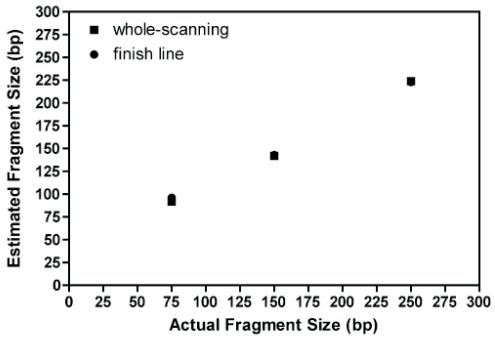

log-log plot	Estimated Size (bp)	
Actual Size (bp)	Panorama	Finish line
75	92	96
150	142	143
250	224	223

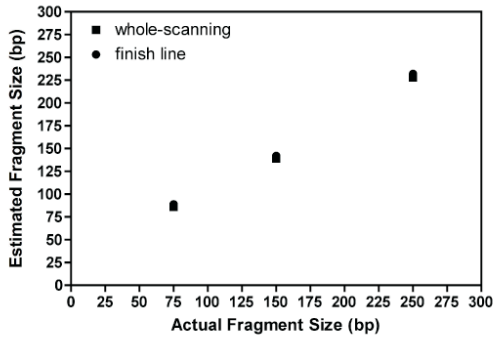

μ vs. 1/ln(M) plot	Estimated Size (bp)	
Actual Size (bp)	Panorama	Finish line
75	86	89
150	139	142
250	228	232

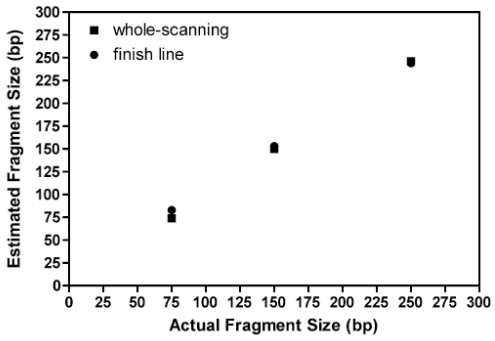

M-S model	Estimated Size (bp)	
Actual Size (bp)	Panorama	Finish line
75	74	83
150	150	153
250	246	244

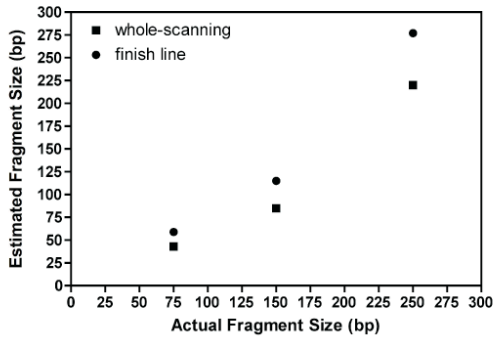

M-S D^E model	Estimated Size (bp)	
Actual Size (bp)	Panorama	Finish line
75	43	59
150	85	115
250	220	277

Figure VI-1. Comparison of sizing results of YOYO-labeled DNA fragments in the whole-gel scanning and finish line modes. Run conditions: 0.5X TBE buffer, $T = 22°C$, and $E = 15$ V/cm.

6.3.2 Effect of running buffers and labeling dyes

The accuracy of these four sizing methods were also evaluated with DNA migration data collected with different running buffers and labeling dyes (Figures VI-2 to VI-5).

The plots of *log-log* and *μ versus 1/ln(M)* have similar sizing accuracy (deviation > 10 bp for 75- and 250- bp fragments; ~ 10 bp for the 150-bp fragment) for separations in both TBE and CM buffers.

The *Mercier-Slater model*, as previously observed, gives the best sizing accuracy among all four methods evaluated here. The closest size estimation came from the combination of YOYO-labeled DNA sample separated in the CM buffer. The differences between the estimated and actual sizes are 2, 1, and 1 bp for the three "unknowns", 75, 150, and 250 bp, respectively.

The *Mercier-Slater dispersion model* still has the worst sizing accuracy for separations in both the TBE and CM buffers, especially for the smaller "unknowns" (75 and 150 bp, respectively). This may result from the fact that the relative sizes of smaller "unknowns" are not large enough to reach the reptation regime, when compared to the gel pore size.

a.

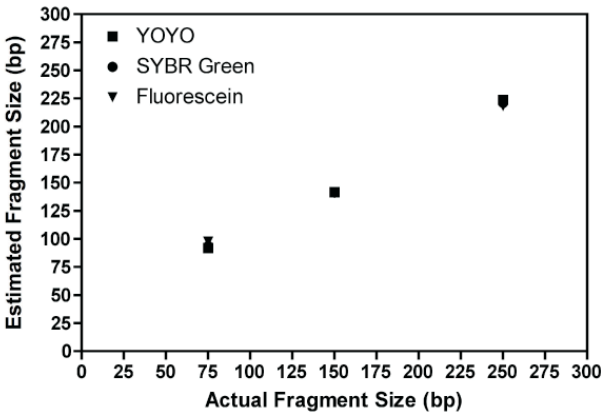

log-log plot	Estimated Size (bp)		
Actual Size (bp)	YOYO	SYBR Green	Fluorescein
75	92	94	98
150	142	141	141
250	224	221	218

b.

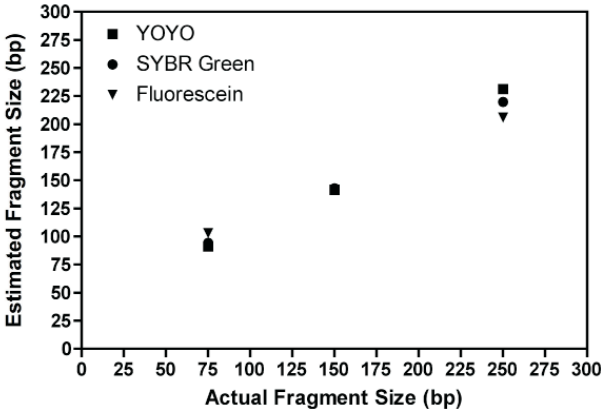

log-log plot	Estimated Size (bp)		
Actual Size (bp)	YOYO	SYBR Green	Fluorescein
75	91	94	103
150	142	143	141
250	231	220	206

Figure VI-2. Results of DNA sizing with the *log-log plot*. (a) 0.5X TBE buffer. (b) CM buffer. Run conditions: $T = 22°C$, and $E = 15$ V/cm.

a.

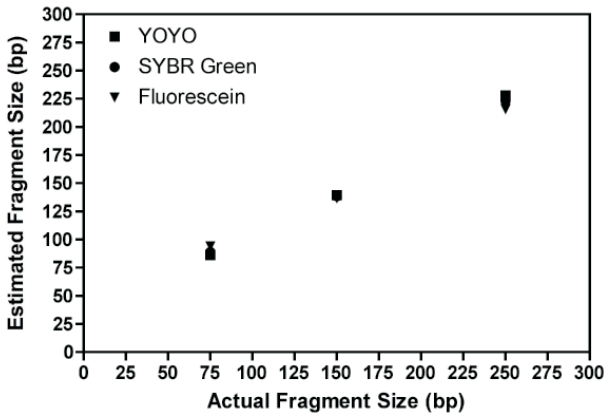

μ vs. 1/ln(M) plot	Estimated Size (bp)		
Actual Size (bp)	YOYO	SYBR Green	Fluorescein
75	86	89	94
150	139	138	137
250	228	223	216

b.

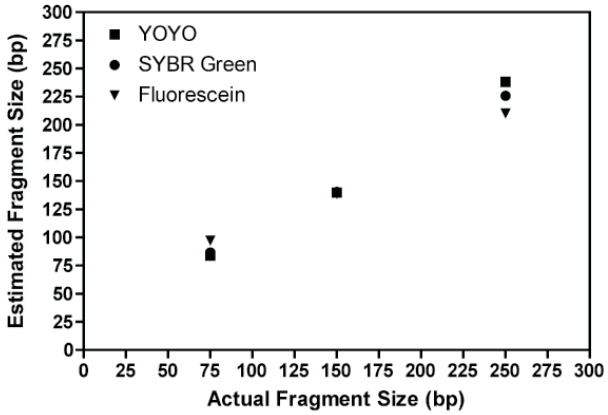

μ vs. 1/ln(M) plot	Estimated Size (bp)		
Actual Size (bp)	YOYO	SYBR Green	Fluorescein
75	84	87	97
150	140	141	139
250	238	226	210

Figure VI-3. Results of DNA sizing with the *μ versus 1/ln(M) plot*. (a) 0.5X TBE buffer. (b) CM buffer. Run conditions: $T = 22°C$, and $E = 15$ V/cm.

a.

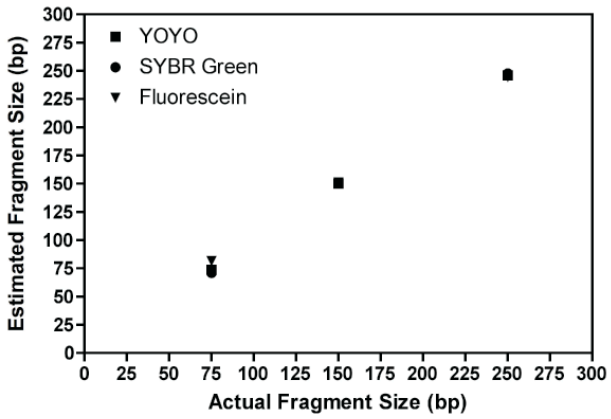

M-S model	Estimated Size (bp)		
Actual Size (bp)	YOYO	SYBR Green	Fluorescein
75	74	71	81
150	150	151	151
250	246	248	245

b.

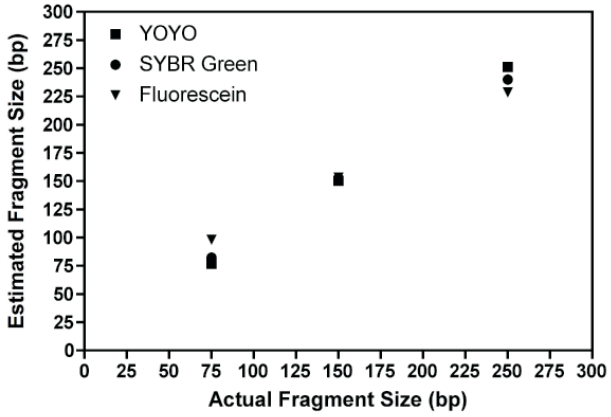

M-S model	Estimated Size (bp)		
Actual Size (bp)	YOYO	SYBR Green	Fluorescein
75	77	82	98
150	151	153	153
250	251	240	229

Figure VI-4. Results of DNA sizing with the *Mercier-Slater model*. (a) 0.5X TBE buffer. (b) CM buffer. Run conditions: $T = 22°C$, and $E = 15$ V/cm.

a.

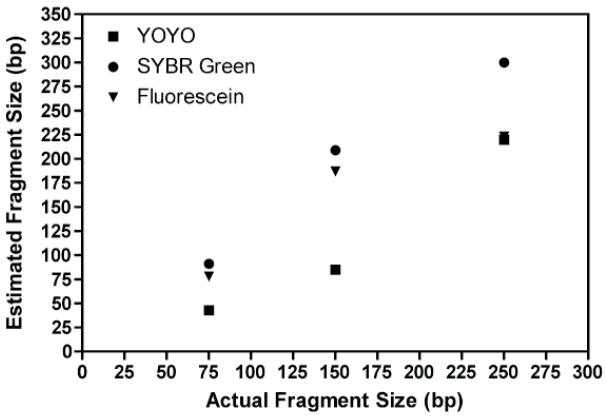

M-S D^E model	Estimated Size (bp)		
Actual Size (bp)	YOYO	SYBR Green	Fluorescein
75	43	91	78
150	85	209	187
250	220	300	223

b.

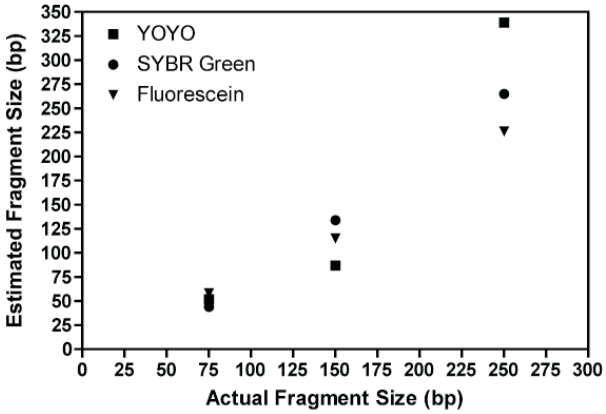

M-S D^E model	Estimated Size (bp)		
Actual Size (bp)	YOYO	SYBR Green	Fluorescein
75	52	44	58
150	87	134	115
250	339	265	226

Figure VI-5. Results of DNA sizing with the *Mercier-Slater dispersion model*. (a) 0.5X TBE buffer. (b) CM buffer. Run conditions: $T = 22°C$, and $E = 15$ V/cm.

6.4 Concluding remarks

In this chapter, we have evaluated four size-calling methods with migration data collected under different buffer and dye conditions and have demonstrated that the *Mercier-Slater model* gives the best sizing accuracy. We have also shown that it is possible to use the dispersion coefficients of DNA fragments migrating in the sieving gel to perform size estimation, although the sizing accuracy was not good for the "unknowns" used in this work. It is expected that this method would work better for DNA fragments with relative sizes in the reptation regime. More work is needed to verify this.

We hope that the results here can help identify a more accurate size-calling method and also help build a systematic procedure for evaluating the accuracy of different DNA size-calling methods used in many genomic analysis assays, so that researchers can consistently compare the performance of different DNA sizing methods.

CHAPTER VII

CONCLUSIONS AND FUTURE WORK

7.1 Conclusions

In this work, we hope to show that microfluidic gel electrophoresis devices, when integrated with our automated rapid whole-gel scanning detection system, can perform fast and low-cost DNA separations.

The ability of our integrated system to acquire in nearly real time both spatial and temporal data of DNA migrating in the gel simultaneously with high resolution provides a more detailed picture of the separation process. It makes us able to observe the evolution of the separation process rather than just analyze the electropherogram after the run is completed and speculate what has happened during the separation process.

Several DNA size-calling methods were evaluated using the migration data collected under different buffer and dye conditions on the integrated microchip gel electrophoresis system. We identified a potential combination of a size-calling method, running buffer and labeling dye for highly accurate DNA sizing.

We also successfully established the predicting capability of separation resolution of DNA gel electrophoresis by measuring fundamental migration parameters (mobility, diffusion, and dispersion) of ssDNA migrating in the sieving gels on a conventional slab

gel DNA sequencer. This capability makes it possible for scientists and engineers to tailor their DNA gel electrophoresis system according to their desired separation resolution by systematically measuring these parameters instead of the old trial-and error process.

7.2 Future work

Although we have successfully designed and built an integrated electrophoresis system for rapid and consistent characterization of the dsDNA separation process, the following are recommended to further improve the performance and capability of our system.

7.2.1 Further automation

Currently, we still need to manually change the polarity of the voltage applied between electrodes to perform sample compaction and separation. The strength of the applied electric field is controlled by manually turning the knob of the power supply. During the DNA separation process, the current is monitored with a multimeter, but any changes in voltage still have to be made by the operator. LabVIEW provides a means for programmable control on personal computers, which makes it possible to automate the sample compaction and separation processes, and to continuously monitor and adjust the voltage for best separation results. The whole separation process can be further streamlined if LabVIEW is integrated into our electrophoresis system.

7.2.2 Separation of ssDNA

We have successfully performed rapid, automated characterization of the separation process of dsDNA in nearly real time on our integrated DNA electrophoresis system. However, more interest is in the characterization of the separation of ssDNA in the sieving gel, because, when compared to dsDNA, there are far less migration data of ssDNA in literature for study of the physics of DNA gel electrophoresis. Currently, we still have problems in imaging ssDNA fragments on our system because of low fluorescence signal. We seek to solve this problem by using a more sensitive CCD camera and sample compaction.

7.2.3 DNA sizing with dispersion data

In this work, we attempted to perform DNA sizing using the dispersion coefficients of dsDNA migrating in the sieving gel. Although current results are not satisfactory (deviation in size calling > 20 bp), this still provides a new way of size calling instead of using only the mobility data. More work on the M-S dispersion model will be needed to make it better capture both qualitatively and quantitatively the trend of dispersion coefficients. Our system can quickly generate such data for model development.

7.2.4 Test of other peak fitting functions

In our work, the peak trace of each separated DNA fragment was fitting to a Gaussian profile [37] to find out the peak width for determination of the diffusion and dispersion coefficients under different run conditions. However, the Gaussian profile does not al-

ways give the best fitting results. Marco *et al.* [104] has collected about ninety empirical functions for peak fitting in their review. It would be of interest to analyze our DNA migration data with these functions to identify potential candidates for better peak fitting results and therefore more accurate diffusion and dispersion coefficients.

7.2.5 *Multiplex DNA separation*

Clark *et al.* performed two-color DNA sizing by mixing two DNA samples labeled with two different intercalating dyes on a capillary electrophoresis system and obtained good sizing results [89]. It is also of interest to perform such separations on our electrophoresis system because it can further increase the throughput of our system.

In addition to linear DNA fragments, the migration behavior of DNA vectors in the gel is also an interesting topic. We have tried to separate a mixture of both linear and vector DNA fragments of the same size to see differences in the mobility and dispersion data and how the conformation of a DNA fragment affects the migration behaviors. More work will be needed to get the detailed information.

REFERENCES

[1] Ugaz, V., Elms, R., Lo, R., Shaikh, F., Burns, M., *Philosophical Transactions of the Royal Society of London Series A-Mathematical Physical and Engineering Sciences* 2004, *362*, 1105-1129.

[2] Service, R. F., *Science* 2006, *311*, 1544-1546.

[3] Stellwagen, E., Stellwagen, N., *Electrophoresis* 2002, *23*, 2794-2803.

[4] Lu, Y. J., Weers, B., Stellwagen, N. C., *Biopolymers* 2001, *61*, 261-275.

[5] Mayer, P., Slater, G. W., Drouin, G., *Analytical Chemistry* 1994, *66*, 1777-1780.

[6] Chen, Z., Graham, R., Burns, M. A., Larson, R. G., *Electrophoresis* 2007, *28*, 2783-2800.

[7] Ogston, A., *Transactions of Faraday Society* 1958, *54*, 1754-1757.

[8] Rodbard, D., Chrambac.A, *Proceedings of the National Academy of Sciences of the United States of America* 1970, *65*, 970-977.

[9] Teraoka, I., *Polymer Solutions: An Introduction to Physical Properties*, Wiley, New York 2002.

[10] Tinland, B., Pluen, A., Sturm, J., Weill, G., *Macromolecules* 1997, *30*, 5763-5765.

[11] Hoagland, D., Arvanitidou, E., Welch, C., *Macromolecules* 1999, *32*, 6180-6190.

[12] Desruisseaux, C., Long, D., Drouin, G., Slater, G. W., *Macromolecules* 2001, *34*, 44-52.

[13] Rousseau, J., Drouin, G., Slater, G. W., *Physical Review Letters* 1997, *79*, 1945-1948.

[14] Lumpkin, O. J., Dejardin, P., Zimm, B. H., *Biopolymers* 1985, *24*, 1573-1593.

[15] Lerman, L. S., Frisch, H. L., *Biopolymers* 1982, *21*, 995-997.

[16] Gennes, P.-G. d., *Scaling Concepts in Polymer Physics*, Cornell University Press, Ithaca, N.Y. 1979.

[17] Slater, G. W., Noolandi, J., *Physical Review Letters* 1985, *55*, 1579-1582.

[18] Slater, G. W., Noolandi, J., *Biopolymers* 1986, *25*, 431-454.

[19] Slater, G. W., Rousseau, J., Noolandi, J., *Biopolymers* 1987, *26*, 863-872.

[20] Viovy, J. L., *Reviews of Modern Physics* 2000, *72*, 813-872.

[21] Heller, C., Duke, T., Viovy, J. L., *Biopolymers* 1994, *34*, 249-259.

[22] Duke, T., Viovy, J. L., Semenov, A. N., *Biopolymers* 1994, *34*, 239-247.

[23] Duke, T. A. J., Semenov, A. N., Viovy, J. L., *Physical Review Letters* 1992, *69*, 3260-3263.

[24] Semenov, A. N., Duke, T. A. J., Viovy, J. L., *Physical Review E* 1995, *51*, 1520-1537.

[25] Slater, G. W., Drouin, G., *Electrophoresis* 1992, *13*, 574-582.

[26] Yan, J. Y., Best, N., Zhang, J. Z., Ren, H. J.*, et al.*, *Electrophoresis* 1996, *17*, 1037-1045.

[27] Pluen, A., Tinland, B., Sturm, J., Weill, G., *Electrophoresis* 1998, *19*, 1548-1559.

[28] Slater, G. W., *Electrophoresis* 1993, *14*, 1-7.

[29] Doi, M., Edwards, S. F., *The Theory of Polymer Dynamics*, Clarendon Press; Oxford University Press, Oxford [Oxfordshire], New York 1986.

[30] Larson, R. G., *The Structure and Rheology of Complex Fluids*, Oxford University Press, New York 1999.

[31] Slater, G., Guo, H., *Electrophoresis* 1995, *16*, 11-15.

[32] Gibson, T., Sepaniak, M., *Journal of Chromatography B* 1997, *695*, 103-111.

[33] Luckey, J., Norris, T., Smith, L., *Journal of Physical Chemistry* 1993, *97*, 3067-3075.

[34] Yarmola, E., Sokoloff, H., Chrambach, A., *Electrophoresis* 1996, *17*, 1416-1419.

[35] Slater, G. W., Mayer, P., Drouin, G., *Methods in Enzymology* 1996, *270*, 272-295.

[36] Slater, G. W., Kenward, M., McCormick, L. C., Gauthier, M. G., *Current Opinion in Biotechnology* 2003, *14*, 58-64.

[37] Giddings, J. C., *Unified Separation Science*, Wiley, New York 1991.

[38] Brahmasandra, S. N., Burke, D. T., Mastrangelo, C. H., Burns, M. A., *Electrophoresis* 2001, *22*, 1046-1062.

[39] Fabrizio, E. F., Nadim, A., Sterling, J. D., *Analytical Chemistry* 2003, *75*, 5012-5021.

[40] Heller, C., *Electrophoresis* 1999, *20*, 1962-1977.

[41] Nkodo, A., Garnier, J., Tinland, B., Ren, H.*, et al.*, *Electrophoresis* 2001, *22*, 2424-2432.

[42] Rousseau, J., Drouin, G., Slater, G. W., *Electrophoresis* 2000, *21*, 1464-1470.

[43] Schmalzing, D., Adourian, A., Koutny, L., Ziaugra, L.*, et al.*, *Analytical Chemistry* 1998, *70*, 2303-2310.

[44] Ugaz, V. M., Burke, D. T., Burns, M. A., *Electrophoresis* 2002, *23*, 2777-2787.

[45] Nkodo, A. E., Garnier, J. M., Tinland, B., Ren, H. J*., et al.*, *Electrophoresis* 2001, *22*, 2424-2432.

[46] Stellwagen, N. C., Gelfi, C., Righetti, P. G., *Biopolymers* 1997, *42*, 687-703.

[47] Barron, A., Blanch, H., *Separation and Purification Methods* 1995, *24*, 1-118.

[48] Mikkers, F. E. P., Everaerts, F. M., Verheggen, T. P. E. M., *Journal of Chromatography* 1979, *169*, 11-20.

[49] Jorgenson, J. W., Lukacs, K. D., *Clinical Chemistry* 1981, *27*, 1551-1553.

[50] Jorgenson, J. W., Lukacs, K. D., *Journal of Chromatography* 1981, *218*, 209-216.

[51] Jorgenson, J. W., Lukacs, K. D., *Analytical Chemistry* 1981, *53*, 1298-1302.

[52] Knox, J. H., *Journal of Chromatography A* 1994, *680*, 3-13.

[53] Brahmasandra, S. N., Ugaz, V. M., Burke, D. T., Mastrangelo, C. H., Burns, M. A., *Electrophoresis* 2001, *22*, 300-311.

[54] Wu, J. Q., Pawliszyn, J., *Analytical Chemistry* 1992, *64*, 224-227.

[55] Beale, S. C., Sudmeier, S. J., *Analytical Chemistry* 1995, *67*, 3367-3371.

[56] Kim, S., Yoo, H. J., Hahn, J. H., *Analytical Chemistry* 1996, *68*, 936-939.

[57] Olivares, J. A., Stark, P. C., Jackson, P., *Analytical Chemistry* 2002, *74*, 2008-2013.

[58] Wu, J. Q., Pawliszyn, J., *American Laboratory* 1994, *26*, 48-52.

[59] Palm, A., Lindh, C., Hjerten, S., Pawliszyn, J., *Electrophoresis* 1996, *17*, 766-770.

[60] Wu, X. Z., Pawliszyn, J., *Electrophoresis* 2002, *23*, 542-549.

[61] Wu, X. Z., Huang, T. M., Liu, Z., Pawliszyn, J., *Trac-Trends in Analytical Chemistry* 2005, *24*, 369-382.

[62] Desruisseaux, C., Slater, G. W., Drouin, G., *Macromolecules* 1998, *31*, 6499-6505.

[63] Desruisseaux, C., Slater, G. W., Drouin, G., *Electrophoresis* 1998, *19*, 627-634.

[64] Ferguson, K. A., *Metabolism* 1964, *13*, 985-1002.

[65] Stellwagen, N., Gelfi, C., Righetti, P., *Biopolymers* 1997, *42*, 687-703.

[66] Kopecka, K., Drouin, G., Slater, G. W., *Electrophoresis* 2004, *25*, 2177-2185.

[67] Mercier, J. F., Tessier, F., Slater, G. W., *Electrophoresis* 2001, *22*, 2631-2638.

[68] Van Winkle, D. H., Beheshti, A., Rill, R. L., *Electrophoresis* 2002, *23*, 15-19.

[69] Rill, R. L., Beheshti, A., Van Winkle, D. H., *Electrophoresis* 2002, *23*, 2710-2719.

[70] Slater, G. W., *Electrophoresis* 2002, *23*, 1410-1416.

[71] Slater, G. W., Mayer, P., Hubert, S. J., Drouin, G., *Applied and Theoretical Electrophoresis* 1994, *4*, 71-79.

[72] Ugaz, V., Burke, D., Burns, M., *Electrophoresis* 2002, *23*, 2777-2787.

[73] Tinland, B., Pernodet, N., Pluen, A., *Biopolymers* 1998, *46*, 201-214.

[74] Ugaz, V. M., Brahmasandra, S. N., Burke, D. T., Burns, M. A., *Electrophoresis* 2002, *23*, 1450-1459.

[75] Ugaz, V. M., Lin, R. S., Srivastava, N., Burke, D. T., Burns, M. A., *Electrophoresis* 2003, *24*, 151-157.

[76] Yanagida, M., Hiraoka, Y., Katsura, I., *Cold Spring Harb Sym* 1982, *47*, 177-187.

[77] Lo, R. C., Ugaz, V. M., *Electrophoresis* 2006, *27*, 373-386.

[78] Djouadi, Z., Bottani, S., Duval, M. A., Siebert, R.*, et al.*, *Journal of Chromatography A* 2000, *894*, 231-239.

[79] Rhee, K. W., Ware, B. R., *Journal of Chemical Physics* 1983, *78*, 3349-3353.

[80] Strachan, T., Read, A. P., *Human Molecular Genetics 2*, Wiley-Liss, New York 1999.

[81] Beck, S., Okeeffe, T., Coull, J. M., Koster, H., *Nucleic Acids Res* 1989, *17*, 5115-5123.

[82] Smith, L. M., Sanders, J. Z., Kaiser, R. J., Hughes, P.*, et al.*, *Nature* 1986, *321*, 674-679.

[83] Glazer, A. N., Peck, K., Mathies, R. A., *Proceedings of the National Academy of Sciences of the United States of America* 1990, *87*, 3851-3855.

[84] Lerman, L. S., *Journal of Molecular Biology* 1961, *3*, 18-30.

[85] Glazer, A. N., Rye, H. S., *Nature* 1992, *359*, 859-861.

[86] Zhu, H. P., Clark, S. M., Benson, S. C., Rye, H. S.*, et al.*, *Analytical Chemistry* 1994, *66*, 1941-1948.

[87] Kim, Y. S., Morris, M. D., *Analytical Chemistry* 1994, *66*, 1168-1174.

[88] Schwartz, H. E., Ulfelder, K. J., *Analytical Chemistry* 1992, *64*, 1737-1740.

[89] Clark, S. M., Mathies, R. A., *Analytical Chemistry* 1997, *69*, 1355-1363.

[90] Reese, H. R., *Biopolymers* 1994, *34*, 1349-1358.

[91] Zeng, Z. X., Clark, S. M., Mathies, R. A., Glazer, A. N., *Analytical Biochemistry* 1997, *252*, 110-114.

[92] Slater, G. W., Desrulsseaux, C., Hubert, S. J., Mercier, J. F.*, et al.*, *Electrophoresis* 2000, *21*, 3873-3887.

[93] Slater, G. W., Guillouzic, S., Gauthier, M. G., Mercier, J. F.*, et al.*, *Electrophoresis* 2002, *23*, 3791-3816.

[94] Tinland, B., Pernodet, N., Weill, G., *Electrophoresis* 1996, *17*, 1046-1051.

[95] Mercier, J. F., Slater, G. W., *Electrophoresis* 2006, *27*, 1453-1461.

[96] Ross, P., Scruggs, R., *Biopolymers* 1964, *2*, 231-236.

[97] Smith, S. B., Bendich, A. J., *Biopolymers* 1990, *29*, 1167-1173.

[98] Ulfelder, K. J., Schwartz, H. E., Hall, J. M., Sunzeri, F. J., *Analytical Biochemistry* 1992, *200*, 260-267.

[99] Mccord, B. R., Jung, J. M., Holleran, E. A., *Journal of Liquid Chromatography* 1993, *16*, 1963-1981.

[100] Edwards, A., Hammond, H. A., Jin, L., Caskey, C. T., Chakraborty, R., *Genomics* 1992, *12*, 241-253.

[101] Rosenblum, B. B., Oaks, F., Menchen, S., Johnson, B., *Nucleic Acids Res.* 1997, *25*, 3925-3929.

[102] Sigmon, J., Larcom, L. L., *Electrophoresis* 1996, *17*, 1524-1527.

[103] Rye, H. S., Yue, S., Wemmer, D. E., Quesada, M. A.*, et al.*, *Nucleic Acids Res.* 1992, *20*, 2803-2812.

[104] Di Marco, V. B., Bombi, G. G., *Journal of Chromatography A* 2001, *931*, 1-30.

VITA

Name: Chih-Cheng Lo (a.k.a. Roger C. Lo)

Address: 16, ALY 2, LN 438, GUANG RONG RD., LO TUNG,
I Lan, 265, TAIWAN

Email Address: rogerlo2004@gmail.com

Education: B.S., Chemical Engineering, National Chung Hsing University, 1997
M.E., Chemical Engineering, Texas A&M University, 2002
Ph.D., Chemical Engineering, Texas A&M University, 2008